공학박사학위논문

효과적인 약물 전달을 위한 마이크로니들 및 생산 공정 개발

Novel microneedle design and fabrication for improved drug delivery

2017 년 8 월

서울대학교 대학원

기계항공공학부

나 상 철

효과적인 약물 전달을 위한 마이크로니들 및 생산 공정 개발

Novel microneedle design and fabrication

for improved drug delivery

지도교수 전 누 리

이 논문을 공학박사 학위논문으로 제출함

2017 년 8 월

서울대학교 대학원

기계항공공학부

나 상 철

나상철의 공학박사 학위논문을 인준함

2017 년 8 월

위 원 장 _____

부위원장 _____

위 원 _____

위 원 _____

위 원 _____

Abstract

Novel microneedle design and fabrication for improved drug delivery

Sangcheol Na

School of Mechanical and Aerospace Engineering

College of Engineering

Seoul National University

Since its invention in 1853 by the British physicians Alexander Wood, the syringe is a basic transdermal injection tool used over 12 billion injections per year by injection drug users (IDU) worldwide. Transdermal drug delivery can avoid hepatic metabolism and absorption differences in relation to gastrointestinal disorders. In addition, it can produce fast effects with small amounts of drugs, but it is accompanied by several problems. According to world health organization estimates in 2014, about 2 million syringe-induced medical accidents occur each year and 25 types of blood-borne viruses have been reported including hepatitis B, C and HIV. In addition to the economic

reasons that vaccination costs increase annually, the use of a syringe should be prescribed by a professional medical practitioner, or at least necessary for undergo relevant profes-sional training. Therefore, development of microneedle is required as a drug delivery technology that can be used by general public without fear of secondary infection.

To this end, this thesis first describes the development of a microneedle that mimics the tip of a hypodermic needle and enables efficient drug administration with invasion. In the backside lithography process, the mask design factors are investigated and applied to easily fabricate complex three dimensional structures with a single UV exposure. The suggested microneedle array combines with the fiber sheet to function as an effective transdermal drug delivery system. It can continuously supply the administered drug using capillary forces and wicking of the fibers. Their functionality is visualized and evaluated in drug delivery tests using agarose gels.

One step further, we demonstrate production of microneedle by injection molding process capable of realizing a low manufacturing cost and a mass production. We achieve the injection molding process of microneedle while solving limitations such as machining of sharp point, gas trap and

generation of burr, etc. Continuous drug administration and diffusion by proposed microneedles can be confirmed in real time through experiments. In addition, *in vivo* drug delivery is successfully confirmed by inserting into the body of actual adult mouse.

The microneedles of this study have various applications as a safe and advanced transdermal drug delivery method that anyone can use. In particular, it will serve as a starting point for solving problems that may arise from drug delivery through existing injections, but also will be a new step for human health and well-being with low production costs and easy accessibility.

Keywords: Microneedle; Backside lithography; 3D microstructure; Injection molding process; Transdermal drug delivery;

Contents

List of Figures

Chapter I

Introduction

1.1 History of microneedle for drug delivery to dermis

Since the approval of the United States in 1979 for administering scopolamine to treat motion sickness as the first transdermal system for administration through the skin, various studies and systems have been developed for effective intravenous drug delivery.[2] Administration through the skin can avoid hepatic metabolism and control the drug dose and method of delivery. It can also prevent absorption differences in relation to gastrointestinal disorders, and is user-friendly. It is relatively safe for pain,

discomfort, and infection risks.[3] The worldwide transdermal patch market is worth $ 31.5 billion,[4] but there are only about 30 commercially available transdermal patch products.[5] The reason for these limitations in transdermal drug delivery depends on the versatile biological barrier properties of the *stratum corneum* which constitutes the outer skin layer.

Our skin consists of *epidermis, dermis/corium and subcutaneous tissues/hypodermis*.(Fig.1.1)[1] The epidermis is mostly a *stratum corneum* composed of keratin-rich dead cells. This outermost 10-15 ㎛ thick *stratum*

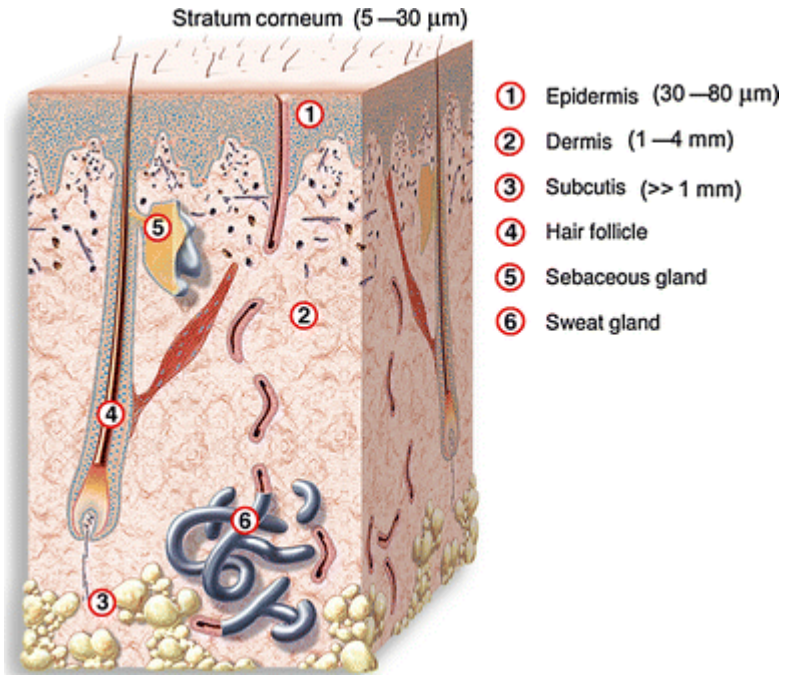

Figure 1.1 Structure of human skin**.** [1]

corneum acts as a major barrier to drug absorption. *Epidermis* does not have blood vessels and is nourished by diffusion from the capillaries present in the *dermis*.[6] *Dermis* is a layer of skin that surrounds the tactile receptors. It has an extracellular matrix (ECM) that contains collagen fibers and a variety of elastic fibers to provide the tensile strength and elasticity of the skin. It has glands of sweat and sebaceous, hair follicles, capillaries, and lymphatic vessels, and is rich in hyaluronic acid and proteoclycan.[7] The *subcutaneous structure* supplies blood vessels and nerves, and attaches the skin to bones and muscles. About 50% of body fat is here.[8] The thickness of epidermis and dermis layer in skin varies greatly from 54.4 to 189.2 ㎛ and 469.2 to 1076.6 ㎛ depending on regions of human body. (Table.1.1)[9]

Due to the structure and properties of these skin, medication through the skin is limited to drugs with low molecular weight below 500 Da. More specifically, it is ideal to have a lipophilic property having a log partition coefficient in the range of 1 to 3.5 and a hydrophilic property capable of dissolving more than 100 ㎍/ml.[10] [11] A drugs with a log P value of greater than 3.5 is so hydrophobic that they interfere with the absorption into the body by interacting with the intercellular lipid of *stratum corneum*. Most

drugs do not meet these conditions. Since they have hydrophilicity or a large molecular weight, they are hard to penetrate the *stratum corneum* layer. [2] Naturally, it is difficult to medicate in the body. Therefore, many strategic research has been conducted by researchers to overcome these challenges.

Table 1.1 Thickness of skin of body regions

Region	Specimens (n)	Epidermis (μm)	Dermis (μm)	E+D (μm)	E/(E+D) (%)
Eyelid	28	54.4±9.6	469.2±119.7	521.2±115.8	7.5
Cheek	28	98.2±26.7	1,076.6±225.0	1,141.1±292.3	8.3
Chin	15	84.0±23.3	763.9±317.1	857.1±247.8	9.9
Front of arm	11	69.2±21.9	943.4±235.6	1,012.6±233.3	6.8
Dorsum of hand	12	189.2±63.1	932.9±121.9	1,065.0±130.4	16.8
Dorsum of foot	13	163.1±18.6	1,001.1±259.2	1,164.4±280.9	14.0

The microneedle array was first presented in 1970 as one of the progressive methods to overcome the *stratum corneum* barrier. [12] However, due to limitations in manufacturing technology, micro-needles began to be realized in the late 1990s when microelectromechanical systems processing technology was developed. In 1998, Henry et al. first processed microneedles through ion etching on silicon wafers to invade the skin and promote delivery of calcein.[13] Over the past two decades, many research into the fabrication and use of microneedle in a variety of materials and designs, including silicon,[14 15 16] metals,[17 18] and polymers.[19 20 21 22] These microneedles penetrate the *stratum corneum* barrier with less pain and form microscopic pores for drug delivery to the target site, such as the epidermis or dermis. There are no reports of skin infections by microneedle, and they are easily inserted into the skin by the user without any additional applicator, without the need for specialized training.[23] Currently developed micro needle can be classified into four different types: solid type, coated type, dissolvable type, and hollow type.[24]

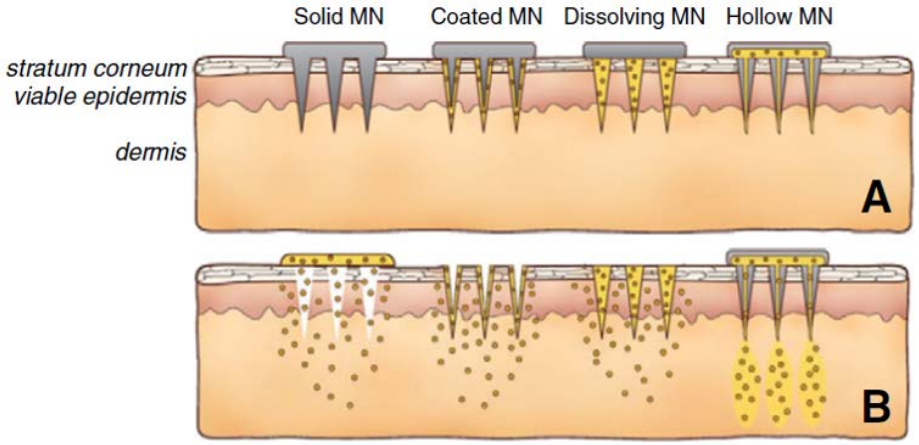

Figure 1.2 Schema of microneedle types[24]

Solid microneedles are used to create pores in the skin. After stabbing, the needle is removed and the drug is embrocated to the skin surface. The drug is diffused and absorbed into the micro pores created by the microneedle. These solid microneedles are made from a variety of materials, including silicon,[25 26] [15] metals such as stainless steel [27] and titanium,[28] non-degradable polymers such as polymethylmethacrylate (PMMA)[29] and polycarbonate,[30] or bio degradable polymers such as poly-lactic-co-glycolic acid (PLGA) and polylactic acid (PLA).[21] Coated microneedles are coated with drug on the surface of the solid type microneedle and inserted into the skin together. When the drug dissolved and absorbed into the body, the microneedle have to be removed separately. The manufacturing process of the coated microneedle

involves the use of various methods such as spray coating,[31] dipping,[32] gas jet,[33] and various agents such as carboxymethylcellulose sodium salt,[31] glycerol,[34] hyaluronic acid.[21] Dissolvable microneedles are made of safe materials that the needle itself absorbs to the skin and disappears after insertion. Most of them are fabricated from filled in a micro-mold cavity and dried or polymerized.[21 35] As another fabrication method, a droplet-born air blowing (DAB) method is proposed, which draws up the viscous liquid containing the medicament and dries it with air.[36] Finally, a hollow microneedle has an empty tube in the microneedle, which can be inserted into the skin and used as a supply channel for continuous drug administration. Due to its microscopic structure, hollow microneedles are generally produced by microelectromechanical systems (MEMS) technology, including deep reactive ion etching of silicon,[37] deep X-ray photolithography,[38] wet chemical etching[37] and laser micromachining.[39] Another production method is drawing a traditional glass micropipette.[40] Additionally, fabrication method is proposed the electrodepositing nickel on a polymer needle made by micromachining[41] or DAB.[42] However, it is clear that it has a big obstacle to mass production and commercialization due to the nature of the structure and process.

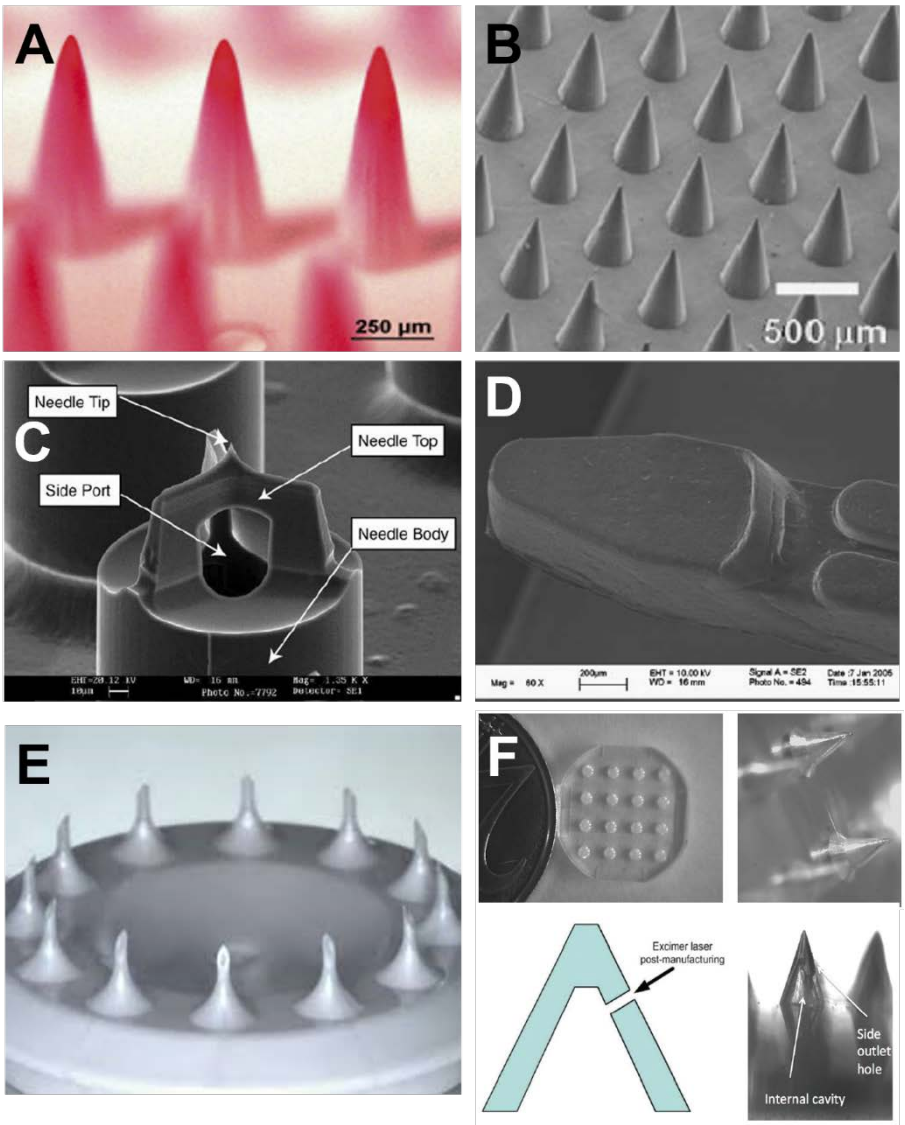

Figure 1.3 Various type of the microneedles (A) S.P. Sullivan *et al*., (2008)[43] (B) J.H. Park *et al*., (2010)[44] (C) P.Y. Zhang et al., (2009) [45] (D) Sammoura et al., (2007) [46] (E) L.A. Dick *et al*., (2015) [47] (F) Lhernould *et al*., (2011) [48]

1.2 Motivation and objective

Among the transdermal drug delivery methods into the body, the most widely used methods to date are drug injection using a syringe. Since its invention in 1853 by the British physicians Alexander Wood, [49] the syringe is now a basic transdermal injection tool used over 12 billion injections per year by injection drug users (IDU) worldwide.[50] Syringes are direct and fast transdermal drug delivery methods, low production costs and regardless of drug types. However, there are statistics that at least 10% of population suffer from needle phobia, which is a major obstacle to the opportunity for patients to receive medical care.[51] [52] Also, There is a risk of infection due to the use of un sterilized syringes or reuse of contaminated syringes. Patients in the developing world are injected with syringes 10-100 times per year, of which at least 50% of the procedures are unsafe. Studies have shown that 20-80% of new hepatitis B infections are due to unsafe injections.[50] For this reason, safe discard is essential to preventing needle stick injuries to the used syringe. World health organization (WHO) estimates that needle stick injuries occur worldwide at 2 million per year.[53] In addition, the use of a syringe should be

prescribed by a professional medical practitioner, or at least necessary for undergo relevant professional training. For these various problems, alternative drug delivery methods offer distinct advantages.

The various microneedles and manufacturing processes presented have various development possibilities, but there are obstacles to overcome for commercialization. Conventional technologies until now are mainly based on a micromachining or semiconductor process technology with high cost and low productivity, so it is not yet available commercially.

The first aim of this thesis is to develop a commercially available transdermal drug delivery system. For this purpose, several factors have to be considered. Development and design constraints are defined like below.

1) Fabrication process capable of mass production at low cost

2) User friendly system that anyone can use

3) Effective drug delivery

4) Biocompatibility and stability

5) Easily disposable without fear of secondary infection

First, we developed a microneedle designed to mimic tip of hypodermic needles for efficient drug delivery and to continuously infuse fluids with skin invasion. The microneedle array demonstrates the superior drug delivery efficacy by embedding fiber or forming a hole in the substrate for sustained drug administration.

Secondly, backside lithography process can be used to produce a array of complex shape microneedles with a large area by only single exposure. In

addition, introducing a novel mold machining method, mass production of microneedle can be realized using injection process to reduce cost and commercialize.

Finally, we demonstrate the functionality of microneedles produced *in vitro* or *in vivo* by drug delivery experiments.

1.3 Thesis overview and contribution

This paper describes the design and production of microneedles, which allow easy infiltration of the *stratum corneum* layer and efficient administration of fluids. It also mentions the development of an injection molding process for its mass production.

This is a step further than the development process and discussion of a number of microneedles presented at the laboratory level, and is significance as a cornerstone that can actually contribute to the well-being of humankind and be spread and used at a low price.

In chapter 2, a complex shape of microneedle is fabricated using the difference in curing shape according to the dimension of the opening area during the backside lithography process. We have considered for a design factor that can create grooves for infusion of fluid into the body after invasion to the skin. The resistance to compressive stress of microneedles made with backside lithography and the force required for injection into skin substitutes

are tested and compared. In addition, we introduce a fiber-embedded microneedles that can enhance fluid administration through fiber capillary force and wicking. Solid microneedles which mimic the tip of hypodermic needles are inserted for skin pretreatment. After forming pores in the stratum corneum and viable epidermis, drugs are diffused through the pores and into the dermis.

Chapter 3 introduces a study on the mass production of microneedles using injection molding. We describe the production of microneedles with grooves to form the microfluidic channels when injected at skin described above. The limitation of the machining process is overcome by proposing the machining method through the assembled core. The cavity is processed by the proposed machining method and the micro needle is produced through the actual injection molding process. In addition, the resistance to compressive stress and displacement of the microneedle are predicted by finite elements method, and the actual failure test and the force required for skin injection are tested.

Chapter 4 describes the practical application of microneedles formed through injection molding. The microneedle is inserted into the hypothetical skin and the amount of fluid absorbed through the fluid outlet connected to the groove is analyzed with time. In addition, an effective *in-vivo* drug delivery is confirmed by inserting a microneedle into an adult mouse.

The main contribution of this research is to provide a novel and innovative microneedle design for efficient fluid administration and development of mass production drug delivery systems for commercialization.

Chapter II

Fiber-based drug delivery microneedle

2.1 Concept

The main microneedle fabrication concept of this research is based on backside photolithography for fabrication of microstructure. Photolithography is a common fabrication technique widely used to manufacture microstructures. [54] [55] In general lithography, a photoresist or UV curable resin is placed on a substrate represented by a silicon wafer, and a microstructure is formed through UV exposure from the front side. [56] [57] This method requires

several iterations for a multi-level 3D structure. However, several recent studies have proposed that a multi-level structure can be formed in one step through backside incidence using a transparent substrate. [58] [59]

One of the objectives of this research is to create microneedles for transdermal drug delivery using backside lithography. Our proposed fabrication method is further developed in a previous study examining the possibility of a microneedle production method with basic conical microneedle array. [60] We develop microneedles that are effective in drug administration, inspired by our previous studies that can control the height, width, and slope of microstructures according to the design of the mask. [58]

The microneedle we propose has a sharp pointed shape which mimic the tip of hypodermic needles that can effectively invade the skin. Also, it has a groove acting as a microfluidic channel that allows fluid to rapidly enter the body. Finally, it is intended to place a fiber between the skin and the substrate of the microneedle allowing continuous fluidic flow through the gap between the skin and the inserted needle groove.

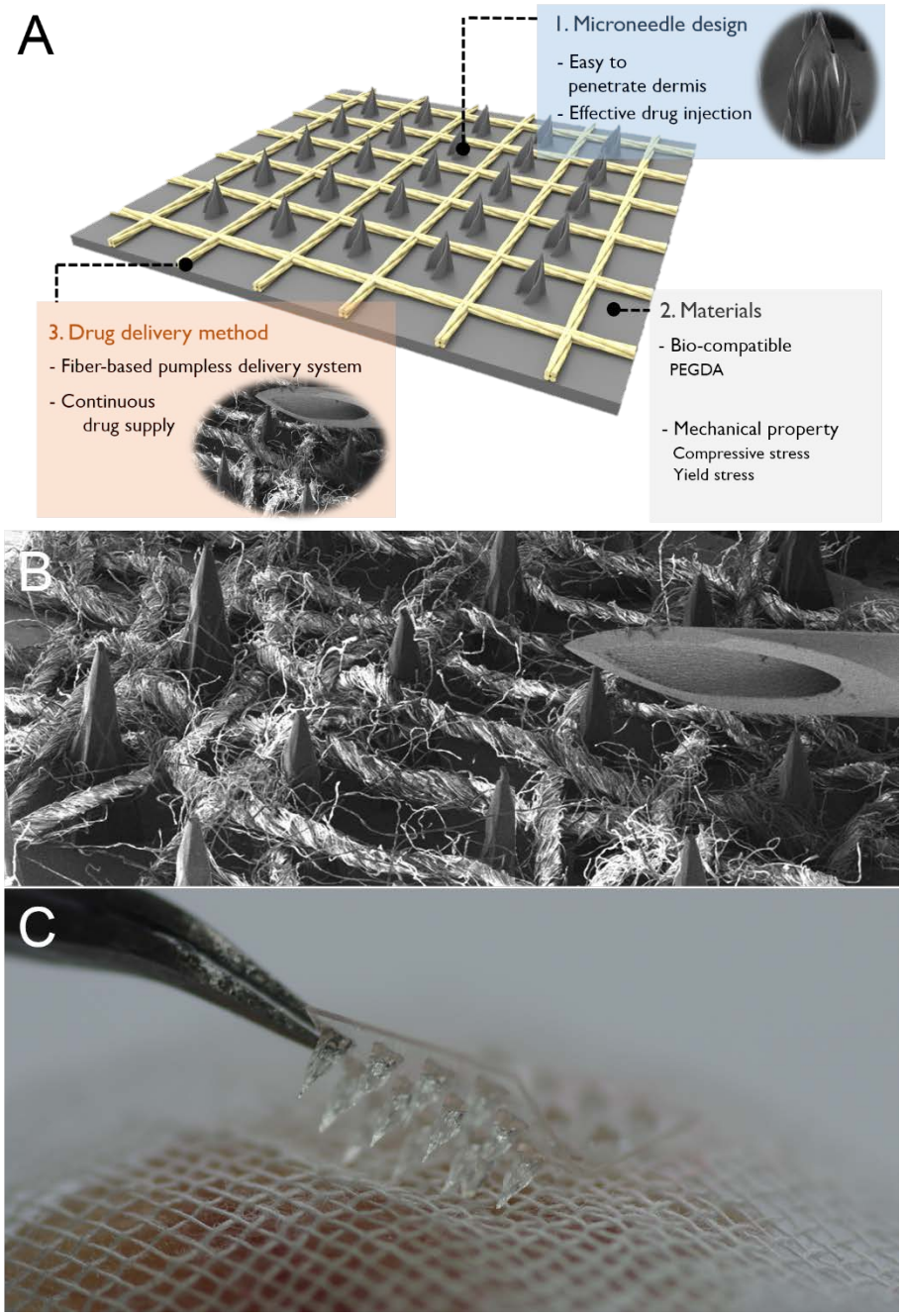

Figure 2.1.1 Schematic diagram and photographs of fiber-embedded microneedle

Schematic diagram and photographs of Microneedle is shown in figure.2.1.1. Fiber-embedded microneedles are comprised of solid microneedles and fiber mesh part. Solid microneedles which mimic the tip of hypodermic needles are inserted for skin invasion. After forming pores in the *stratum corneum* and *epidermis*, drugs are diffused through the pores and into the dermis. To effective drug delivery, we recognize the need of extra method using wetting of the cotton fiber. Wetting force which driving liquid type drug allows continuous and stable drug supply without any extra pump. Compare to simple solid microneedle, fiber-embedded microneedle represent the significantly increased efficiency. This fiber-embedded microneedles can be useful in the field of vaccination, clinical trials for macromolecules and other applications.

2.2 Microneedle fabrication using backside lithography

2.2.1 Preparation of microneedle array

We fabricated microneedle structures of various scales on PET substrate. In this study, polyethylene glycol diacrylate (PEG-DA) (Sigma-Aldrich, MO, USA) resin are used. PEG-DA is widely used in radical-free copolymer crosslinking reactions. PEG-DA mixture solution consists of 3% photo-initiator (Igarcure 184, CIBA specialty chemical, Switzerland) in PEGDA-200. The mixture is cured by reaction of the acrylic group of PEG-DA and photo-initiator when a sufficient amount of UV light is irradiated. The crosslinking of PEG-DA mixture solution initiates at the exposed surface proximal to UV light.

We used commercially available polyethylene terephthalate (PET) film (Item No. H4588, SKC, Korea) as a transparent substrate for backside lithography. According to the specification of manufacturer, the thickness of PET film is 188 ㎛. The glass transition temperature of the film is 140°C,

which is significantly higher than the 70°C temperature during the drying in the fabrication process. PET film has very exceptional resistant to chemicals; it is not dissolved or degraded by the chemicals involved in the developing process. In this study, we used pure ethyl alcohol as the developer. The adhesion between PEGDA structure and PET film is remarkably excellent since the surface of the PET film is coated with an acrylic group. When the PEGDA mixture solution is cured by UV light, this acrylic group reacts and crosslinks not only to form a microstructure but also to adhesion to the film. Before using, PET substrates are cleaned with pure ethyl alcohol and dried with a nitrogen blower.

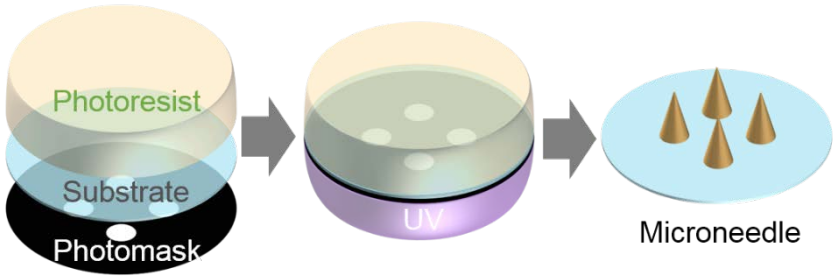

Figure 2.2.1 Microneedle fabrication process using backside lithography

Figure 2.2.1 shows an overview of microneedle fabrication process using a backside lithography. The PEGDA mixture solution is filled with petri dish and the PET film is placed thereon. A mask determining the shape of the microneedle is placed on top of film. A glass plate is used to improve contact between the film and the mask. An UV aligner (Shinu MST, South Korea) with i-line filter (365nm) is used for exposure. Intensity of UV light is 17.2 mW/cm^2 and decreased by about 7.4% as it passes through a 1.8mm thick glass plate. Exposure time is controlled to obtain specific 3D microneedle structure. After the exposure process, the microneedles on the film can be obtained. product is washed with ethyl alcohol to remove the uncrosslinked PEGDA mixture. After drying the alcohol and solution using a dry oven (70°C), the residual PEGDA polymer is crosslinked in a UV exposure

machine.

2.2.2 Method and experiment parameter setting

The major factor that can affect the shape of a microneedle in fabrication process using backside lithography is the shape and size of the hole in mask and the exposure time. Microneedle structure is formed as a PEGDA polymer crosslinking by UV light. This means that light path, intensity, and dose can be important variables in microneedle fabrication. Experiments are carried out to explore the conditions of forming the desired shape and size of microneedle. According to the Huygens-Fresnel principle, light is diffracted and focused as it passes through narrow slit. As the width of the slit increases, the amount of light passing through increases. 365 nm UV light was used in this study.

To experimentally estimate the height of microneedle, the circle hole, which is the simplest shape according to the UV light dose, is assumed. This mask consisted of circular holes with diameters ranging from 100 ㎛ to 1000 ㎛. The UV light dose ranged from 100 mW/cm^2 to 400 mW/cm^2. In preliminary experiments, the increase in microneedle length by UV dose was

almost reduced at dose of 400 mW/cm^2 or more, so that the range was defined as such.

In the structure of the skin, the *epidermis* is distributed from the skin surface at a depths of 50 ㎛ to 200 ㎛ or less. The fact that the *dermis* is distributed in depths of more than 800 ㎛ can be an important factor in the design of the microneedle length.

2.2.3 Microneedle geometry analysis according to various process conditions

The figure 2.2.2 show the shape and length of the microneedle formed according to the size of the circular hole and UV light dose. Overall, the length of the microneedle increases with the opening size. However, as the diameter of the hole increases to a certain size or more, the length of microneedle becomes gradual and eventually saturated. Especially, at UV dose of 100 mW/cm^2, it can be confirmed that the increase in microneedle length reaches saturation at a hole diameter of 300 ㎛. In addition, the increase in microneedle length is gentle on the condition when the hole size reaches 600 ㎛ at UV dose of 200 mW/cm^2 and when the hole size reaches 900 ㎛ at UV dose of 300 mW/cm^2.

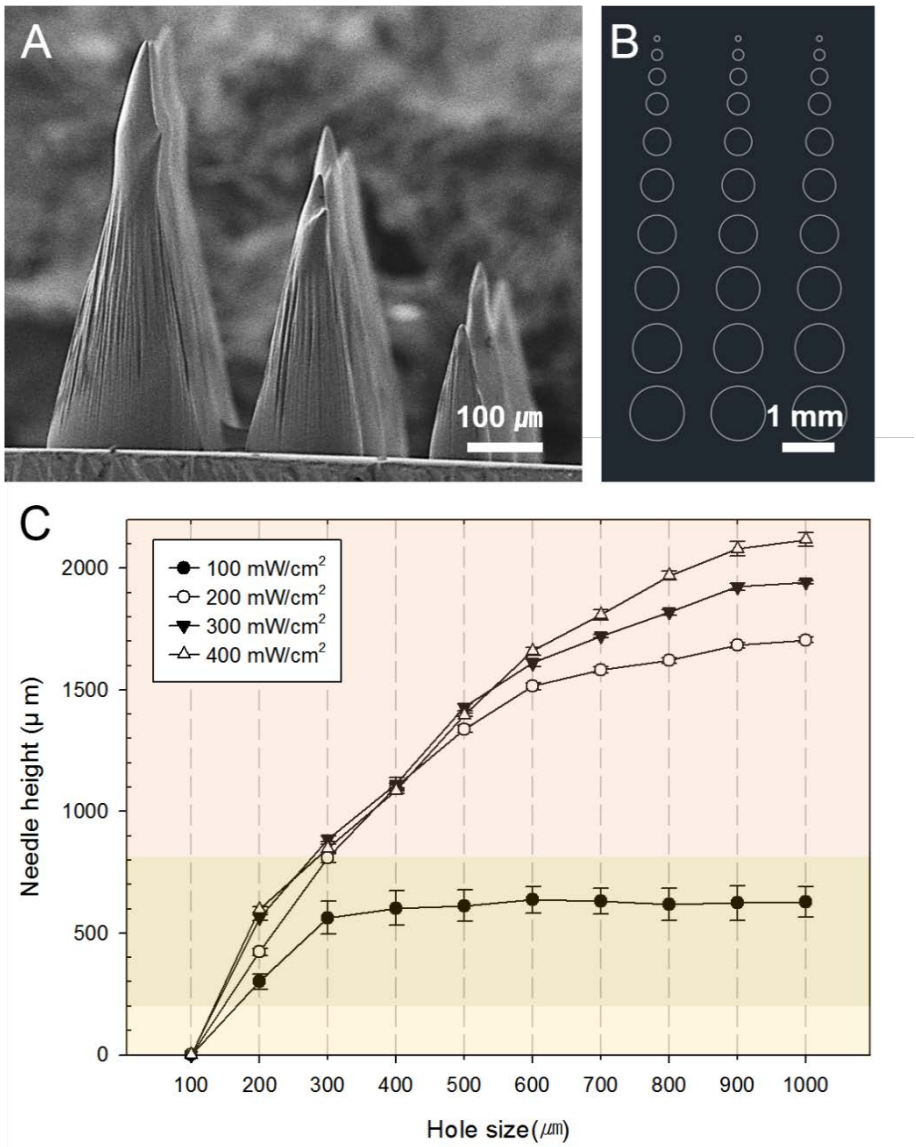

Figure 2.2.2 Appearance of circular microneedle fabricated by backside lithography**.** (A)SEM image and (B) drawings. Length distribution of the microneedle formed according to the size of the circular hole and UV light dose

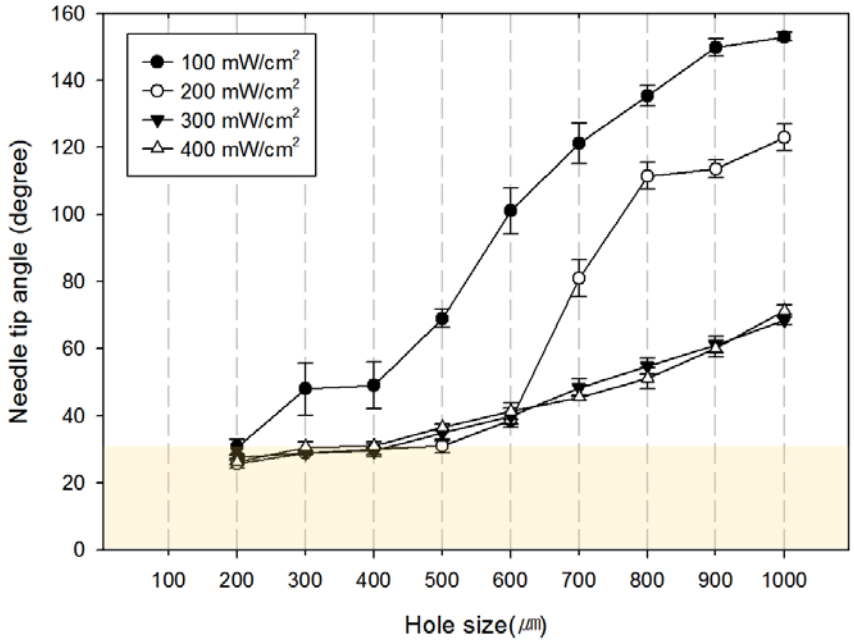

Figure 2.2.3 Change of the tip angle according to the size of the circular hole and UV light dose

The tip angle of the microneedle is as important as the length of the microneedle, which has a great impact on skin penetration. Microneedles with pointed end require less force to penetrate the sin and relieve pain to the recipient. The figure 2.2.3 shows the tip angle of the microneedle formed according to the size of the circular hole and UV light dose. Overall, the graph appears to form sigmoidal curves. Under the condition of 100 mW/cm^2 UV

dose, the tip angle maintains less than 50 degrees at hole size of 400 ㎛ or less. Thereafter, as the hole becomes larger, it shows an increasing tendency. After reaching a hole size of more than 900 ㎛, the tip ends are no longer sharp and form a gentle round shape, forming a very large tip angle of more than 140 degrees. This tendency seems to show a similar although there is a difference in an absolute value of the tip angle depending on the UV dose. However, as the UV dose increases, the tip angle tends to become sharp. It is assumed that the sharp angle limit has been reached in the circular microneedle design at UV dose above 300 mW/cm^2. As a result, microneedle fabrication through circular hole with a size of less than 400 ㎛ shows a tip angle of less than 30 degrees.

Above mentioned microneedle manufacturing using circular holes, it is difficult to reduce the tip angle of microneedle when producing a needle over a certain size. Focusing on this point, the microneedle is formed to better performance through the modification of the hole design.

The larger hole area in the mask, the greater amount of incoming light. As a result, the crosslinking amount of the UV curable resin is increased, and a large structure could be formed. First, we can assume that a basic hole is opened at the same distance with all directions from center (simply circular hole). In order to reduce the amount of crosslinking at the edges of the microneedle base, we designed a hole with a variable distance from the center to the edge. Figure 2.2.4 and table shows a schematic concept. Compared with the radius r of the circle, the rhombus shape has a minimum distance of 0.707r and the star shape has a minimum distance of 0.5r. In addition, we can compare the area of circle shape(πr^2), rhombus shape($2r^2$) and star shape ($\sqrt{2}\ r^2$). The ratio of each area is about 1: 0.636 : 0.45 (circle : rhombus : star). This suggests that the amount of light concentrated near the center can

be reduced by hole shape modification. This reduced light can control the amount of UV resin cured and consequently change the shape of the microneedle.

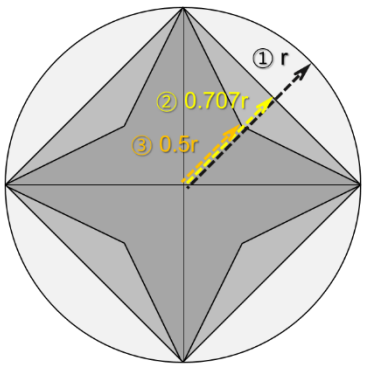

Shape	The shortest distance from the center	Opening area	Area ratio
Circle	r	πr^2	1
Rhombus	0.707r (=$\frac{1}{\sqrt{2}}$ r)	$2r^2$	0.636
Star	0.5 r	$\sqrt{2}r^2$	0.450

Figure 2.2.4 & Table 2.2.1 Schematic concept of hole shape modification and parameters

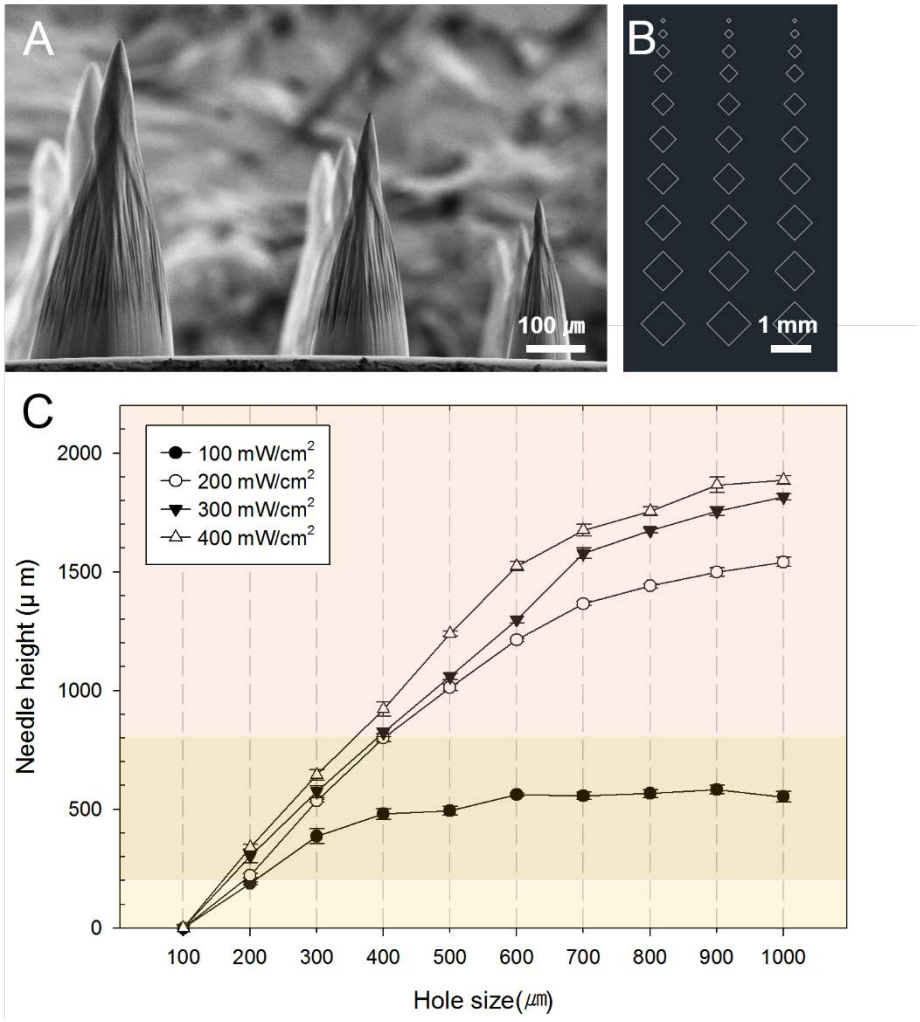

Figure 2.2.5 Appearance of rhombic microneedle fabricated by backside lithography**.** (A)SEM image and (B) drawings. Length distribution of the microneedle formed according to the size of the circular hole and UV light dose.

The shape of the hole is modified to make the microneedles with high height while making sharp tip angle. The figure 2.2.5 shows the length of the microneedle formed according to the size of the rhombic hole and UV light dose. Similar to above described the circular microneedle fabrication, the length of microneedle increases as the hole size increases. Overall, the rhombic microneedles from hole size of 500 ㎛ or less show a length distribution of about 71~80% compared to a circular shape. With a hole size of 700 ㎛ or more at 200, 300, 400 mW/cm^2 UV dose, it has a length distribution of about 85% ~ 92% compared to a circular microneedle, and the increase in length is gentle compared to the increase in hole size. The rhombic microneedle lengths are also saturated near the 300 ㎛ hole size at 100 mW/cm^2 UV dose. The saturated height is formed at 550 ㎛, 85% or the circular shape.

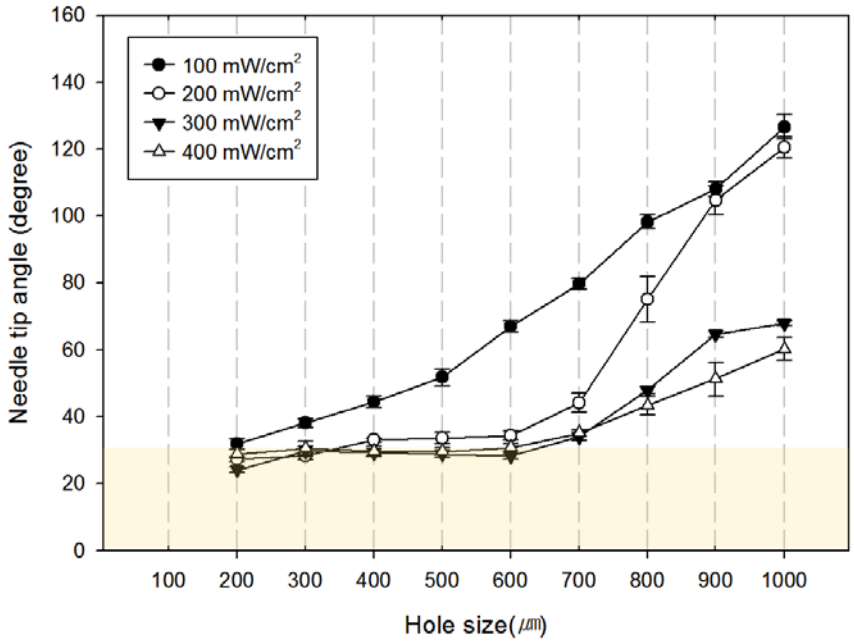

Figure 2.2.6 Change of the tip angle according to the size of the rhombic hole and UV light dose.

However, it is the angle of tip end that shows the large difference according to the hole shape modification. The figure 2.2.6 shows the tip angle of the microneedle formed according to the size of the rhombic hole and UV light dose. Microneedles has a sharper angle as the dose of UV light increases when using masks of the same size and shape. Similar to fabrication using a circular mask, the tip angle of the microneedle increases as the size of

the hole increases with a 100 mW/cm^2 UV dose. Under the condition of 200 mW/cm^2 UV dose, the tip angle maintains an angle value of 35 degrees or less in 600 ㎛ hole size or less. Microneedles made with larger than 600 ㎛ hole size have rapidly increase in tip angle. Under the condition of 300, 400 mW/cm^2 UV dose, it shows similar pattern. The tip angle shows less than 30 degrees to a range of 600 ㎛ hole size and displays a gradual increase in the larger hole size range. Compared to a circular-shaped hole, a sharp-pointed microneedle shape can be obtained with a higher height using rhombic-shaped hole.

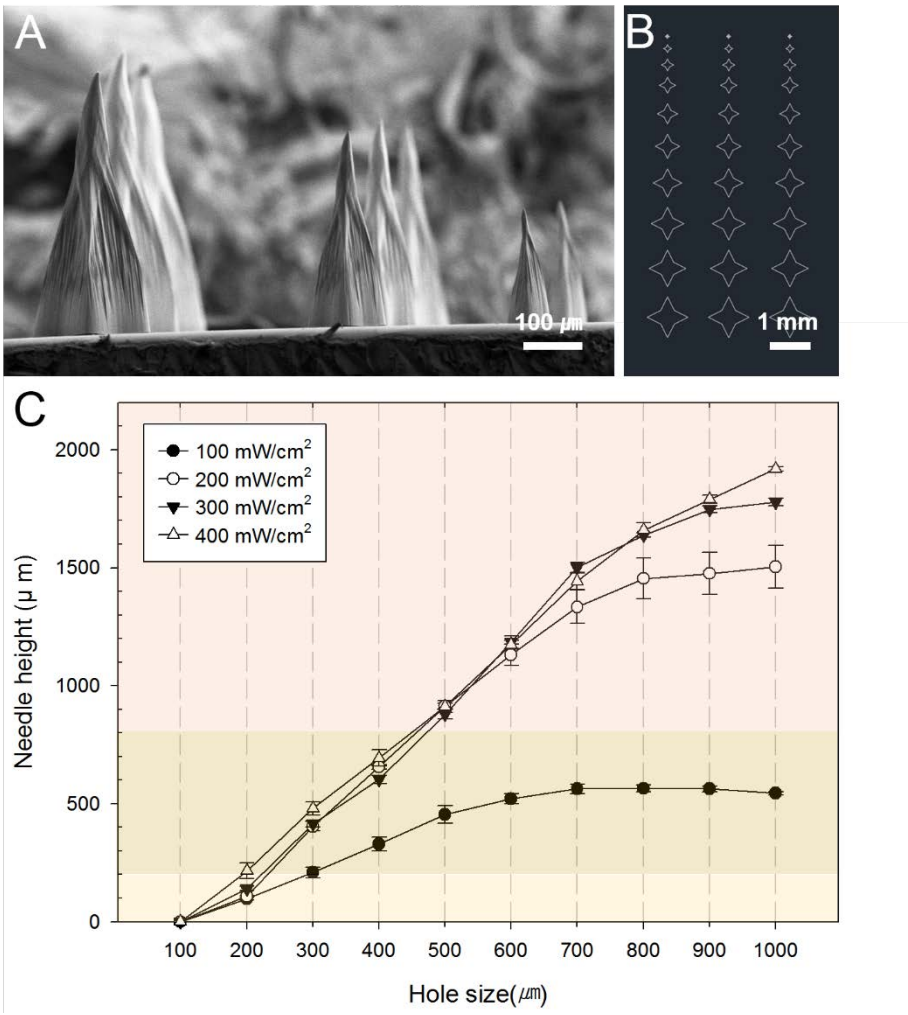

Figure 2.2.7 Appearance of star shape microneedle fabricated by backside lithography**.** (A)SEM image and (B) drawings. Length distribution of the microneedle formed according to the size of the circular hole and UV light dose.

Compared to the microneedle shape we made earlier, we designed a star shape hole to get a more sharp microneedle. The figure 2.2.7 shows the length of the microneedle formed according to the size of the star shape hole and UV light dose. As in the previous experiments, the length of the microneedle increases as the hole size increases. Overall, the star-shape microneedles from hole size of 500 ㎛ or less show the needle length distribution of about 66~75% compared to a circular shape. In the case of 100 mW/cm^2 UV dose, the height of microneedle is saturated at 600 ㎛ hole size, and then it is about 530 ㎛. In other cases, the graph of 200 mW/cm^2 UV dose tends to increases continuously, but it also reaches the saturation point in the 800 ㎛ hole size and then maintains the height of 1450 ㎛. In the 300 and 400 mW/cm^2 UV dose, the increasing tendency of the microneedle length becomes slower at larger than 700 ㎛ hole size, and it has a length distribution of about 80% ~ 88% compared to a circular microneedle.

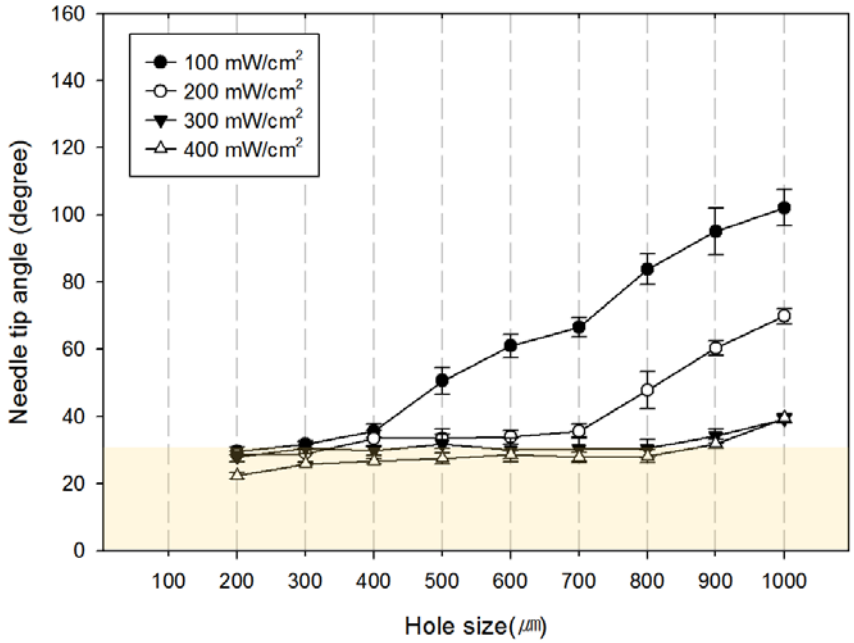

Figure 2.2.8 Change of the tip angle according to the size of the star shape hole and UV light dose

Similar to the rhombus type microneedle, tip end angle comparisons in microneedle fabrication using star shape holes show a more significant result. Compared to the previous two results, the angle of tip is remarkably reduced as whole. It shows a sharp shape of tips which have less than 35 degrees to 700 ㎛ hole size condition at a UV dose of 200 mW/cm^2 or more. In the case of 300 and 400 mW/cm^2 UV dose, the tip angle of less than 35 degrees is

maintained even in a hole of 800 ㎛ size. Especially at a dose of 400 mW/cm^2, the tip ends are formed with very sharp ends of about 28 degrees. Overall, modified mask allows sharp tips to be formed at high dose and large hole sizes. Accordingly, it is possible to form a microneedle closer to the original purpose of ‘epidermal invasion and penetration’.

2.3 Microneedle compressive stress and insertion testing using multi-functional adhesion/scratch test system

2.3.1 Resistance test against compressive stress

Measurements of compressive stress were carried out using multi-functional adhesion/scratch test system (Neoplus INC, Seoul, Korea) This system can measure the adhesive force using a pressure-sensitive load cell. The microneedle is mounted on the moving part of the system and moved toward the fixed block. The fixed microneedles on the mount moves in a transverse direction at a rate of 20 ㎛/s until a failure occurs by contact with the block. (Fig. 2.3.1)

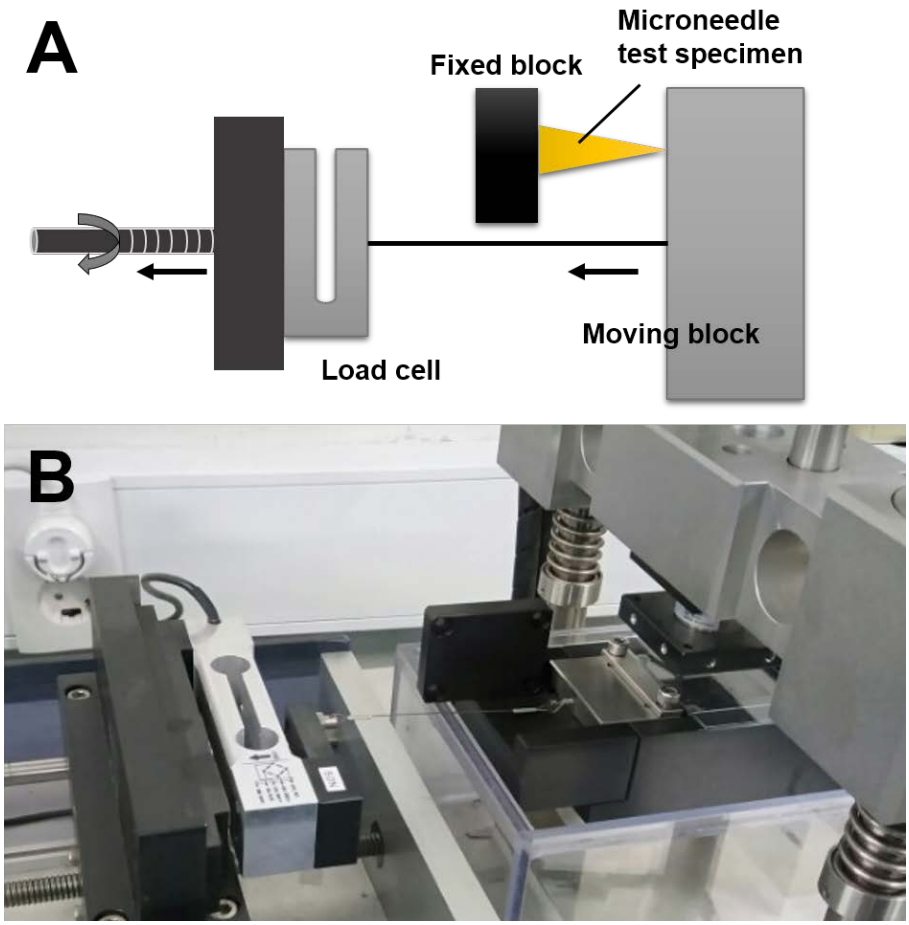

Figure 2.3.1 Illustration and photograph of experiment setup

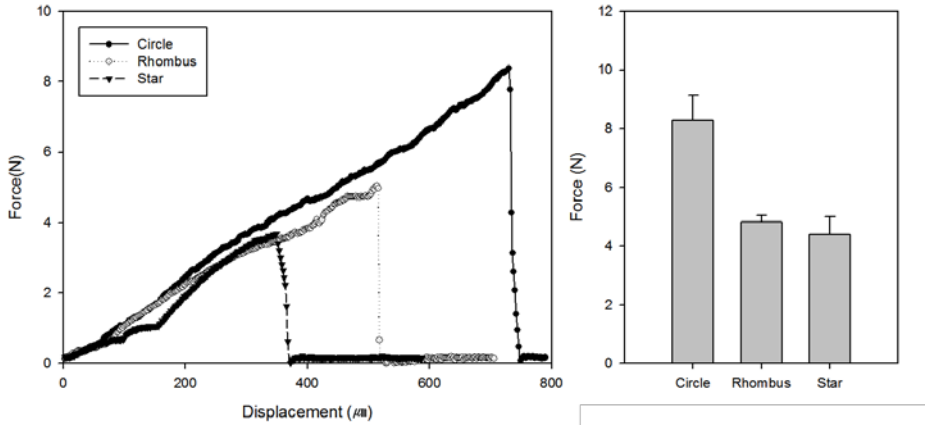

Figure 2.3.2 Graph of resistance to compressive stress for various microneedle type.

Experiments are designed to measure the difference in compressive stress sustained by different microneedle shape. The needle size which is root length of 800 ㎛ and height of 1600 ㎛ controlled the size variable and three types of needles such as circular shape, rhombic shape and star shape microneedles were prepared. The figure 2.3.2 shows the compressive stresses received by each microneedle and the deformed length distribution until fractured. The experiment proceeded with four samples each. The circular microneedle showed maximum compressive stress of 8.27N (SD 0.86) and showed deformity of 730 ㎛, but it was fractured. The rhombic microneedle

had a maximum compression stress of 4.82N (SD 0.24), deformed by 510 ㎛ and fractured. The star shape microneedle shows a maximum compressive stress of 4.40N (SD 0.60) and a maximum strain of 350 ㎛.

2.3.2 Insertion test of microneedle array

The insertion pressure test is performed assuming injection into the skin to check (i) how much stress is applied to the inserted microneedle into the skin, and (ii) whether it is within the compressive stress range identified above, and (iii) whether it does not break. A microneedle array with various densities is formed on a 7mm x 7mm (49mm^2) PET film as described above section. Four different microneedle arrays are used. (Fig. 2.3.3 & Table 2.3.1) The shape of microneedle is star type and unified to a base length of 800 ㎛ and a height of 1600 ㎛, which are the same dimension as used in the previous compressive stress test.

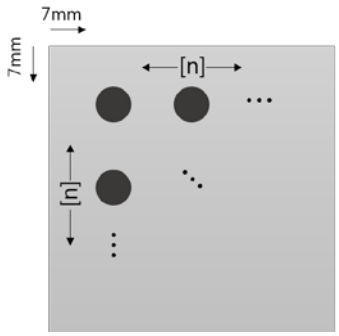

MN distribution	MN per sample	Interspacing at base
5 x 5 array	25	500㎛
4 x 4 array	16	1000㎛
3 x 3 array	9	1500㎛
2 x 2 array	4	2000㎛

Figure 2.3.3 & Table 2.3.1 Parameter values for Insertion pressure test according to needle interval

Parafilm M®(PF) film is used as an alternative to actual skin. The parafilm is folded to obtain a ten-layer (~1mm) specimen. [61] Larrañeta, Eneko, et al. reported that parafilm can be used as a substitute virtual sin for actual skin tissue for microneedle injection experiments. According to these, although there is a slight difference that skin is inserted by microneedles about 10% more, distribution of insertion results show similar tendency. It can be used as a good model of needle performance comparison experiment using this method.

The experiment is carried out using the multi-functional adhesion/scratch test system described above. The ten-layer parafilm is mounted on the moving part of the system and moved toward the microneedle array on the fixed block. The fixed ten-layer parafilm on the mount moves in a transverse direction at a rate of 20 ㎛/s until fully inserted.

The maximum forces required for insertion at 800 ㎛ depth are reduced as microneedle density decreases, i.e., 19.85N (SD 2.05), 14.48N (SD 2.05), 10.67N (SD 0.65), 5.97N (SD 0.33) on the microneedle array of 5×5, 4×4, 3×3 and 2×2.(Fig. 2.3.4 A) In other words, it can be confirmed that the force required for insertion is reduced in proportion to the interval length

between the needle and needle. For example, the force required when inserting at 500 ㎛ interval is four times as much as the force at inserting 2000 ㎛ interval.

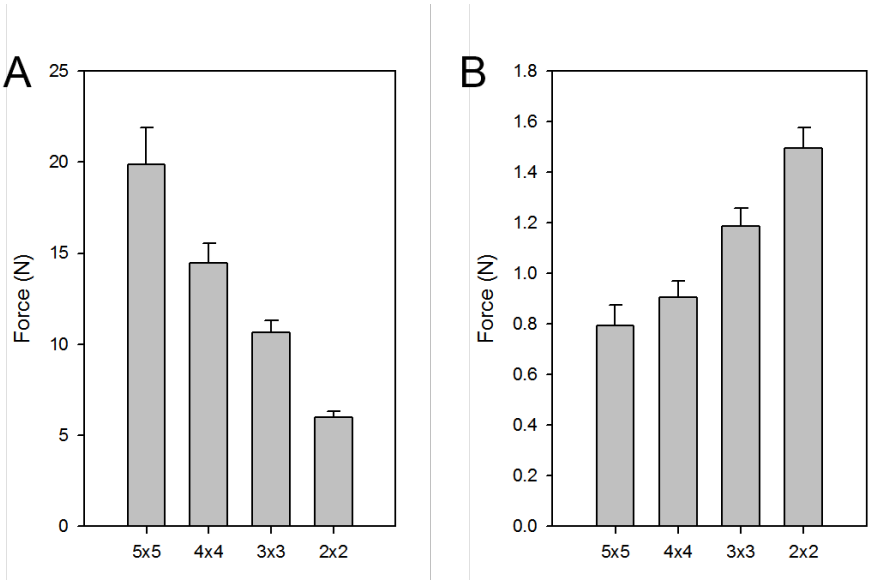

Figure 2.3.4 (A) The maximum forces required for microneedle insertion to parafilm ten-layer. (B) Maximum force applied to each individual needle at insertion.

Previous studies have shown that a maximum force of about 30 N can be applied when pressing an area of 1 cm^2 with a thumb on a human subject. [62] In another reported case, it was reported that the force applied to the elevator button or postage stamp for 30 seconds was about 19N for women and 21N for men. [61] Comparing the results of our experiments above, it can be concluded that the force of about 19.85N is required for insertion, which is close to the limit of force applied by a general adult. In the case of the above-mentioned needles, the spacing between the needles is required to be 500 ㎛ or more. If the spacing of the microneedle in the array is more than 1500 ㎛, it can be easily inserted with less than 50% of the force applied by thumb of normal adult.

The amount of compressive stress per needle in each array is smaller as the density of the needle is higher. The force applied to the entire area is divided in proportion to the number of needles, so that small amount of stress is applied to each of the tight needle arrays. (Fig 2.3.4 B) The force applied to each needle is as follows, i.e., 0.79N (SD 0.08), 0.91N (SD 0.07), 1.19N (SD 0.07), 1.49N (SD 0.08) on the microneedle array of 5×5, 4×4, 3×3 and 2×2. That is, the maximum stress in this experiment is less than 1.5N. Since the

compressive stress to the fracture shown in the previous experiment is less than about 4N, the function of the microneedle can be performed without any fracture problem in insertion.

2.4 Geometry improvements of microneedle for enhanced functionality

2.4.1 Concept

In the previous experiment, the relationship between the shape of the hole and the microneedle shape is confirmed. An experiment was conducted to analyze the shape of the needle by reducing the minimum distance of the hole radius from the circular shape to the star shape. As a result, we found that the shape of the hole that reduces the crosslinking of the edge can form a sharp shape of the microneedle in the higher height. It has also been reported in previous articles that UV curable resin is highly crosslinked in a wide opening area. [58] [63] Here, through modification of the opening area shape used in the backside lithography process, the microneedle is improved to functional shape that allows fluid to flow after the skin invasion while maintaining sharpness. The shallow grooves created in the microneedles from the star shaped holes are further emphasized.

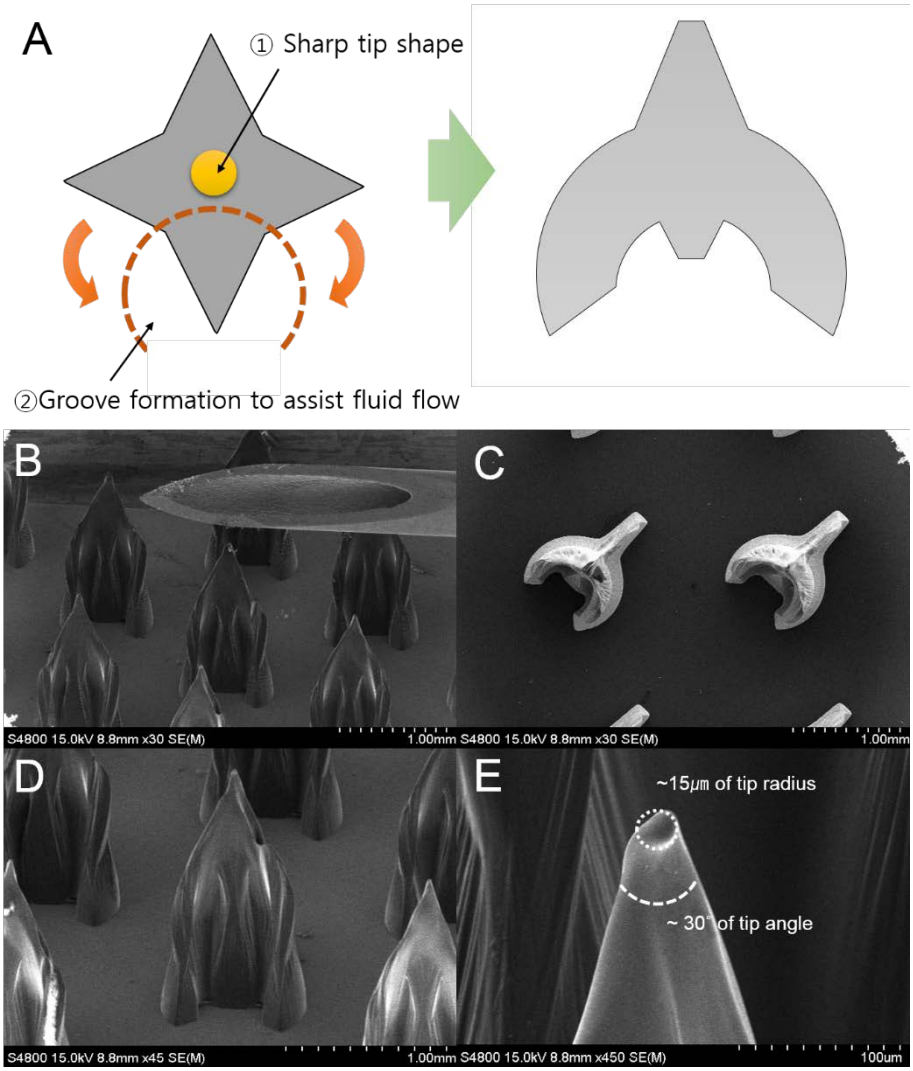

Figure 2.4.1 Design concept and SEM image of trident shape microneedle mimicking tip of hypodermic needles

Fig. 2.4.1 shows the microneedle shape of the modified design like trident. The new trident shape microneedle that resembles the tip of hypodermic needles maintains a high and sharp tip angle similar to the star shape. Especially, the arm originating from the central axis is lowered toward the edge, and it bends and forms a large groove around the center. This arm forms an oblique grooved channel from the tip end to the base of the needle. This large groove is intended to serve as a channel for administering the fluid after microneedle skin invasion. Forming microstructure through these exposures can be deduced from the difference in shape of the microneedle due to UV exposure differences at the center and at the edges. The shape data according to the hole dimension of modified microneedles are as follows.

2.4.2 Geometry analysis of modified microneedle

The figure.2.4.2 A shows the height distribution of the microneedle formed according to the size and dose of the newly designed hole in mask. Similar to the length distribution found in previous experiments, the height of microneedle increases with increasing size of hole. Overall, the hole size of 600 ㎛ or less shows a height distribution of about 65~80% compared to the circle shape. At UV dose of 100 mW/cm^2, the point which the increase in length is slowed seems to be after a hole size of around 800 ㎛. For other exposure conditions of 200, 300, 400 mW/cm^2 UV doses, the height increases continuously after 700 um hole size, but continues to increase steadily.

The angle of the tip end is generally sharp compared to that of the rhombic microneedle.(Fig. 2.4.2 B) Trident shape microneedle shows a higher tip angle than star shape microneedle, but it appears to form about 30 degrees of tip angle. This seems to be due to the design derived from the star shape, which relatively reduces UV crosslinking far from the center of microneedle core. Especially, as the UV dose increases, the angle of tip tends to be sharp. Especially, even in microneedle made with a relatively large 800 ㎛ mask, the

tip radius is 14.7 ㎛. This form is considered to be an excellent form of skin invasion.

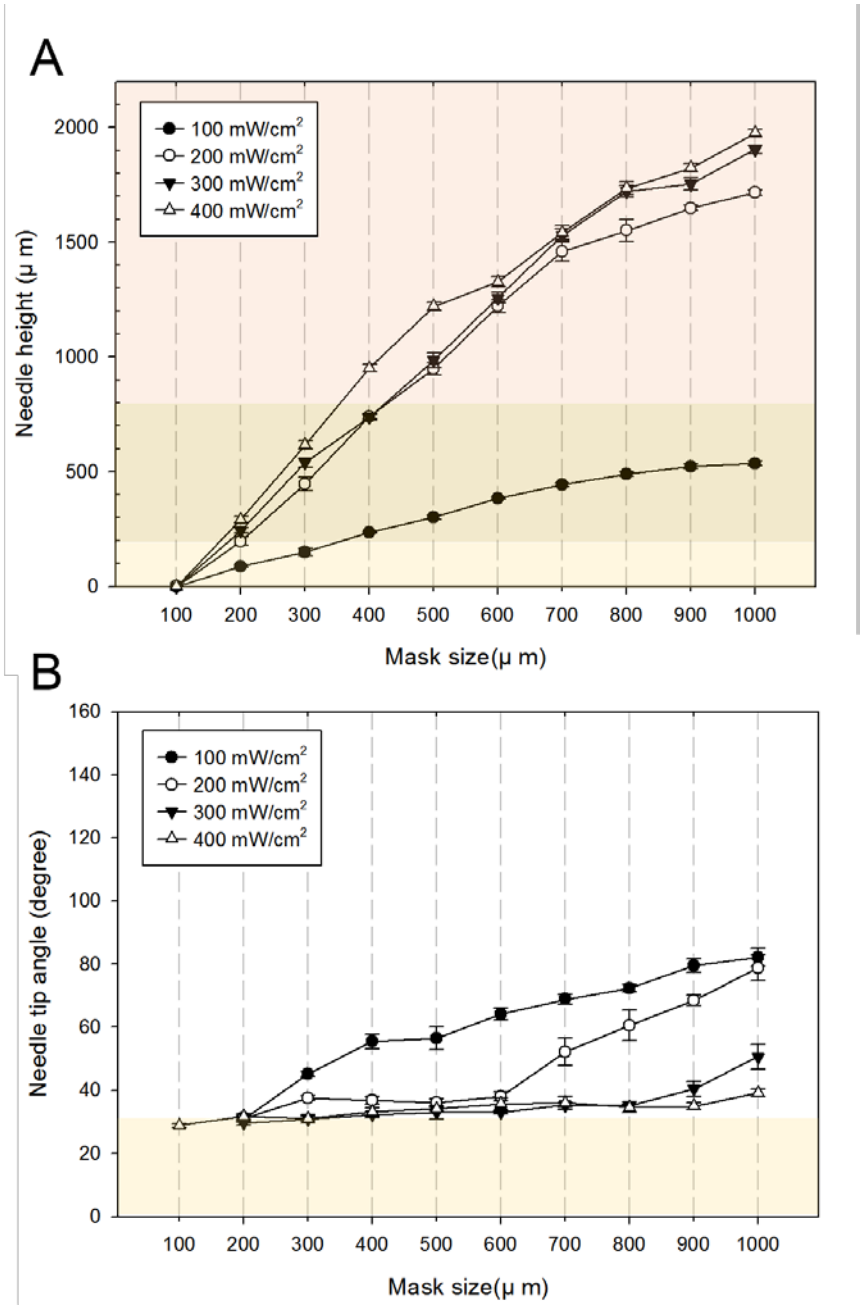

Figure 2.4.2 The height distribution and tip angle of the microneedle formed according to the size and UV dose

2.4.3 Compressive stress test and comparison

The compressive stress test is carried out in the same method as described above. The size of the MN is the same as a root length of 800 ㎛ and height of 1600 ㎛, and the multi-functional adhesion / scratch test system is used. Trident shape microneedle showed maximum compressive stress of 5.83N (SD 0.26). Figure 2.4.3 shows weak compressive stress resistance than circular microneedle but shows stronger resistance than rhombic microneedle as well as star-shaped microneedle.

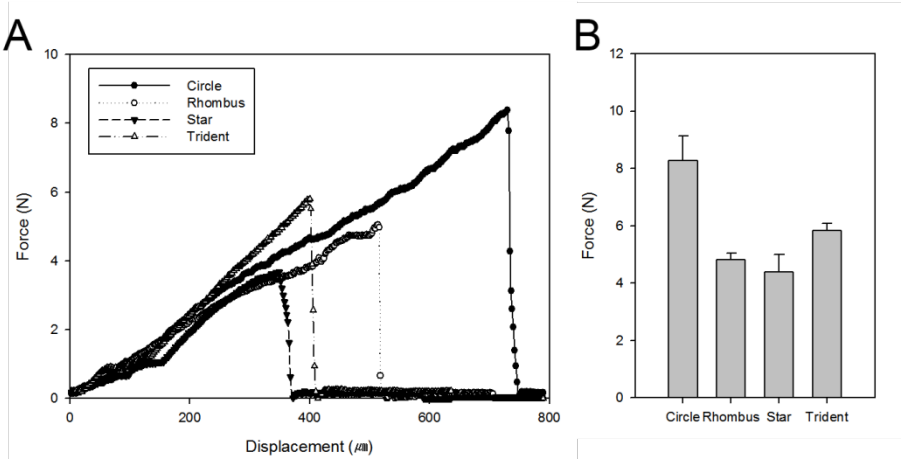

Figure 2.4.3 Resistance to compressive stresses of various microneedles

2.5. Fiber-embedded microneedles for pumpless drug delivery

2.5.1. Drug delivery in agarose gel

The microneedle formed by the backside lithography process can be inserted into the skin to check the drug delivery and drug diffusion profile to confirm the function of skin invasion and fluid delivery. To confirm the delivery of the drug in real time, the specimen used in the insertion experiment is found to be transparent and possess a water absorption property similar to the human body. There are a number of studies that have experimentally or theoretically identified drug diffusion characteristics using agarose gel as a surrogate of human tissue. [64 65 66 67 68 69]

A 100 ㎛-thick parafilm is used as the role of the epidermis layer, including the *stratum corneum* layer, which acts as a barrier to prevent drug penetration from the outermost part of the skin. The dermis layer is replaced with 1% agarose gel. Agarose (Duchefa, Haarlem, Netherlands) produces 1% aqueous solution in distilled water in a mass ratio. Then, sterilize at 121℃ in the autoclave and prepare by gelling at room temperature. 20×20×20 mm

sized agarose block is prepared as a surrogate of the skin with closely adhering parafilm cut at 20 x 20 mm. After that, a 2×2 microneedle array is inserted over the parafilm. Water soluble red dye is used as a drug and 2 $\mu\ell$ is administered in each experimental case. Cosmetic mask which made of polystrene is used as fiber sheet for fiber-embedded drug delivery systems. All procedures are time-lapse imaging with digital single lens reflex (DSLR) camera for more than 5 minutes, allowing real time monitoring of dose area over time. Acquired images are measured using imageJ (NIH, MD) for the area of drug absorption.

2.5.2. Result and discussion

The comparative experiments are conducted to compare the drug delivery capacity of a typical microneedle with the trident shape microneedle that we presented. The microneedle used as a control is the star shape microneedle as described in chapter 2.2.3 above. All the needles used in the experiment have the same root length and height. Figure.2.5.1 and 2.5.2 shows the time-lapsed images of diffusion profile from an injection surfaces. Red water soluble dyes are transferred to the agarose gel via pores caused by the microneedles in the parafilme. The injected area for the first 1 minute shows a proposed trident shape microneedle about 5 times as wide as the normal microneedle. In the first minute, the trident shape microneedle dose ($0.62mm^2$) delivered about 5 times larger area than the normal microneedle dose ($0.11mm^2$). In particular, the difference between the amount administered and the area transferred is drastically widened as time passes. This indicates that the design of the microneedles intended to deliver the drug continuously to the invaded site is successful.

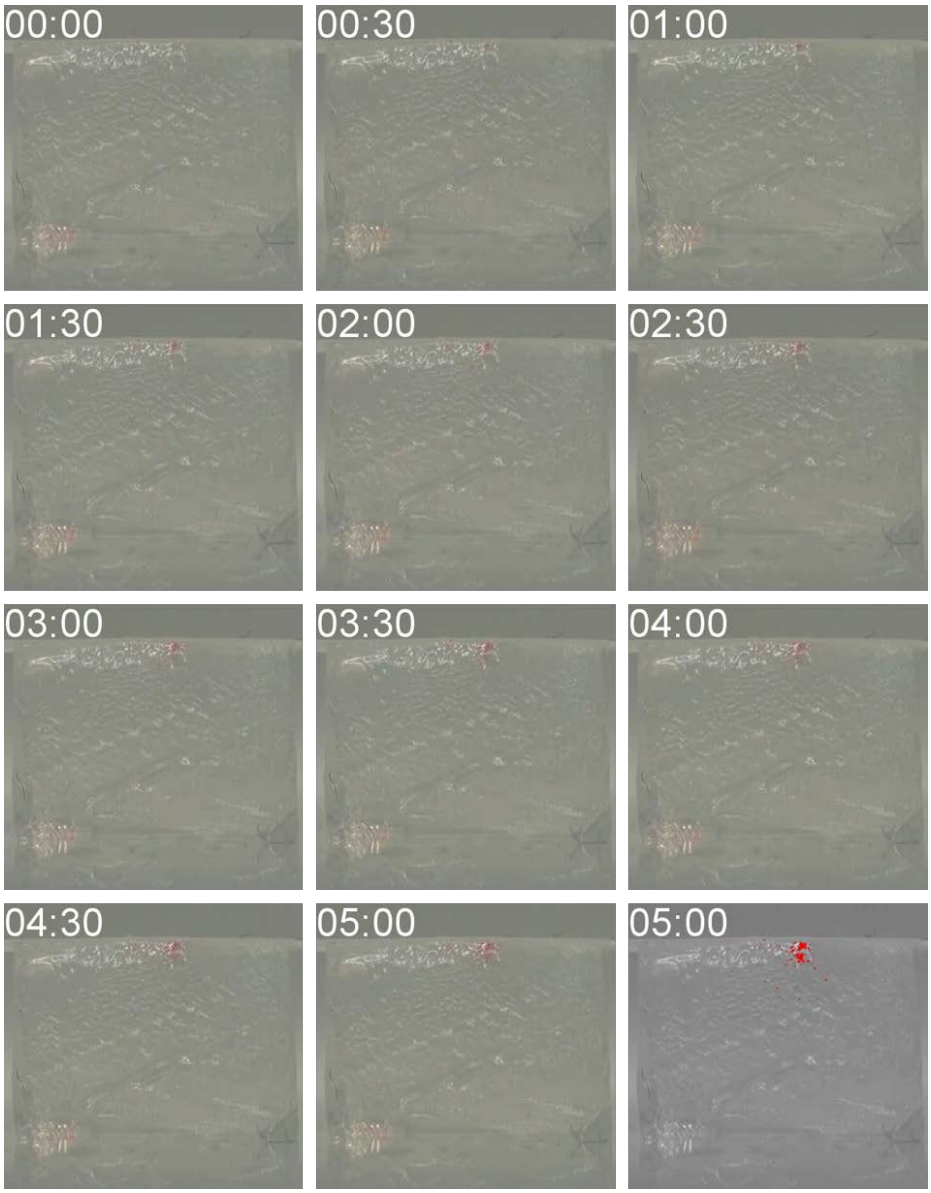

Figure 2.5.1 Time-lapse images in case of typical microneedle drug delivery with embrocation at 1% agarose gel

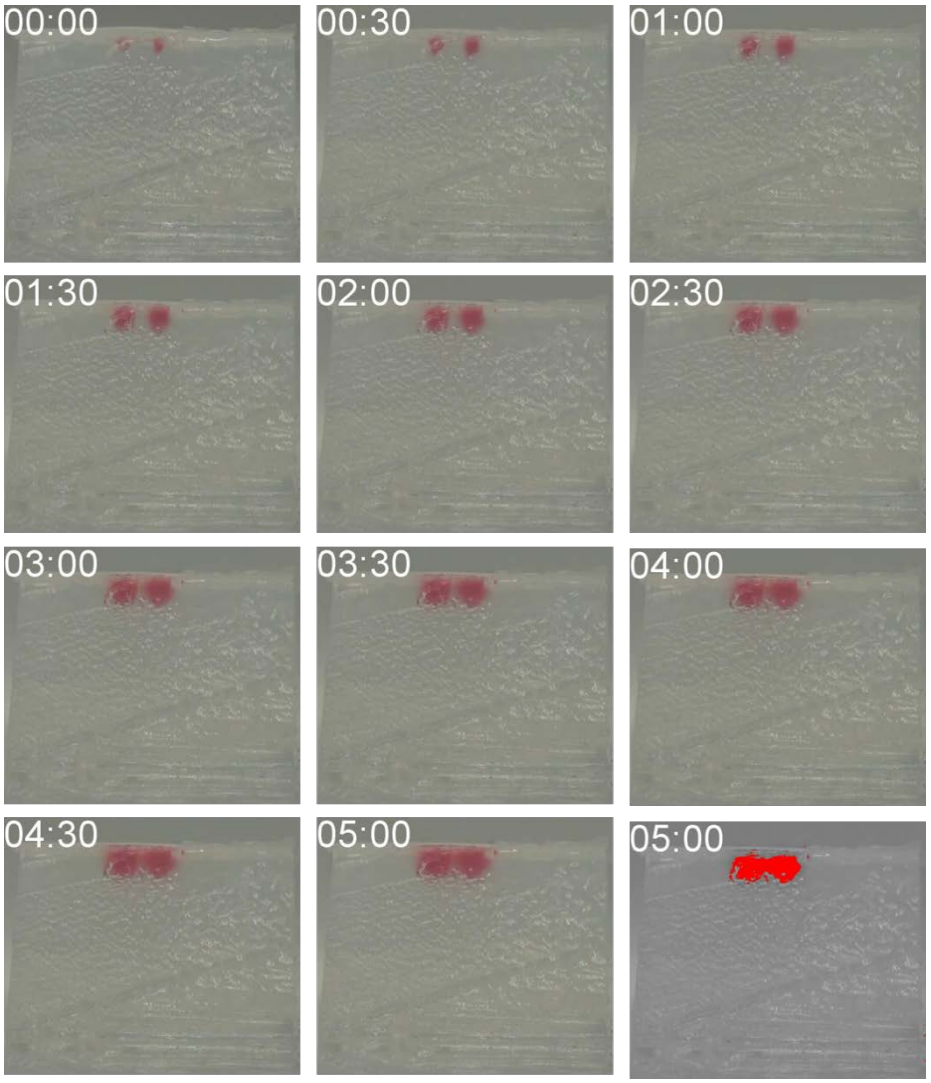

Figure 2.5.2 Time-lapse images in case of trident shape microneedle drug delivery with embrocation at 1% agarose gel

To further increase the delivery of drugs, we propose the fiber-embedded microneedle systems that induce pumpless drug delivery systems. In conventional drug delivery methods using solid microneedles, the micro-needle creates pores in the stratum corneum and the epidermis, and the surrounding drug is transported through the pores. For effective drug delivery, we perceive the needs of an extra method using cotton fiber wetting. By embedding fibers between the substrate and the skin surface where the array of microneedles are located, it is expected that continuous drug delivery around the pore will be possible. The capillary force and wicking phenomenon of the fiber ensures continuous and stable supply of the drug without the pump. This method can be enhanced with a more efficient drug delivery system by combining with the trident microneedle, which facilitates fluid administration. Figures.2.5.3 and 2.5.4 show the diffusion tendency of the drug when inserting a microneedle through a fiber sheet. Red water soluble dyes absorbed 2 μl of the same amount as the other method into the fiber sheet, and inserted the microneedles thereon.

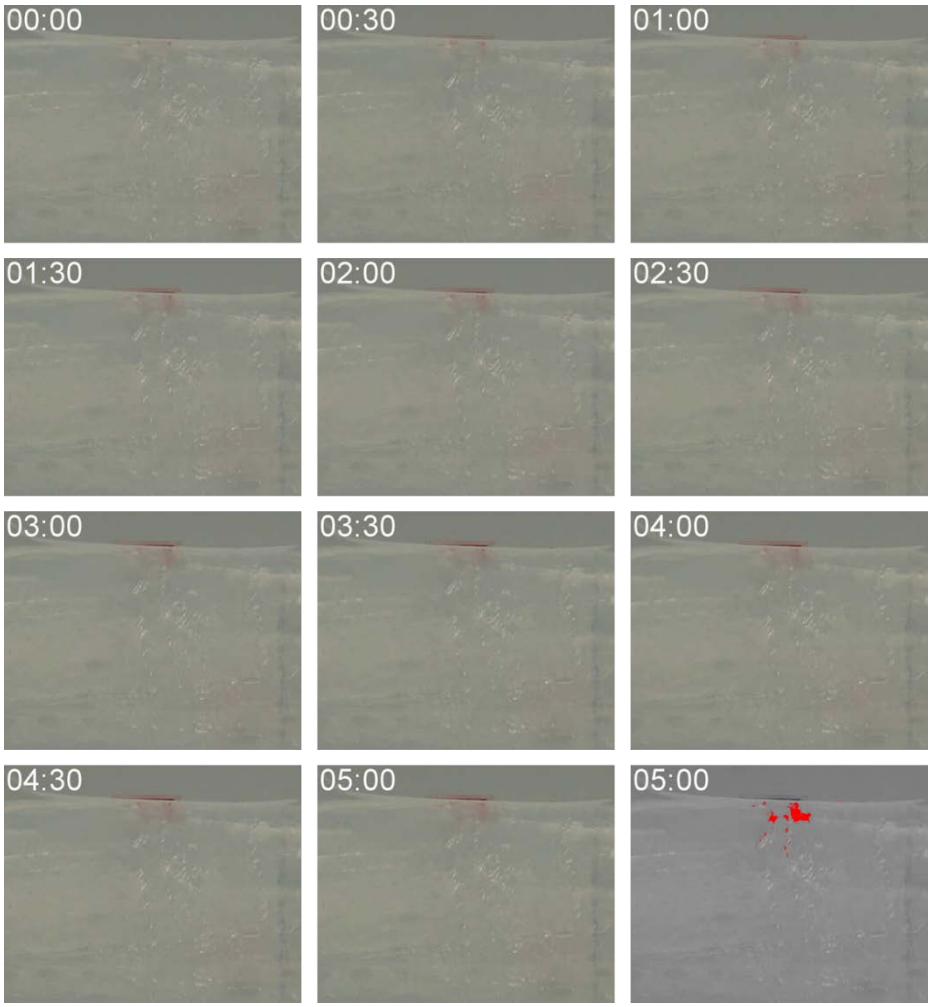

Figure 2.5.3 Time-lapse images in case of typical microneedle drug delivery with fiber sheet at 1% agarose gel

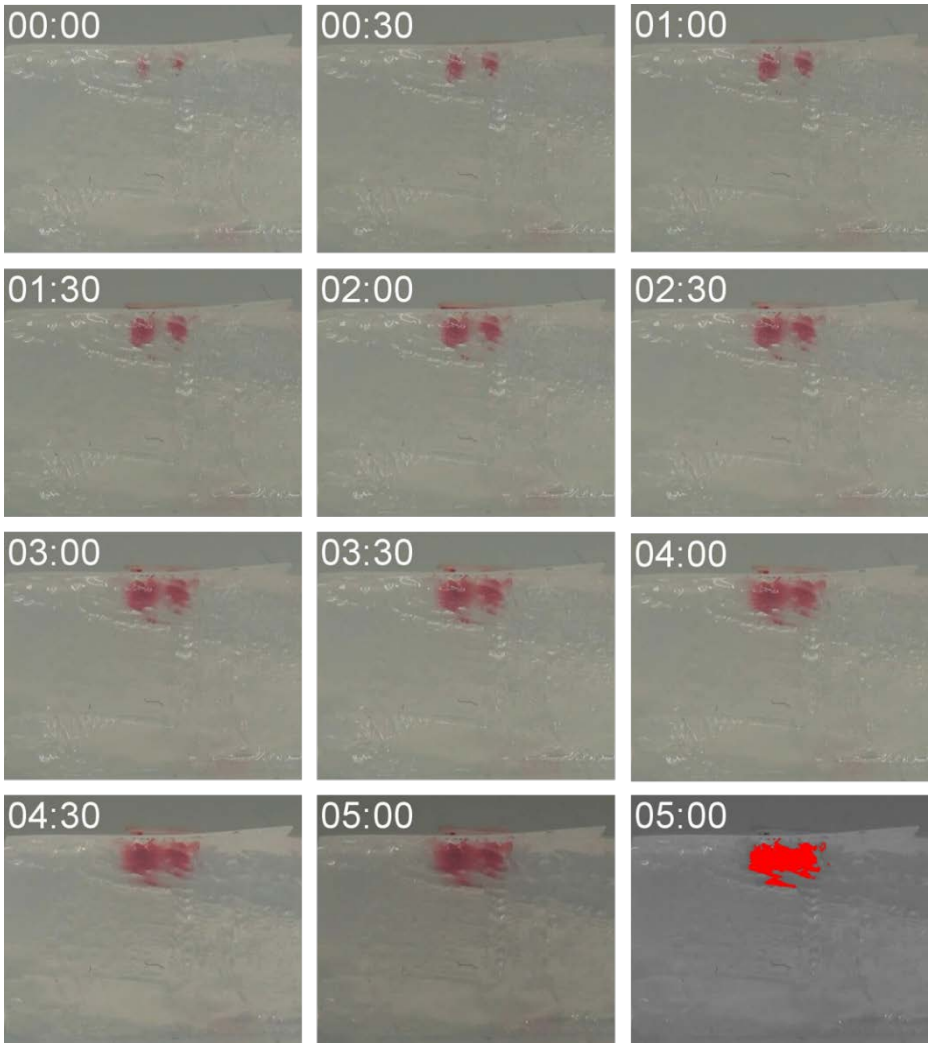

Figure 2.5.4 Time-lapse images in case of trident shape microneedle drug delivery with fiber sheet at 1% agarose gel

Figure 2.5.5 demonstrates the plot of the cross-sectional area dimension of diffusion against times and type of insertion method. The method of inserting a micro needle using a fiber sheet showed a high absorption rate regardless of the kind of the microneedle. The effect of fiber embedding in general micro needle is increased about 2.16 times compared with that of trident type micro needle about 2.92 times. Compared with the microneedle results described above, the fiber-embedded trident shape microneedle shows a remarkably superior drug delivery effect than the normal microneedle by 20 times more.

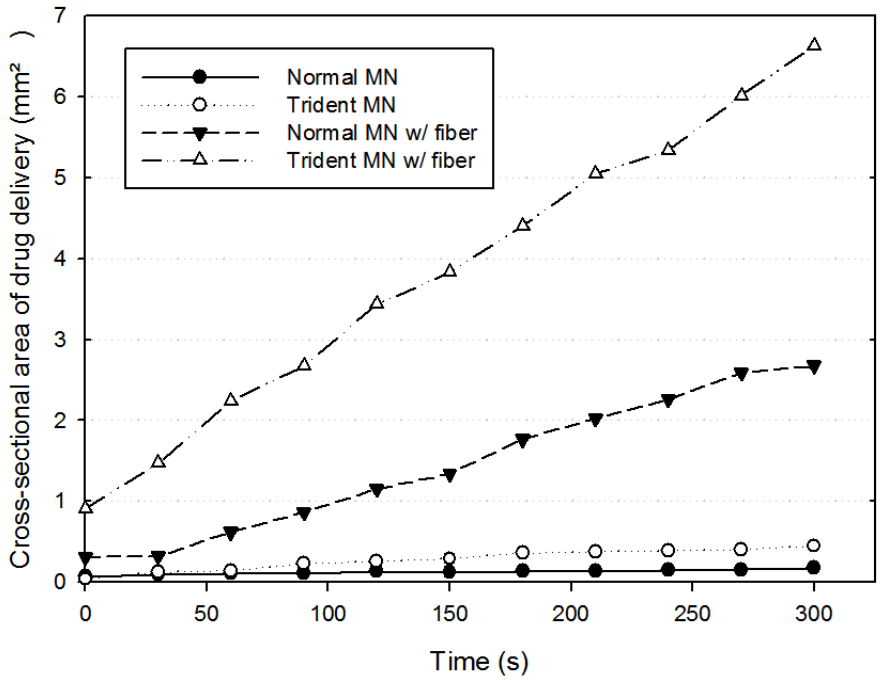

Figure 2.5.5 The plot of the cross-sectional area dimension of diffusion against times and types of insertion method.

Chapter III

Development of microneedle production method using injection molding

3.1. Concept

3.1.1. limitations in microneedle mold making.

The cutting process basically produces a planar or cylindrical cutting surface by causing the tool or the workpiece to linearly or rotationally move relative to each other. (table 3.1.1) The drilling process can be further processed such as boring, tapping, and reaming in the processed holes. The

milling process can be done in a wide variety of ways including plain milling, grooving, sawing, angular milling, face milling, contour milling, gear cutting, helical milling and form milling. [70]

Table 3.1.1 Types of machining and its characteristics

Cutting process	Cutting motion	Feed motion	Tool	Machined surface
turning	rotation of workpiece	linear motion of tool	single-point tool(bite)	cylindrical outer surface
planing	linear motion of workpiece	linear motion of tool	single-point tool(bite)	flat surface
drilling	rotation of tool	linear motion of tool	multi-point tool(drill)	cylindrical inner surface
milling	rotation of tool	linear motion of workpiece	multi-point tool(drill)	flat surface

However, it is difficult to create sharp grooves or cone shape hole with such machining. The dimensions of holes or grooves formed through machining are absolutely dependent on the size of the end diameter of the end mill due to inherent problem. It is not a problem when drilling a cylindrical groove or hole through machining. However, when making a conical or tapered shape hole, the flat bottom is inevitably form as proportional to the diameter of the end mill. Radius of the machined bottom exists even using a

ball-type end mill. In general drilling machining, the machining limit is limited to the diameter of the end mill, which is in the range of more than 100 ㎛. As another working method that can be attempted, electric discharge machining (EDM) processing can be performed by manufacturing a micro needle-like electrode, and using a physical and mechanical action that occurs while discharge. An Electroforming process can also be presented as an alternative. It is a method of making a mold by nickel electroforming on a master made by MEMS process or backside lithography described above. However, these methods are relatively costly and time consuming compared to machining. So, we propose the method of machining a sharp microneedle mold using a conventional machining.

3.1.2. Concept of milling process and mold design

Basically, machining can be used to obtain cylindrical cut surface or a hexahedral cut surface with minimal radius of the end mills at the edges. As a way of forming a sharp edge by machining a straight line, we are inspired by the processing method of the weapon 'bamboo spear', which was easily made in the ancient Orient. This method of cutting a round cylindrical bamboo at an angle of about 20 degrees with a diagonal line to form a sharp tip is remarkably simple. In modern times, the leading edge of the syringe and the straw is similarly diagonally cutting processed to form tip.

Due to the nature of the mold in the form of an intaglio, a method of forming a slit-cut cylindrical hole is conceivable. We proposed a method of machining holes with oblique lines at the corners of metal blocks and bringing them into contact with other block surfaces. Figure 3.1.1 shows the schema for this machining process concept.

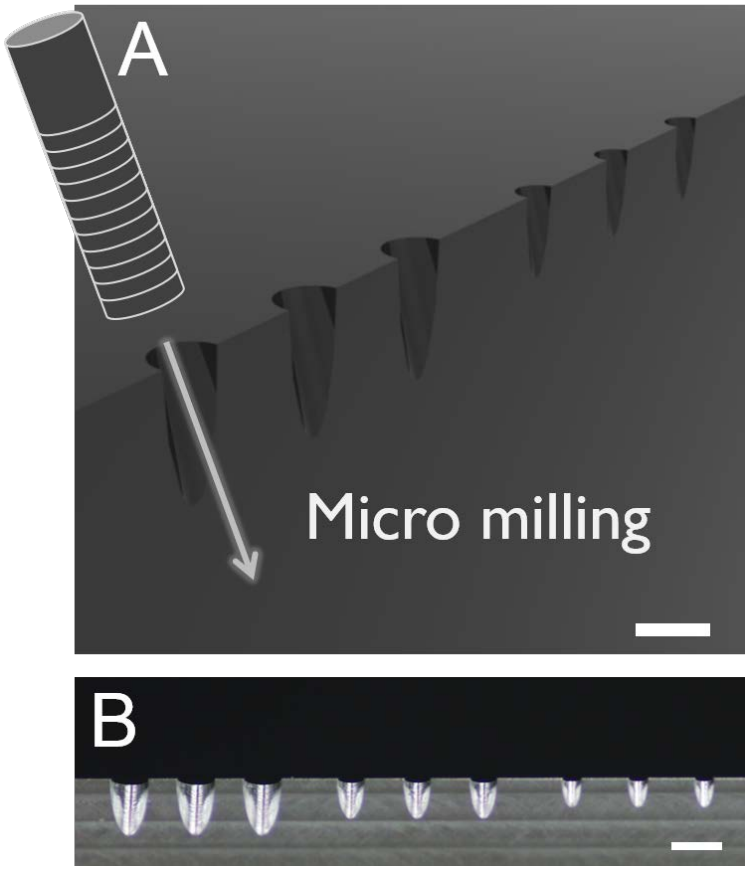

Figure 3.1.1 Concept of milling process (A) corner of the block can be processed diagonally to create a sharp cavity. (B) Image of the actual processed cavity. Scale bar indicates 1mm.

In the proposed mold, the following contents are considered.

1) Using the assembled mold, it is possible to reduce the influence of the gas trap which may occur at the tip end.

2) A thin rib type support is provided on the other side of the main needle, so as to have rigidity against compressive stress and bending stress applied to the microneedle.

3) After insertion of the microneedle, it is intended to flow liquid into the dermis through the groove formed by the ribs. We have devised a microneedle with grooves to aid in subcutaneous administration of the fluid presented in chapter 2.

4) A square boss is designed to create a fluid outlet connected to the groove for continuous fluid supply. It is expected to act as a semi-hollow needle capable of continuous administration.

Overall, a simplified molding experiment is carried out to verify the design and molding possibilities before the entire injection molding process. First, we made an assembled mold using aluminium metal to check the limit of machining. Second, we have tested microstructure molding with thermoplastic resin such as poly lactic acid (PLA). Finally, with the results and experience of these experiments, microneedles are injection molded through quick delivery molding (QDM).

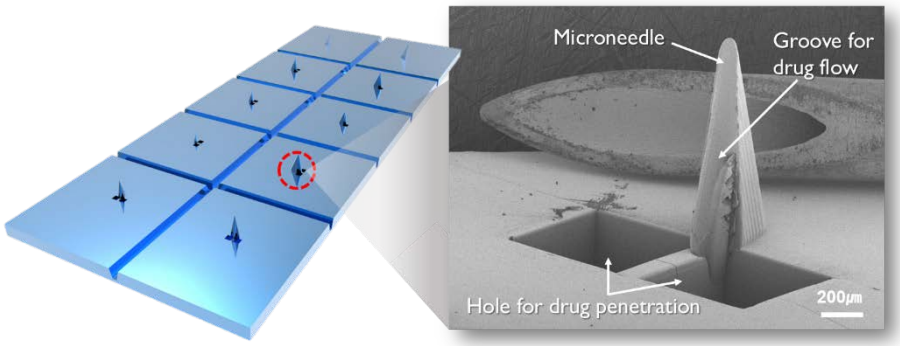

Figure 3.1.2 Schematic and SEM image of MN fabricated by injection molding

3.2. Materials & Method

3.2.1. Simple mold design

Mold cores are made with aluminium alloy for convenience in machining process. We divided the needle design into three major parts. i) There is only a main needle without a rib (type 1), ii) a rib is present at center of mainneedle (type 2), and iii) a rib is asymmetrically biased toward one side of mainneedle (type 3).(Fig. 3.2.1) A cavity is formed using an end mill as oblique line at the corner of block A. The diameter of the half-hole forming the main needle is determined by the diameter of the end mill to be processed. In block B, there is a square boss to create a fluid outlet for fluid injection, and a rib for groove formation to serve as a guide for fluid flow.(Fig. 3.2.2)

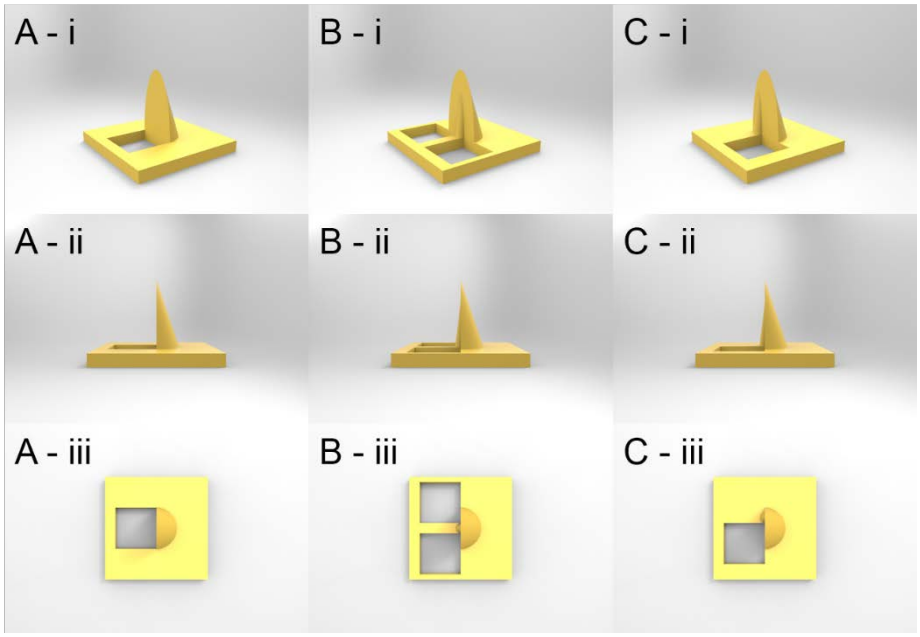

Figure 3.2.1 Schema of microneedle drawn by computer aided design. (A) only a main needle without a rib (type 1), (B) a rib is present at center of mainneedle (type 2), (C) a rib is asymmetrically biased toward one side of mainneedle (type 3)

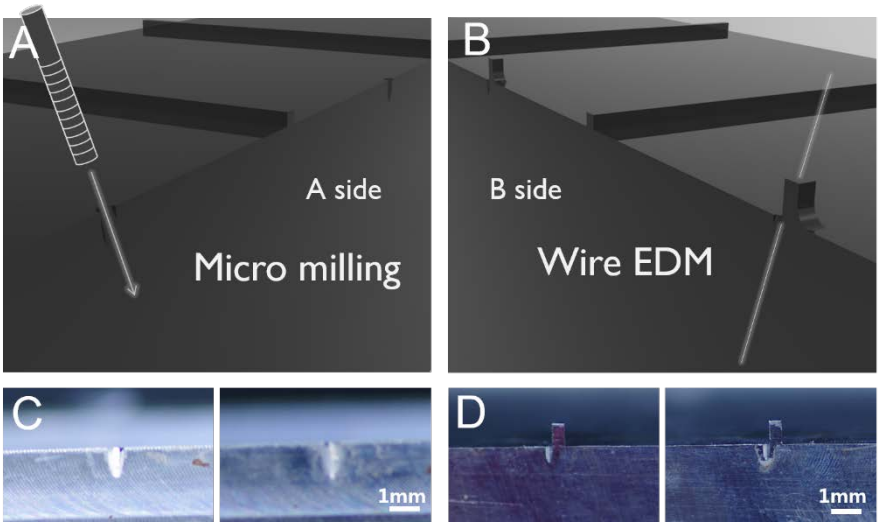

Figure 3.2.2 Machining process and mold image (A) a cavity is formed using an end mill as oblique line at the corner of block A, (B) in block B, there is a square boss to create a fluid outlet for fluid injection (C,D) actual magnified image of mold.

As the size of the needle is reduced, the limitation of the micro-milling process has limited the size and position of the square boss to make the fluid outlet. Our machining capability is that the minimum r level to make the rib part is 150 ㎛ level, so that the rib is biased to one side and the fluid outlet is designed to be in close contact with the groove surface.

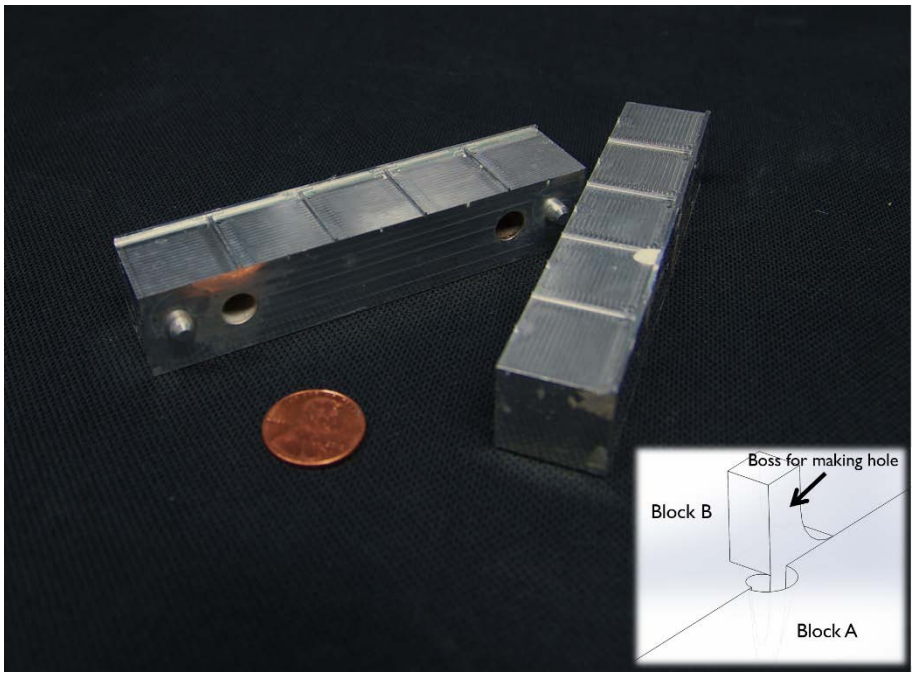

Figure 3.2.3 Image of in-house aluminium alloy mold core for micro-needle molding.

Photographs given in figure 3.2.3 show the in-house aluminium alloy mold core for micro-needle molding. Magnified photographs in A of figure 3.2.3 show an half-hole for molding the main needle part of block A and a square boss for creating fluid outlet and half-hole for creating the rib of block B, respectively.

Both blocks are fixed with square bosses and fastened with screws. The dimension of the main needle is 300 ㎛ in radius and 1000 ㎛ in height. The angle of microneedle tip determined by the machining angle of the drilling is 16.7 degrees. The radius of the rib is 150 ㎛ and the height is 800 ㎛, supporting the main needle. There are five types of designs, types 1, 2 and 3 according to the position and the presence of the ribs described above, and different lengths (1000 ㎛, 1200 ㎛, 1400 ㎛) of the type 3. A custom stainless steel jig (SUS 304) is designed and machined provide uniform pressure and directional heating during molding with thermoplastic resin. (Fig.3.2.4)

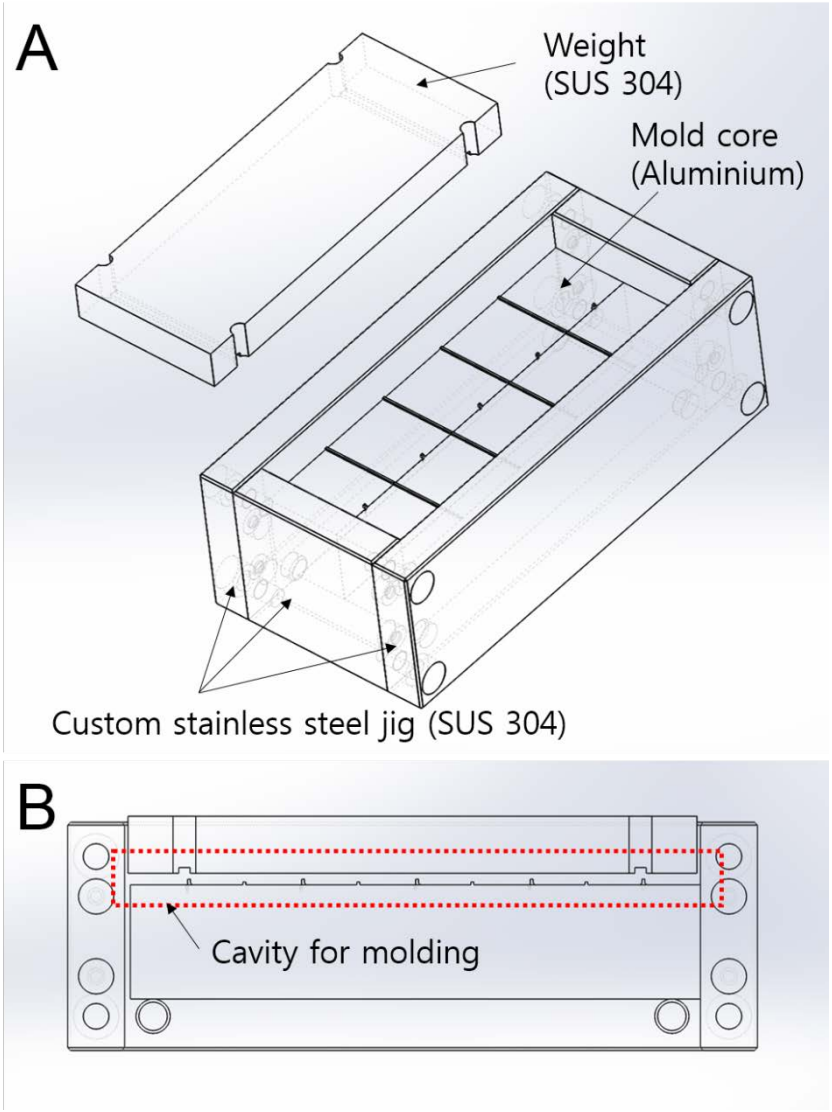

Figure 3.2.4 Assembled molds and jigs for simple molding (A) The weights and jig are made by machining the SUS 304 alloy. Material of mold core is aluminum alloy. (B) All parts are assembled, the resin can be put into the cavity and molded.

3.2.2 Material and molding process

Poly (lactic acid) (PLA) thermoplastic polymer is a biodegradable polymer produced in renewable resources such as corn, potatoes and sugarcane. [71] It is a material that has strong physical and mechanical properties and is completely biodegradable after use. [72] PLA is used as the molding resin, and the filament of the 3D printer is cut into a fillet having a length of 5 mm. PLA filaments for 3D printers are produced with a melting point of about 200℃. The mold core designed as described above for molding is joined with a square jig fastened with a screw. Fill the fillet with 6g and cover with the weight to form the cavity. Heat source (digital hot plate, PMC, USA) was placed on the bottom. When the setting value of the hot plate is reached, the molding is carried out for 20 minutes while maintaining the temperature. After cooling to room temperature, mold release to complete microneedle production.

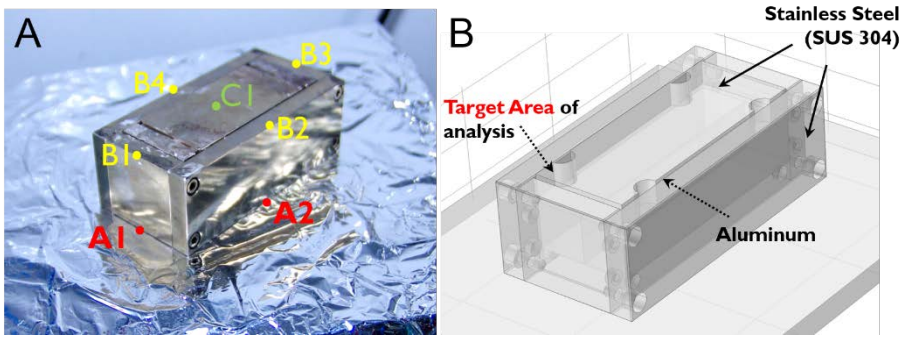

Figure 3.2.5 Photograph of assembled mold and 3D modelling image

During the molding process, it is impossible to directly measure the temperature inside the mold. To estimate the temperature inside the mold during the molding process, the steady state temperature at each point shown in figure 3.2.5 is measured. This temperature value measured with a thermocouple is applied to the 3D model. The temperature of the cavity is predicted by the boundary element method (BEM) using the measured temperature value and graphically analyzed image in figure 3.2.6.

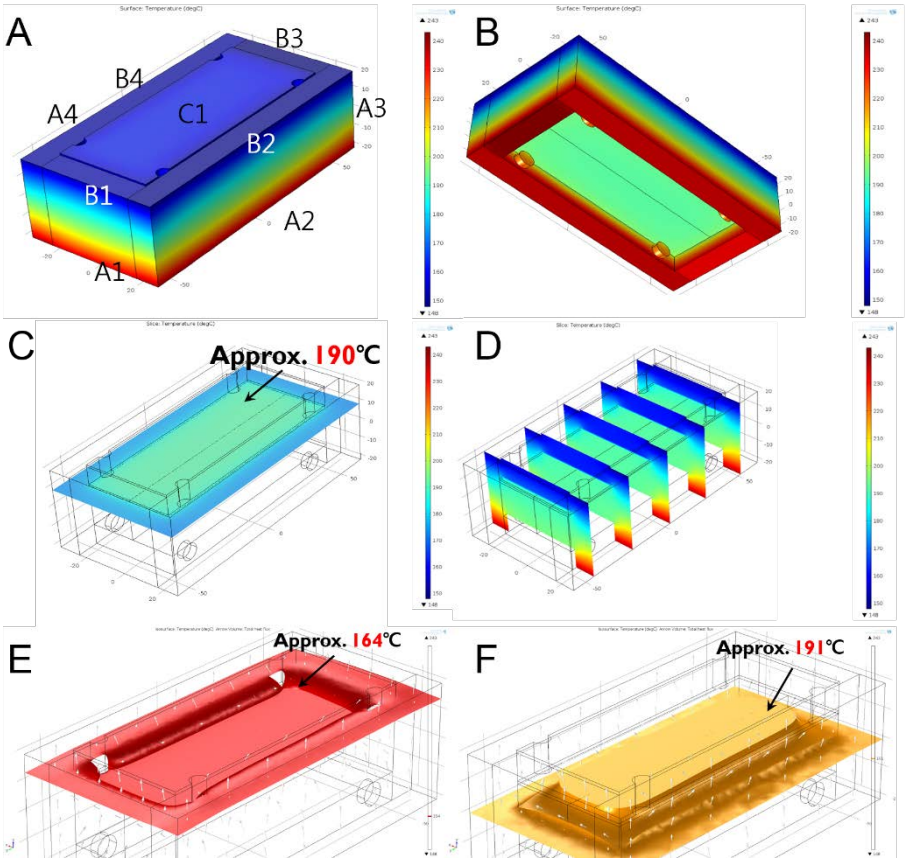

Figure 3.2.6 Estimation of steady state temperature inside mold.

Table 3.2.1 Measurement of steady state temperature at mold

	A1	A2	A3	A4	B1	B2	B3	B4	C1
Temperature(℃)	238	234	243	238	150	153	153	148	142

When the set value of the hot plate is 250℃, according to the analysis result, the maximum temperature of the cavity is approximately 191℃. In addition, a temperature gradient appears in the cavity and the minimum temperature is about 164 degrees. The most important position, the needle shape part, is maintained at about 190℃, so that the thermoplastic resin is melted with maintain the fluidity, and the molding can be performed to a fine structure.

Table 3.2.2 integration results according to SV of hot plate and pressurization

SV of hot plate(℃)	pressurization	Result
< 240	Weights	The upper part of cavity does not melt and the structure is not formed.
240~260		Fine structure molding.
> 260		Excessively melted and attached to the surface polished surface. Carbonized above 280℃
240~260	No weights	Holes and some microstructures unformed.

The results of the molding according to various temperature range and the presence or absence of weight are shown in Table 3.2.2. At setting temperatures lower than 240℃, the temperature of the mold core is low and the thermoplastic resin does not melted enough to have sufficient fluidity, resulting in the microstructure being unformed. Especially, due to the temperature gradation, it can observed that the resin above the cavity is not completely melted. At a set temperature of 260℃ or higher, the resin melts well and is advantageous for molding. However, it is very difficult to release because it is closely attached to the polished surface without clearance. Particularly, it can be observed that the carbonization proceeds partly, due to the high temperature. When molding is carried out without weight, it is difficult to form a fluid-outlet by a square boss, and the microneedle structure is not well formed because of weak inflow of resin.

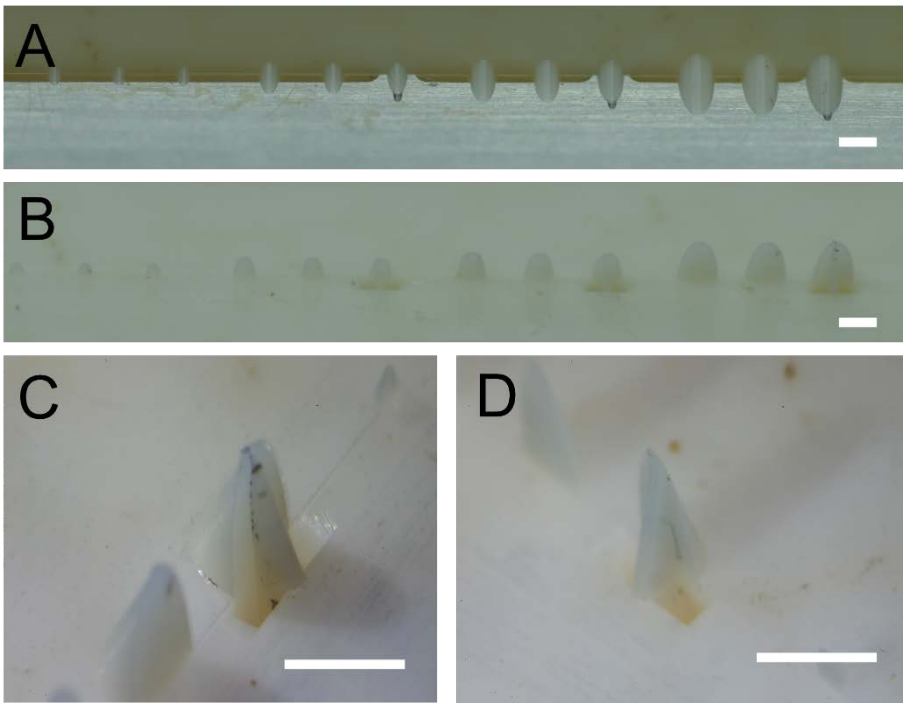

Figure 3.2.7 Photograph of microneedle with molding. Polylactic acid is used as the material, and the molten resin is well filled in the fine cavity. Scale bar indicates 1 mm.

3.3. Compressive stress and insertion testing using multi-functional adhesion/scratch test system

3.3.1. Prediction of microneedle deformation for compressive stress using finite elements method

To predict the deformation according to the load of the microneedles molded through the above-described concept, we used a commercial finite element method (FEM) solver (COMSOL). Figure 3.3.1 shows the schematic diagram of the microneedles and Table 3.3.1 lists the dimensions. This is the type 1, 2 and 3 of the previously processed mold. A boundary is set assuming injection of 300 ㎛ length from the tip end of the needle, and the vertical force is applied at this portion to confirm needle deformation. The material of the analytical microneedles was data of the polymer in the COMSOL library.

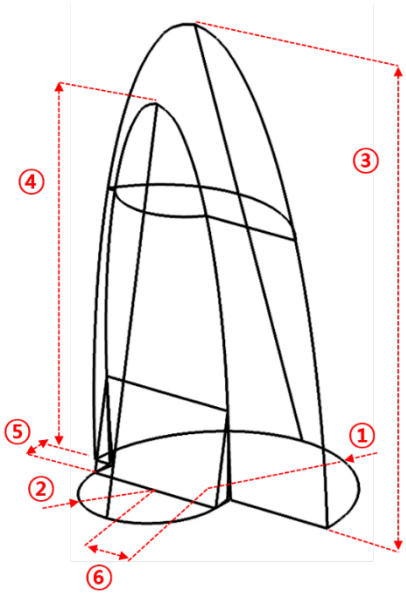

Figure 3.3.1 The schematic diagram of the microneedles modeling

Table 3.3.1 A list of dimensions corresponding to the numbers in figure 3.3.1

Dimension no.	Type 1 (μm)	Type 2 (μm)	Type 3 (μm)
1	300	300	300
2	-	150	150
3	1000	1000	1000
4	-	800	800
5	-	50	50
6	-	-	100

Figure 3.3.2 and 3.3.3 show the distribution of deformation and Von mises stress of the structure in the performed analysis as a graphical analysis image. The displacement of microneedle structure is plotted in contour at a force of about 2N. When the same force is given, the amount of deformation is less in order of type 2 microneedle with rib supporter in the center, type 3 microneedle with rib supporter in asymmetric position, and type 1 microneedle without rib supporter. At this time, the maximum deformation amounts are represented by 51.1 ㎛, 31.5 ㎛, and 36.9 ㎛, respectively. The displacement of the microneedle due to the applied force at various amounts is shown in figure 3.3.4. Compared to type 1 microneedles, the deformation of type 2 and 3 microneedles are 61.6% and 72.3%, respectively. The difference in deformation according to the position of the rib is 17.5%. This indicates that adding a rib supporter gives durable resistant to compressive stress.

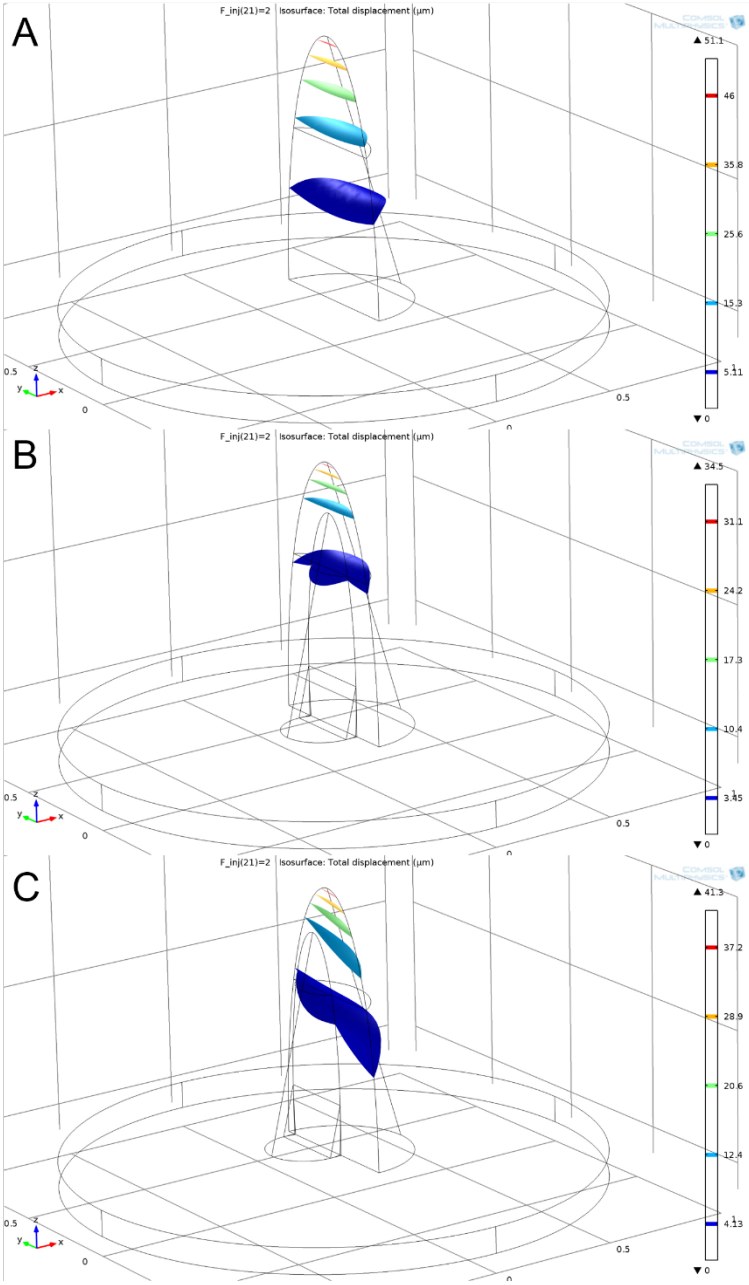

Figure 3.3.2 The displacement of each microneedle structure is plotted in contour at a force of about 2N.

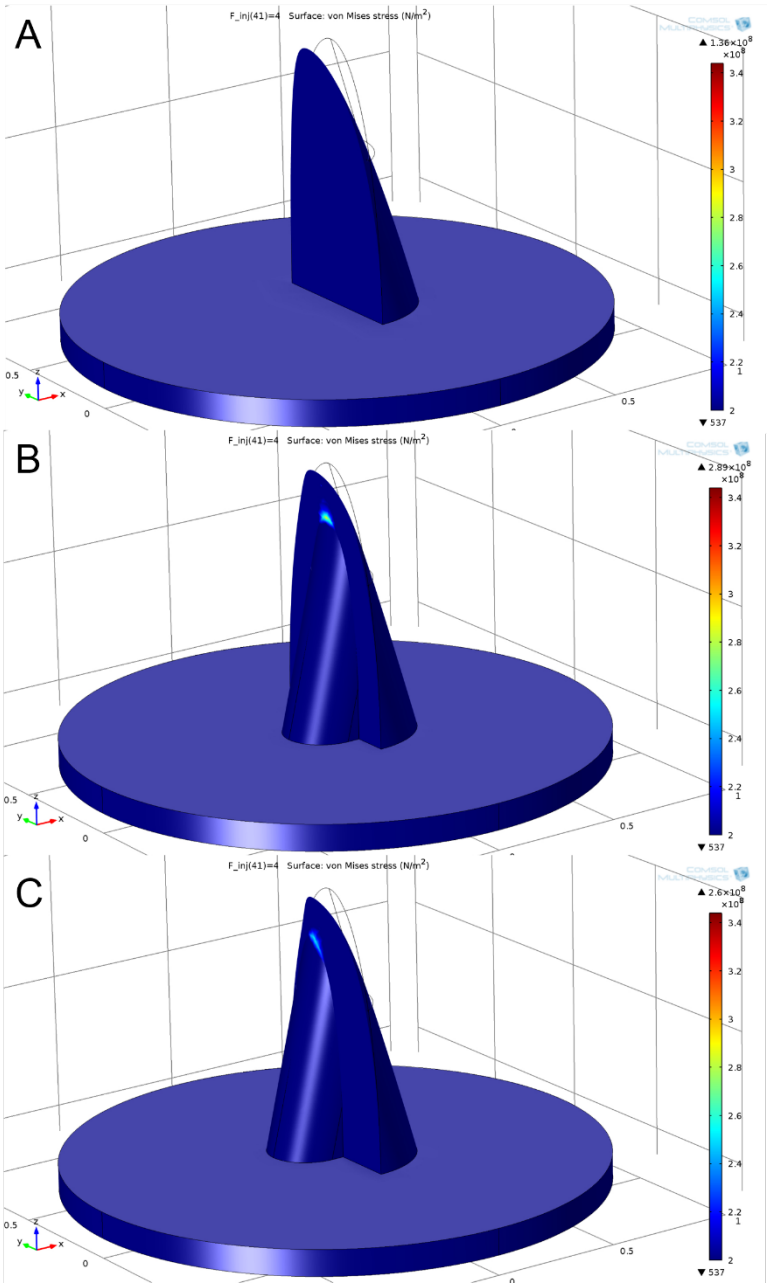

Figure 3.3.3 A graphical analysis image of von mises stress distribution at a force of about 2N.

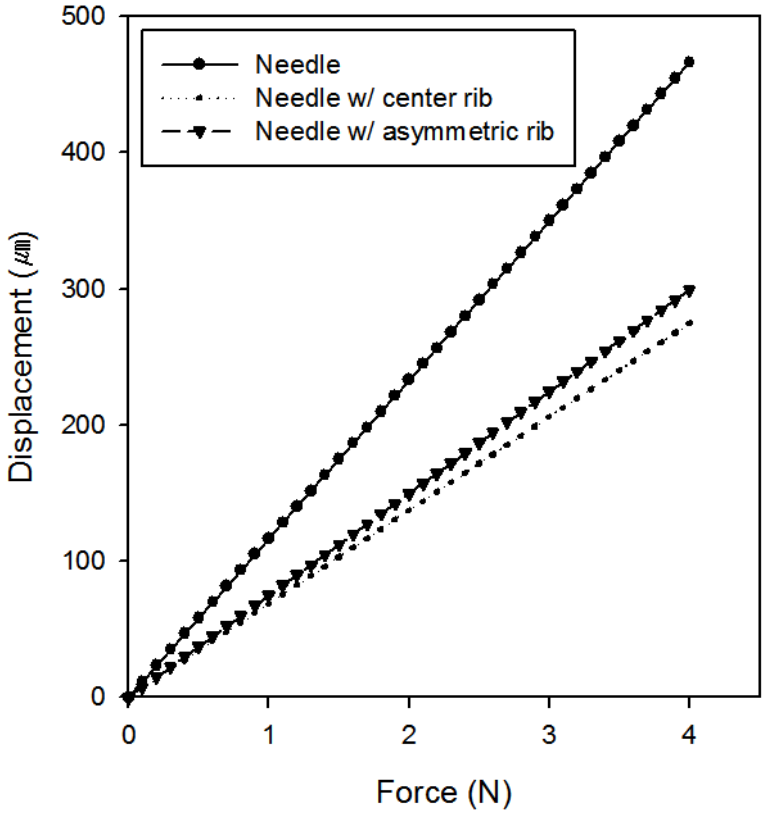

Figure 3.3.4 The displacement of the microneedle due to the applied force at various amounts.

3.3.2. Compressive stress test according to microneedle design

Microneedles are formed from PLA material as described previously in the molding process part. First, the each type of microneedle is subjected to a failure test according to compressive stress. The experimental method is the same as that of chapter 2 using the multi-functional adhesion/scratch test system (Neoplus INC, Seoul, Korea). The dimensions of the needle are the same as those given in the previous schematic diagram of the microneedles and tale 3.3.1.

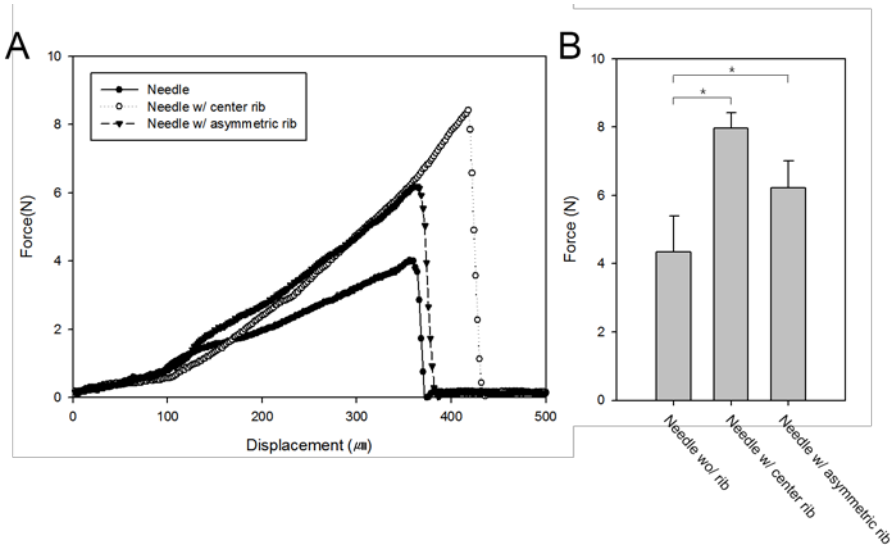

Figure 3.3.5 Compressive stress test according to needle shape

The figure 3.3.5 shows the compressive stresses received by each types of microneedle and the deformed length distribution until fractured. The experiment proceeded with four samples each. The type 1 microneedle without rib supporter showed maximum compressive stress of 4.34N (SD 1.05) and showed deformity of 360 ㎛, but it was fractured. The type 2 microneedle with rib supporter in the center had a maximum compression stress of 7.96N (SD 0.44), deformed by 420 ㎛ and fractured. The type 3 microneedle with rib supporter in asymmetric position shows a maximum compressive stress of 6.21N (SD 0.79) and a maximum strain of 380 ㎛.

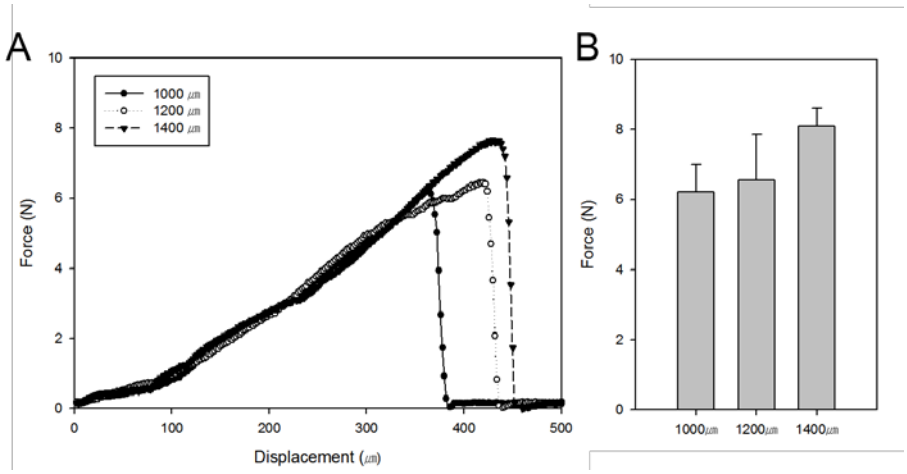

Figure 3.3.6 Compressive stress test according to needle length

The compression resistance along the length of the needle is also tested. The compressive stress resistance is tested using various height of the type 3 microneedles. The height of each needle is 1000 ㎛, 1200 ㎛, and 1400 ㎛, and the length of the rib supporter is 80% of the needle length. The experiment proceeded with four samples each. Figure 3.3.6 shows the deformation profiles of each needle when applying compressive stress. A microneedle of 1000 ㎛ height shows a maximum compressive stress of 6.21N (SD 0.79) and a maximum deformation amount of 380 ㎛. Microneedles of 1200 ㎛ and 1400 ㎛ show the maximum compressive stress of 6.56N (SD 1.29) and 8.09N (SD 0.52), respectively, and the

maximum deformation of 430μm and 450μm. Although the absolute strain amount seems to be more deformed in long microneedle, the relative strain amount of needle length shows 38%, 35.8% and 32.1% strain rate, respectively. As a result, the longer the length, the lower the maximum strain and can be sustained at relatively higher compressive stresses.

3.4. Microneedle production using injection molding process

3.4.1. Mold design and injection molding conditions

Through the simplified molding shown above, we can confirm i) the mold making performance of the micro needle using machining and ii) the possibility of molding using thermoplastic resin. Based on these results, we are try to improve the productivity by real injection molding using Quick delivery molding. Quick delivery molding (QDM) is a system that can quickly create starting molds and prototypes for new product development. First, the mold core is machined on the basis of the CAD drawing and mounted on the standardized mold base. Through the injection molding, we can get the prototype and explore the problems that may occur before proceeding to the mass production mold. All this process is completed in five days, and although it depends on the material of the core, the mold durability is limited to 5000 shots or less.

In the production process using QDM, we can confirm the follows.

1. Is the cavity shape of the mold finely machined into a microstructure shape?

2. Is the molten resin filled into a fine cavity and molded? Do the burrs exist where the core pieces are in contact with each other? Did thin passages between assembled core pieces prevent gas traps?

3. Is the position and size of the eject pin applied well so that it does not stick when the product is ejected?

4. Is it possible for the microneedle produced by injection molding process to penetrate the skin and to administer the fluid as intended?

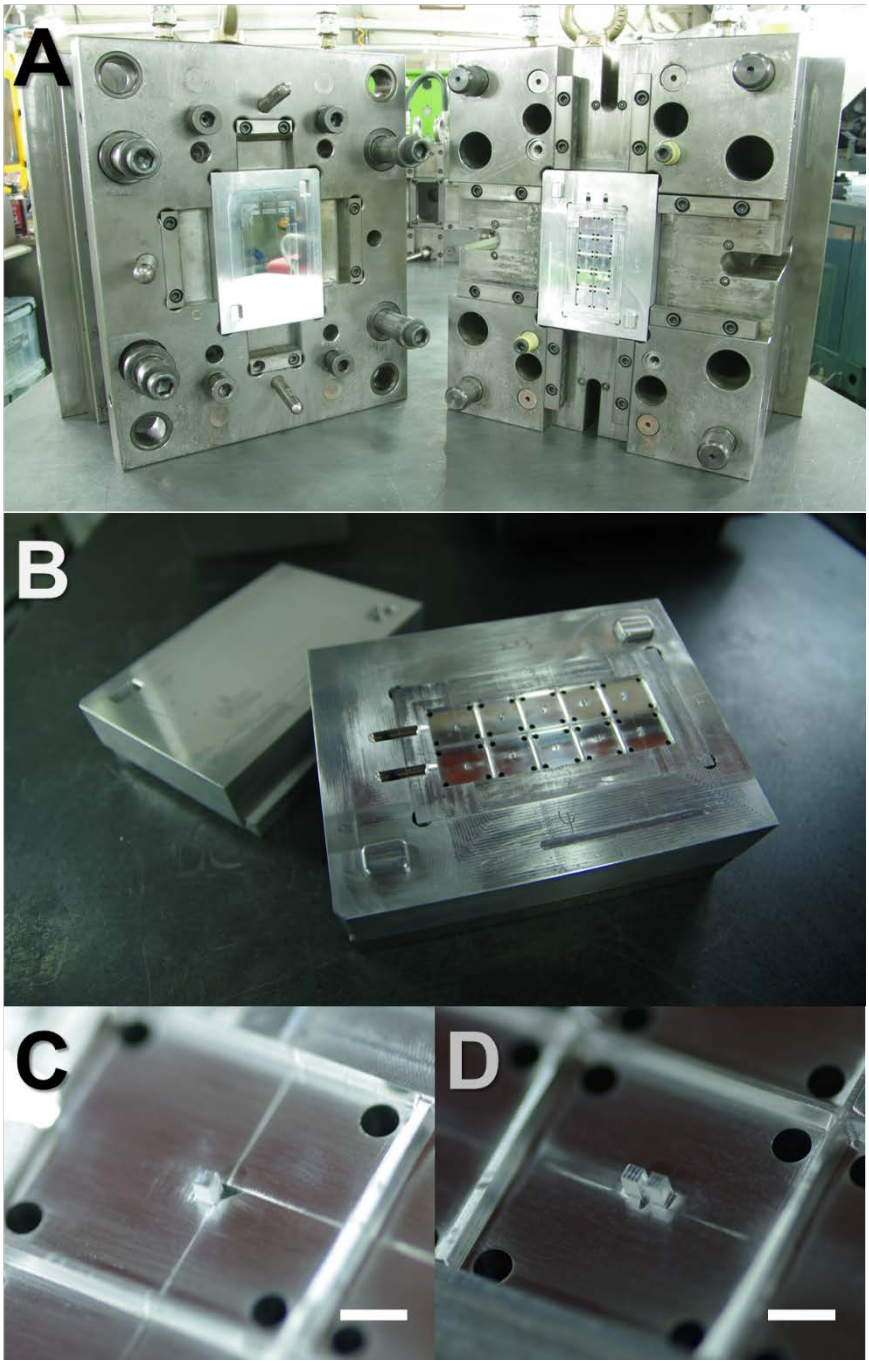

Figure 3.4.1 Photograph of mold core and base.

The production and injection of QDM are conducted in collaboration with suppliers (R & D Factory, Suwon, Korea). The mold is processed using an aluminium alloy (AL 7075, duralumin). Duralumin is an aluminium alloy invented by German A. Wilm of 1909, containing 3-5% copper, 0.2-0.75% magnesium and 0.4-1% manganese. It is low in corrosion resistance, but has high hardness and excellent mechanical properties. [73] Each microneedle cavity is machined into two or three parts according to the proposed machining concept. Mold core with ten microneedle cavities consists of 5 blocks, and is inserted into the mold base in assembled state and used for molding (Fig.3.4.1). The cavity of microneedle is designed with four types, and explored the problems that may occur in the injection process. The description of each design is as follows.

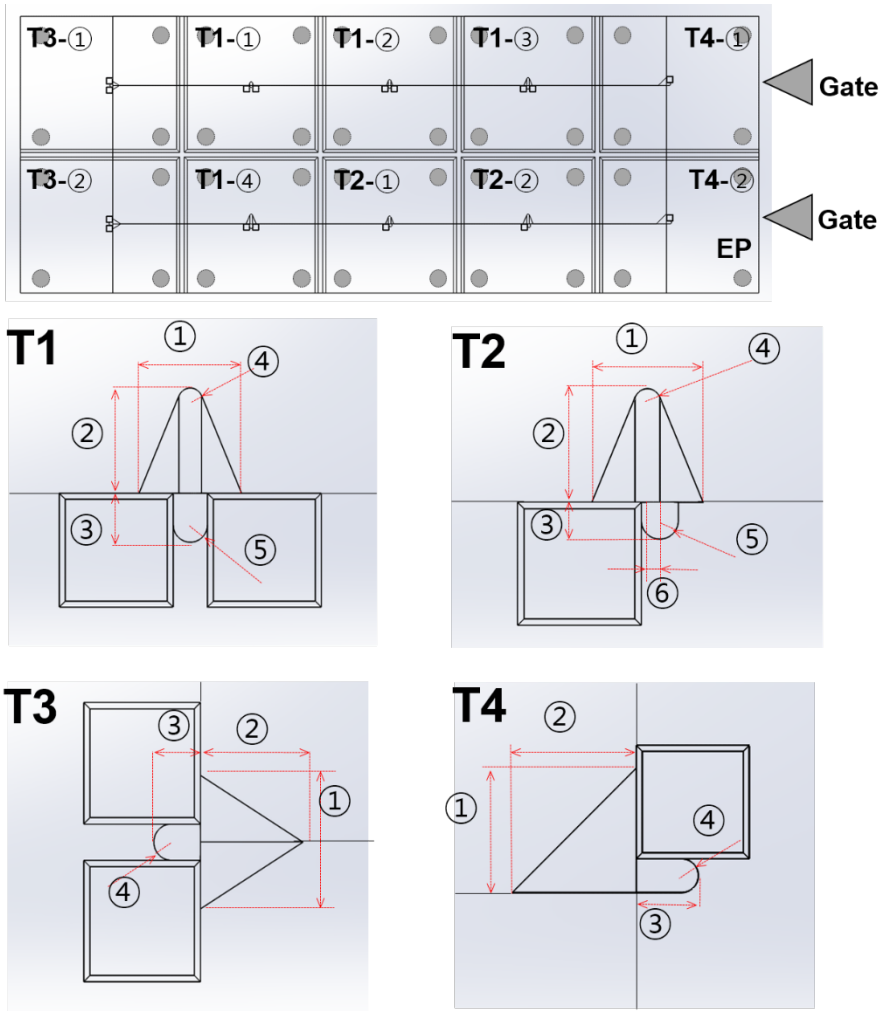

Figure 3.4.2 Drawing of mold core. A total of five blocks are assembled to complete the core, which is designed in 10 different designs. EP indicates eject pin position.

Table 3.4.1 A list of dimensions corresponding to the numbers in figure 3.4.1

	T1-①	T1-②	T1-③	T1-④
①	500	700	900	1100
②	490	710	920	1130
③	230	330	430	520
④	110	110	110	110
⑤	150	150	150	150
Height	1510	1960	2440	2920

	T2-①	T2-②
①	900	1100
②	920	1130
③	430	520
④	110	110
⑤	150	150
⑥	100	100
Height	2440	2920

	T3-①	T3-②
①	900	1100
②	720	880
③	300	400
④	150	150
Height	2250	2750

	T4-①	T4-②
①	900	1100
②	900	1100
③	450	550
④	150	150
Height	2250	2750

Type 1 microneedle has a rib supporter with a center portion and two fluidic outlets on either side of the groove for fluid flow. The tip end of the main needle (indicated by ④ in Fig.3.4.1.T1) inevitably has a minimum r due to the ball endmill radius, which is 110 ㎛ in size. Type 2 microneedle has an asymmetric rib support and a groove with a fluidic outlet contacting more area. Type 3 microneedle consists of two assembled blocks with main needle. This allows the cavity to be formed without machining radius which is inevitable for machining. Type 4 microneedle also eliminates the rounded shape of the needle tip using the assembled mold and consists of a mold with one rib supporter and fluidic outlet. Most structures, including the square boss, have a gradient of at least 1.5 degrees for ease of ejection, except for the side of the microneedle present at the junction of the block. The gate is determined as a side gate and shown in figure.3.4.1 with the position of the eject pin. The dimensions of all these structures can be found in table.3.4.1.

We carry out a parametric study to find materials suitable for injection molding with the various resin of Acrylonitrile-Butadiene-Styrene (ABS), Polycarbonate (PC), Polycarbonate (PMMA), Polypropylene (PP), Polystyrene (PS). Table 3.4.2 shows the properties of resin such as melt flow index and mechanical properties. We select PC (1301EP, LG chemical) and GPPS (25SPi, LG chemical) with high melt flow index (30 g/10min or more) for filling the molten resin to fine cavities. They has also good mechanical properties. Comparing the microneedle shape formed by PC and GPPS, the fine structure at the tip is not formed due to uncharging.(Fig. 3.4.3)

Table 3.4.2 List of candidate resins in the injection process

Manufacturer	Product name	Material	Melt flow index (g/10min)	Tensile strength (MPa)	Flexural strength (MPa)	Flexural modulus (MPa)
LG Chem	TR558A	ABS	25	50	80	2420
Cheil Industries	SC-1220R	PC	22	63	90	2260
LG Chem	1301EP	PC	30	60	96	2340
LG Chem	IF-850	PMMA	12.4	62	125	3300
Altuglas	V150	PMMA	14.5	69	98	3040
LG Chem	TE5008B	PP	30	26	-	1600
LG Chem	25SPi	GPPS	38	50	94	3260

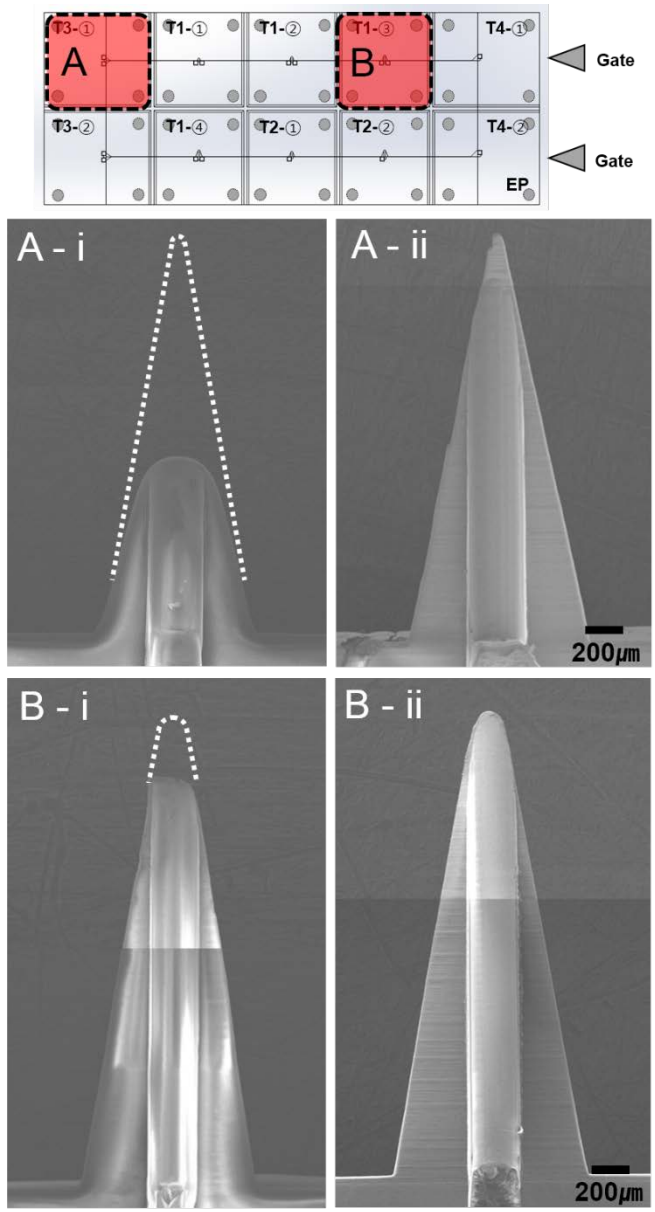

Figure 3.4.3 Comparison of injection results with PC (i) and GPPS (ii). Depending on the position of the cavity in the mold core (A,B) and resin materials (i,ii), the difference in molding can be observed.

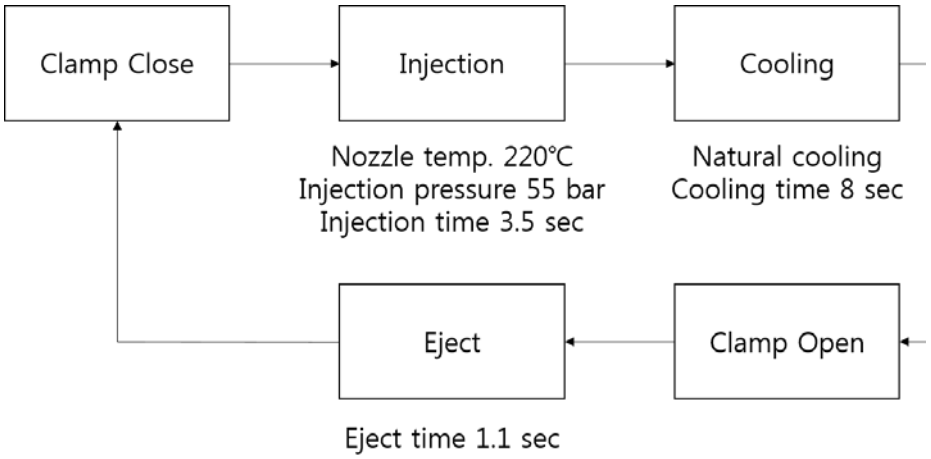

Figure 3.4.4 Flow chart of the injection molding process including important parameters at each step.

Finally, the thermoplastic resin used is a general purpose polystyrene (25SPI, LG chemical, Korea) and the shrinkage rate is assumed to be 5/1000. When combining the blocks to create the core, intentional margin of 5/1000 is applied between each assembled core block to minimize gas trap and burr or flash. Figure.3.4.3 shows the overall injection process and parameters. The nozzle temperature is 220℃, and the filling time of the mold cavity is 3.5 seconds. The injection product is naturally cooled at room temperature for 8 seconds. The clamping force is 110 tons and the maximum injection pressure is 55 bar.

3.4.2. Product inspection and compressive stress test

Imaging with scanning electron microscope (SEM) is performed to check the appearance of the microneedles made using injection molding. Through this process, it is possible to confirm whether the molten resin is well filled in the cavity and the fine end is well formed. Also, it is possible to confirm whether gas traps that may occur in the concave portion of the tip end and whether or not a burr or flash is generated at the coupling portion of the assembled core.

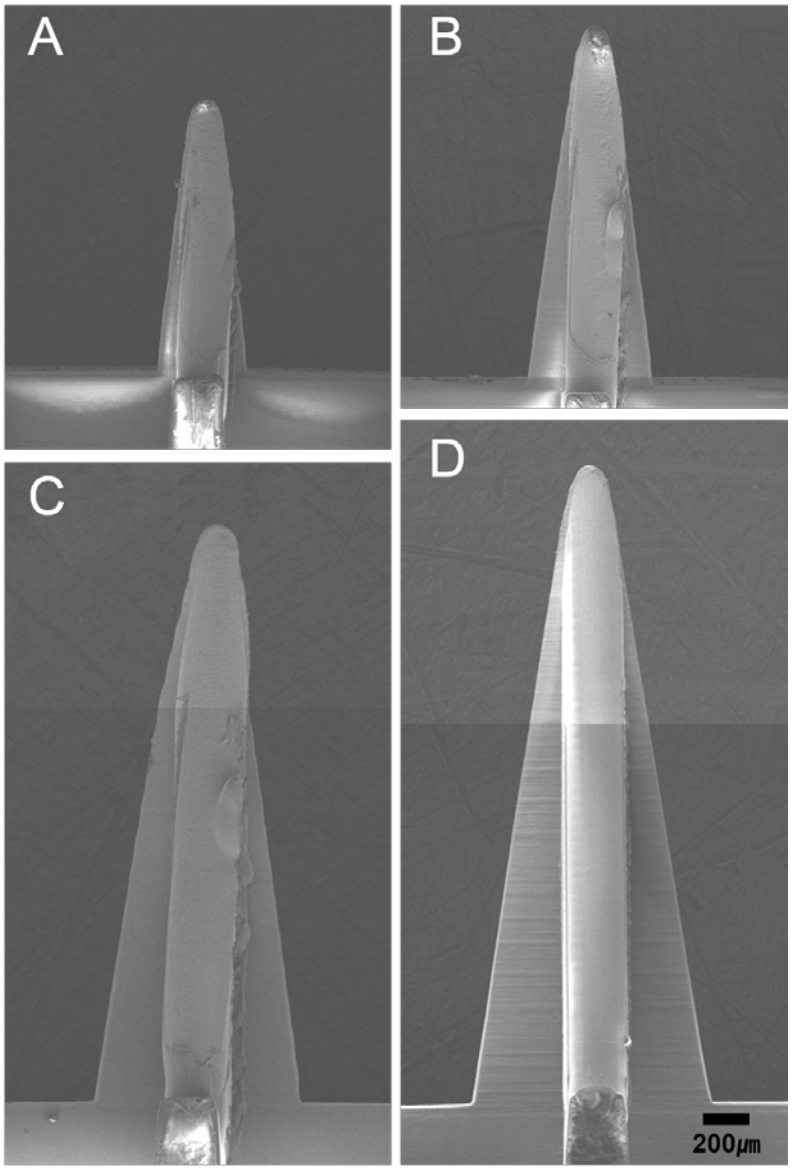

Figure 3.4.5 Microneedle (T1-①, T1-②, T1-③, T1-④) inspection using SEM. They have a tip radius of 54 ㎛(T1-①), 54 ㎛(T1-②), 74 ㎛(T1-③), and 63 ㎛(T1-④), respectively.

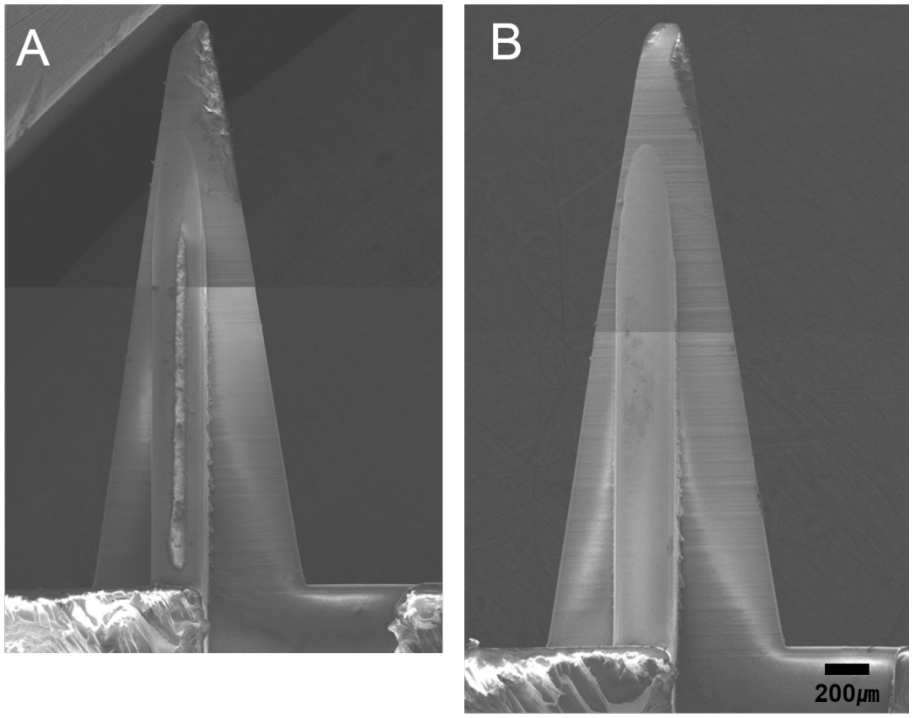

Figure 3.4.6 Microneedle (T2-①, T2-②) inspection using SEM. They have a tip radius of 63 ㎛(T2-①) and 71 ㎛(T2-②), respectively.

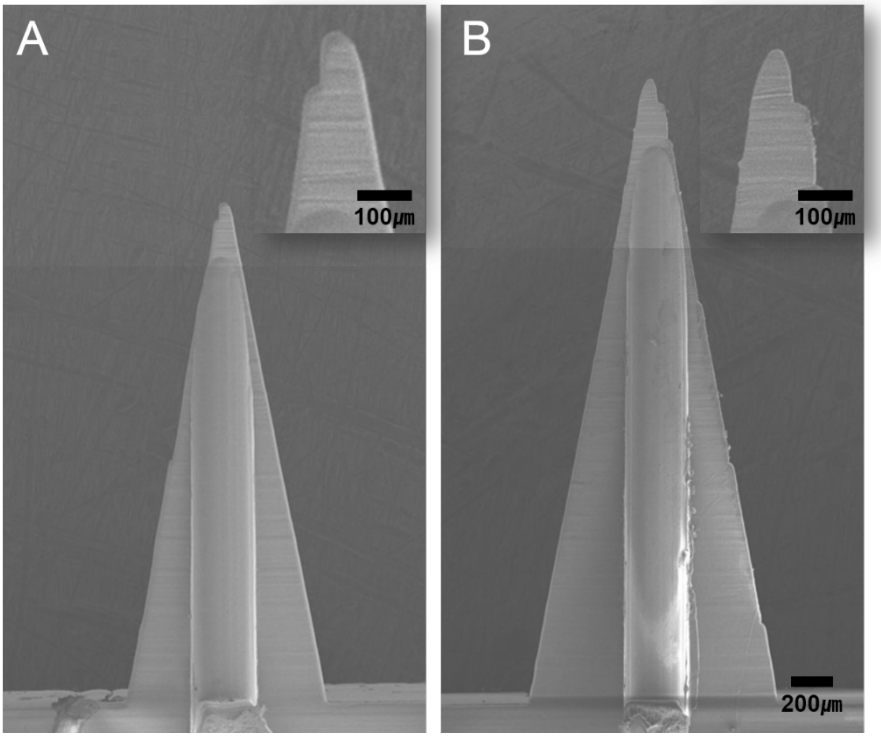

Figure 3.4.7 Microneedle (T3-①, T3-②) inspection using SEM. They have a tip radius of 31 ㎛(T3-①) and 18 ㎛(T3-②), respectively.

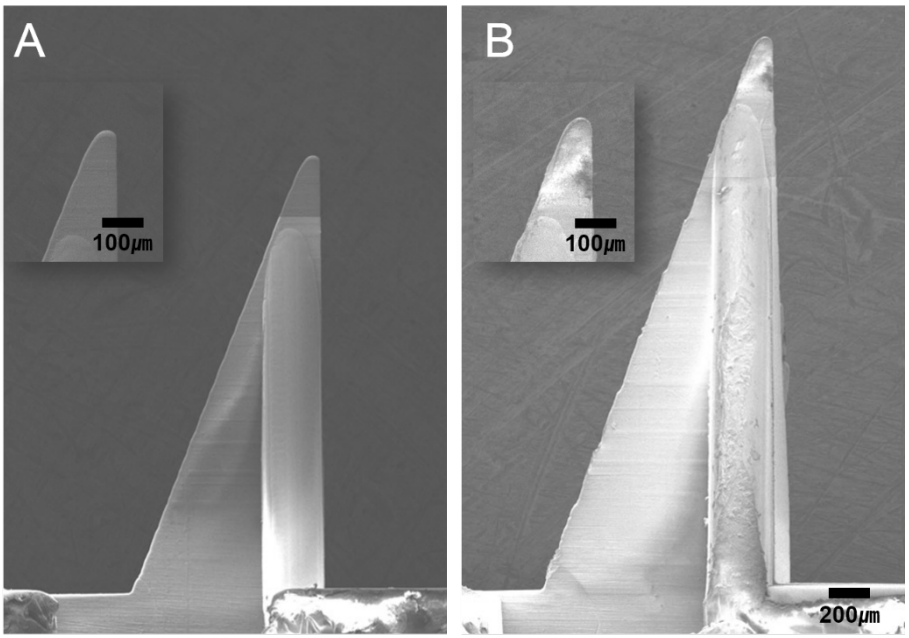

Figure 3.4.8 Microneedle (T4-①, T4-②) inspection using SEM. They have a tip radius of 33 ㎛(T4-①) and 36 ㎛(T4-②), respectively.

Figure.3.4.5 to 3.4.8 shows the image of each needle appearance taken with SEM. Please refer to table.3.4.1 and figure.3.4.2 given above for each sample name, shape and dimensions. As can be seen in figures, burr or flash does not occur in all shapes and it can be seen that tip radius of microneedle differs according to core production method. Tip of type 1 and 2 microneedles are well formed as the shape of cavity decided by the radius of

the ball endmill used in the machining. It is observed that the tip radius is 54 ~ 74 ㎛ due to no gas trap, and the tip angle is about 18 degrees. The cavity of type 3 and 4 microneedle are made by assembling block of chamfer, so tip radius can be determined by filling of molten resin and gas trap. The type 3 microneedles, which are a cavity shape with two chamfered faces, show the tip radius of 18 ㎛ (T3-①) and 31 ㎛ (T3-②). Type 4 microneedles, a cavity shape made with one block of chamfer, show a tip radius of 33 ㎛ (T4-①) and 36 ㎛ (T4-②). The tip angles are 20 degrees (type 3) and 21 degrees (type 4).

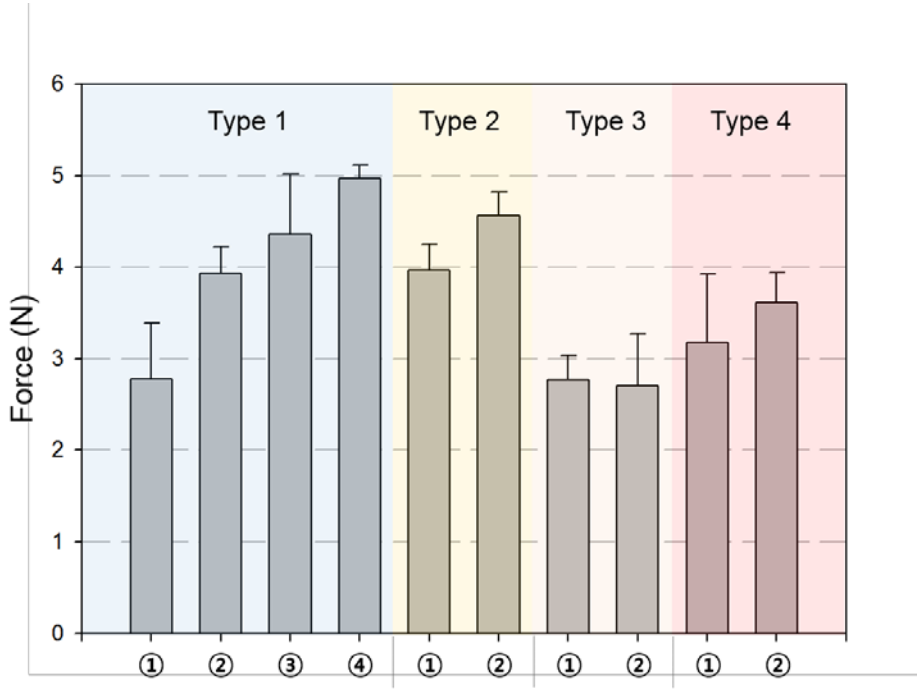

Figure 3.4.9 The force to break for each type of microneedle

The failure test by compressive stress and insertion test is carried out using the multi-functional adhesion/scratch test system described chapter 2. All experiments are repeated 4 times. The force to break for each type of needle is shown in figure. 3.4.9. Type 1 and 2 microneedles show higher compressive stress resistance than type 3 and 4 microneedles due to the shape of the tip end. In particular, type 3 shows that the tip of the needle is easily broken.

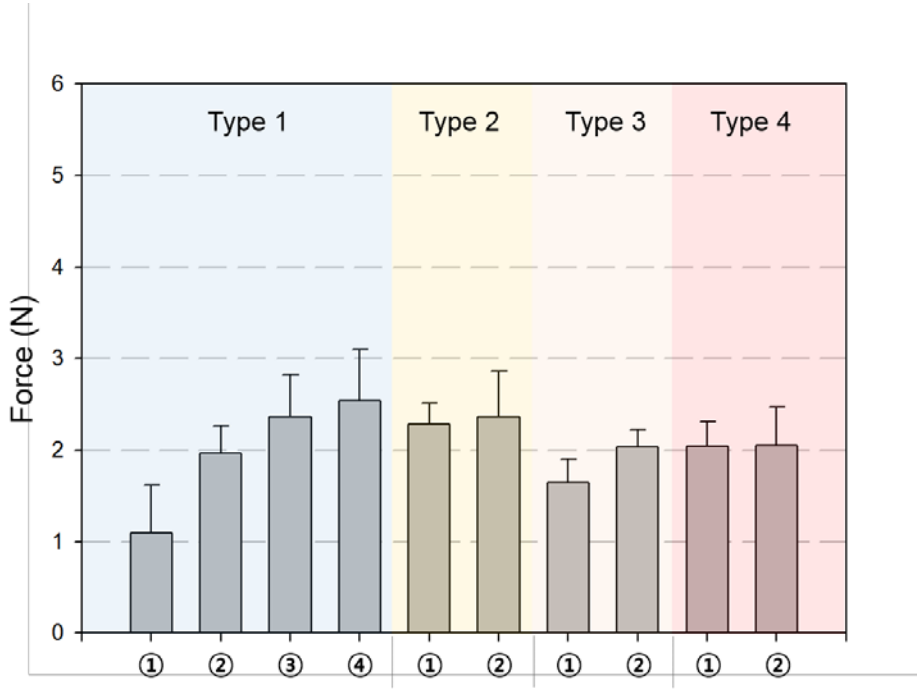

Figure 3.4.10 The force required for insertion according to the shape of each needle.

Figure.3.4.10 shows the force required for insertion according to the shape of each needle. Microneedle of types 3 and 4 with small tip radius can be inserted with relatively less force than microneedle of types 1 and 2. However, this difference does not vary significantly enough to affect the insertion function itself. As shown in the failure test by compressive force, the type 1 and 2 microneedles are more competitive because of the possibility of the tip ends being broken.

Chapter IV

Practical application of microneedle

In this chapter, we describe the practical drug delivery of microneedles made using injection molding. Experiments are conducted using a transparent skin substitute to observe the efficiency of drug delivery. When each designed micro needle is inserted, time-lapsed imaging analyzes and evaluates the diffusion of the water soluble red dye assuming the drug. In addition, we compare the drug delivery with the proposed microneedle made with injection molding to the actual mouse through the embrocation.

4.1 Evaluation of drug delivery functionality

Functionality evaluation tests are conducted to estimate drug administration efficiency when inserting microneedles into the skin. The function of the microneedle for efficient fluid administration can be confirmed by confirming the drug delivery and drug diffusion profile. Described in 2.5.1 drug delivery in agarose gel, a block made of parafilm and agarose gel is used as a surrogate of human skin in this experiment. Through this experiment, the amount of absorption can be visually displayed, and the depth and area of the drug delivered to the skin can be evaluated according to the size of the needle.

First, the delivery experiment is carried out using a type 1 microneedle to check the area of drug delivery according to the size of the needle. A total of 2 ㎕ of water soluble red dye is administered via a fluidic outlet in each microneedle (T1-①, T1-②, T1-③, T1-④) inserted onto the parafilm. Real time imaging is performed for more than 5 minutes using digital single lens reflex (DSLR) camera, which can be seen in the following figure. Acquired images are measured using imageJ (NIH, MD) for the area of drug absorption.

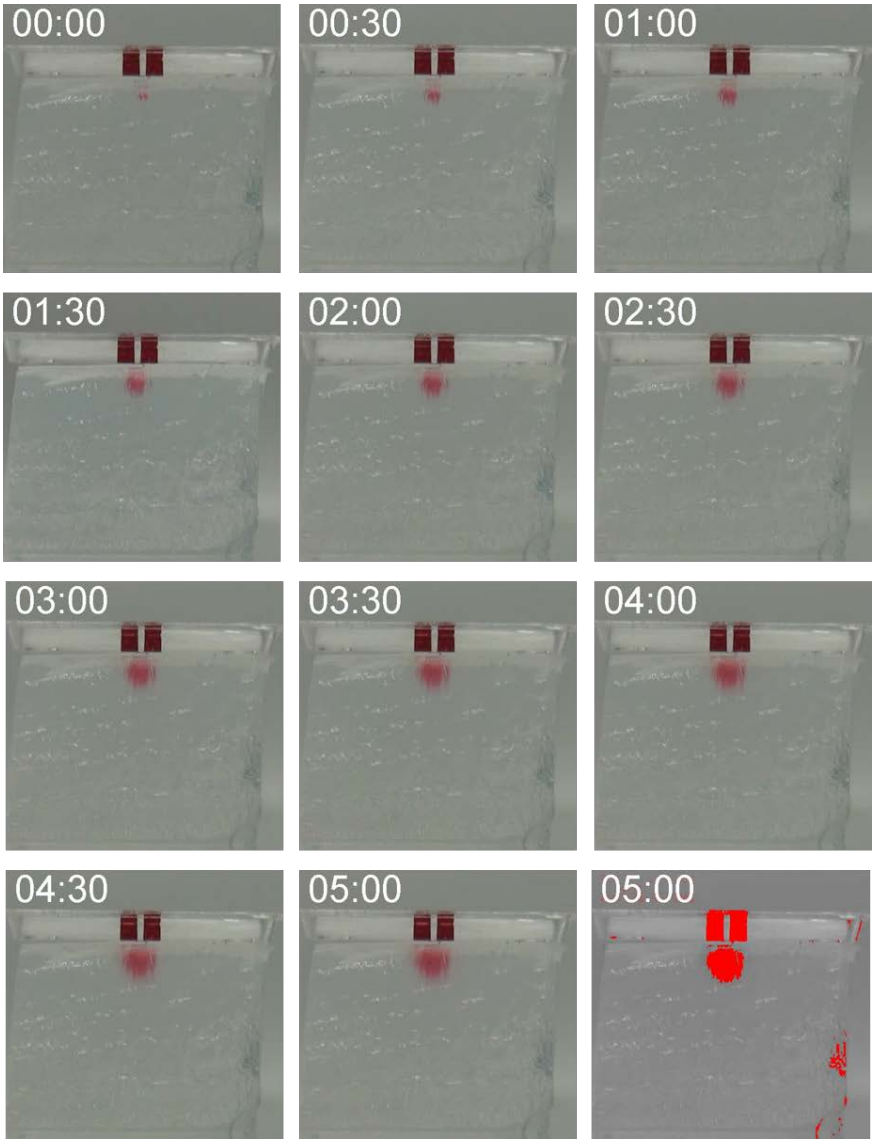

Figure 4.1.1 Time-lapse images in case of T1-① drug delivery at 1% agarose gel

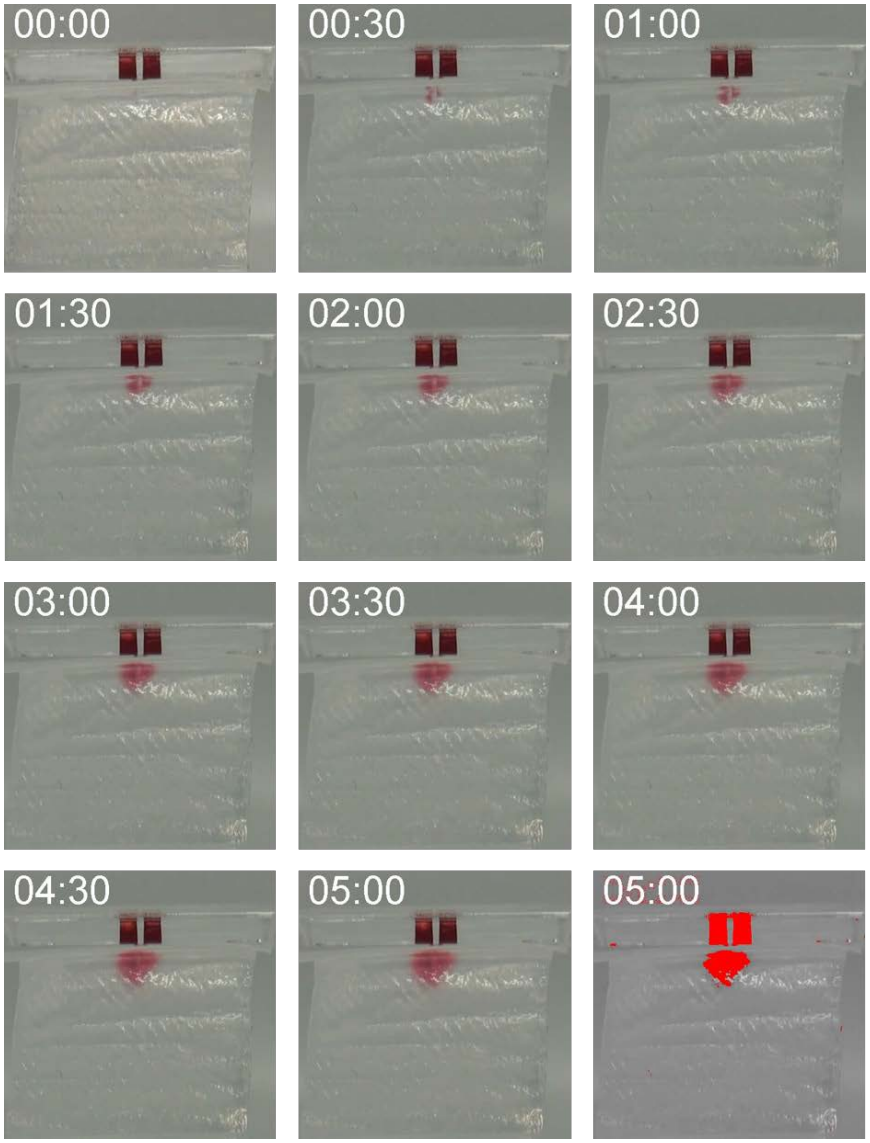

Figure 4.1.2 Time-lapse images in case of T1-② drug delivery at 1% agarose gel

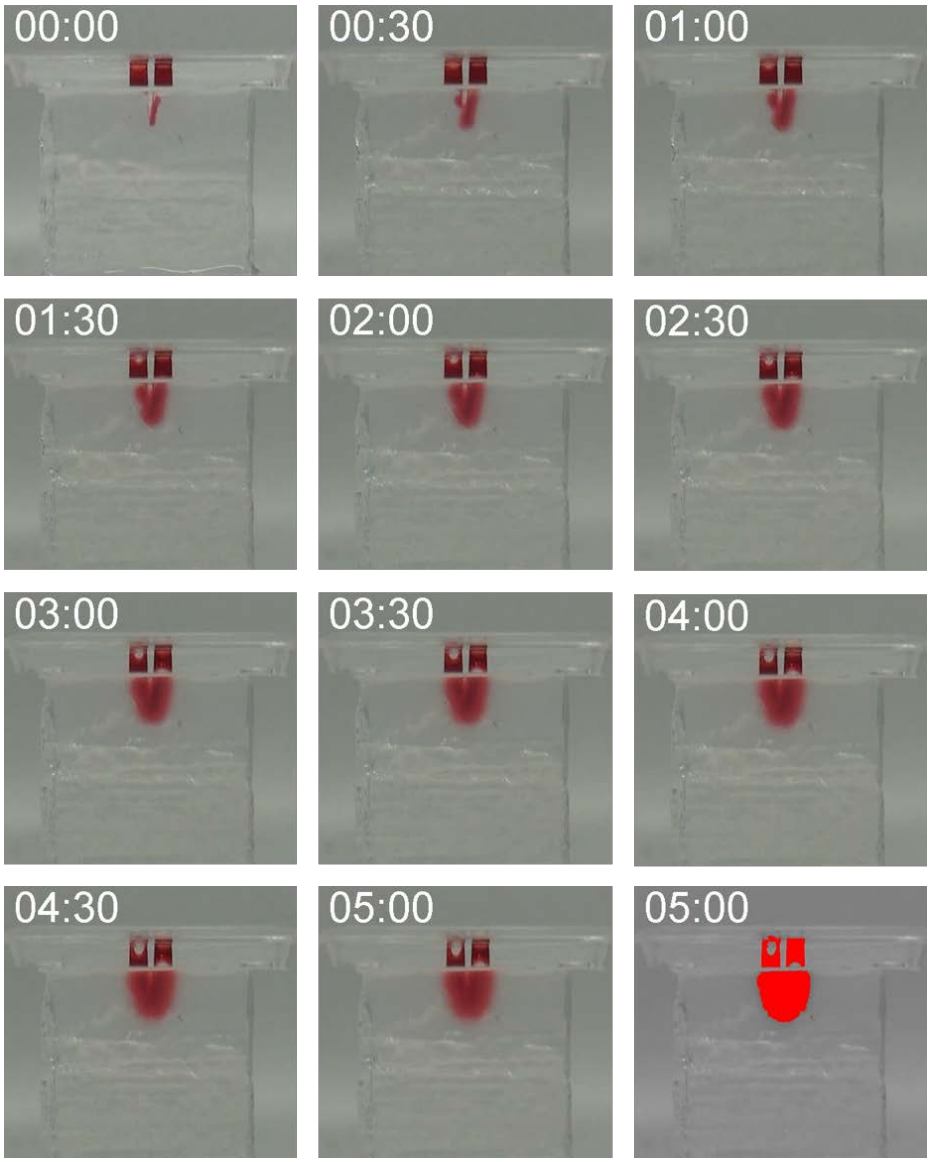

Figure 4.1.3 Time-lapse images in case of T1-③ drug delivery at 1% agarose gel

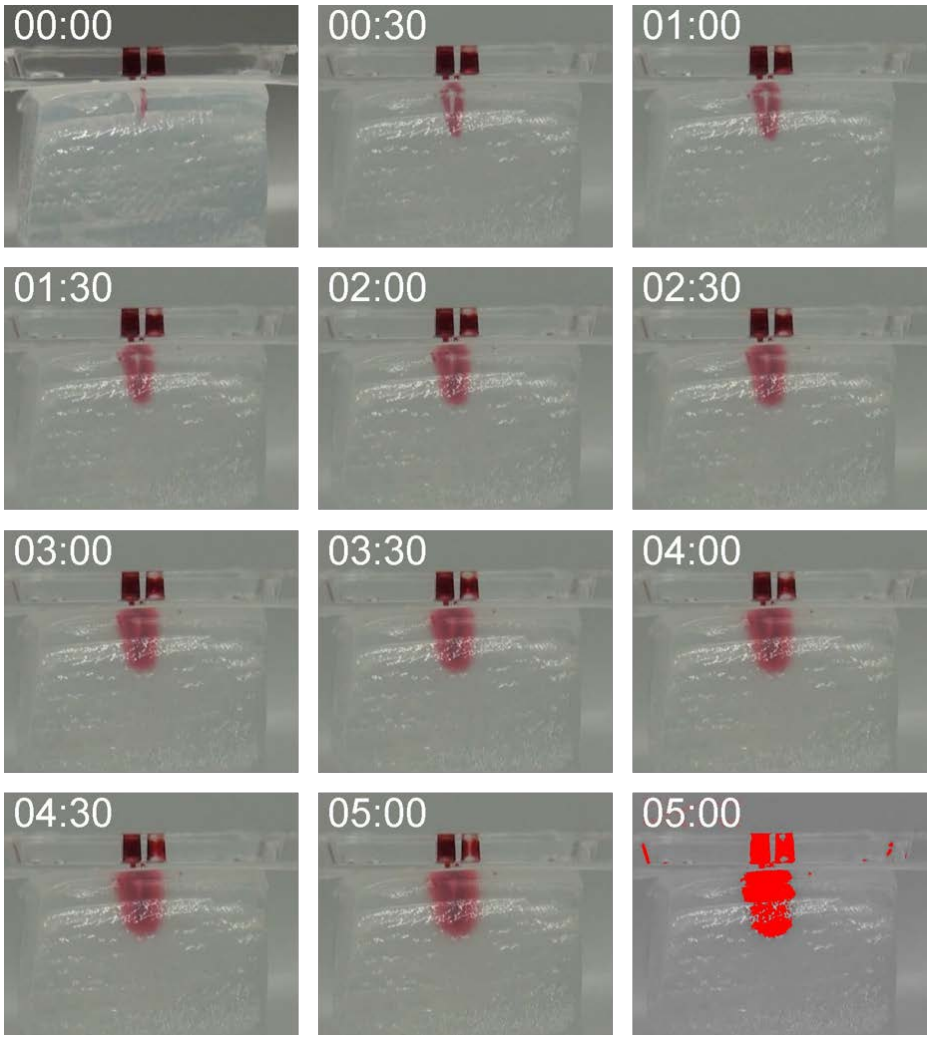

Figure 4.1.2 Time-lapse images in case of T1-④ drug delivery at 1% agarose gel

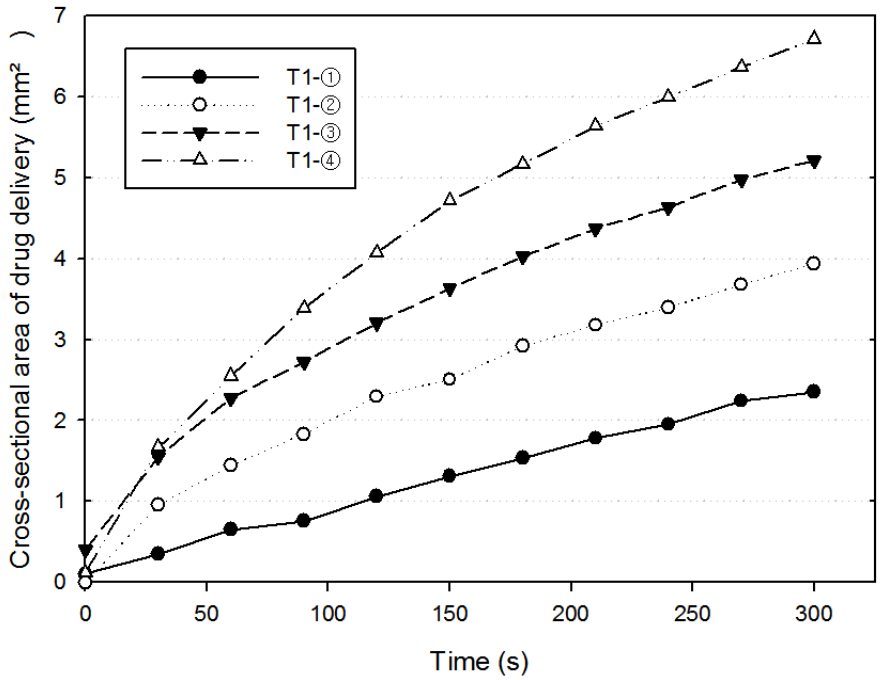

Figure 4.1.5 Plot of the cross-sectional area dimension of diffusion against times and type of microneedle (T1-①, T2-②, T1-③, T1-④)

Figure.4.1.1 to 4.1.4 demonstrates the time-lapsed images of diffusion profile from an injection surfaces. Figure 4.1.5 demonstrates the plot of the cross-sectional area dimension of diffusion against times and type of microneedles (T1-①, T2-②, T1-③, T1-④). Red water soluble dyes administered to the outlets are confirmed to be delivered and diffused through

the grooves formed in the microneedles. The drug delivery area to the length of the microneedle is generally distributed proportionally. Especially, the cross-sectional area of diffusion tends to increase rapidly at the initial stage after insertion. This refers the ability to deliver drugs rapidly in a short time. Compared with the dose of T1-④, the area of drug delivered for the first 1 minute is 25.6% for T1-❶, 56.6% for T1-②, and 89.4% for T1-③.

Next, we compare the type 1 microneedle insertion, type 2 microneedle insertion, and the insertion on the embrocated surface without additional drug influx. The microneedle, assuming a case without a fluid influx, sealed the hole with polydimethylsiloxane (PDMS) on the micro needle of T2-①. The drug is applied with 2 $\mu\ell$ to the site to be inserted and microneedle is inserted directly on the side.

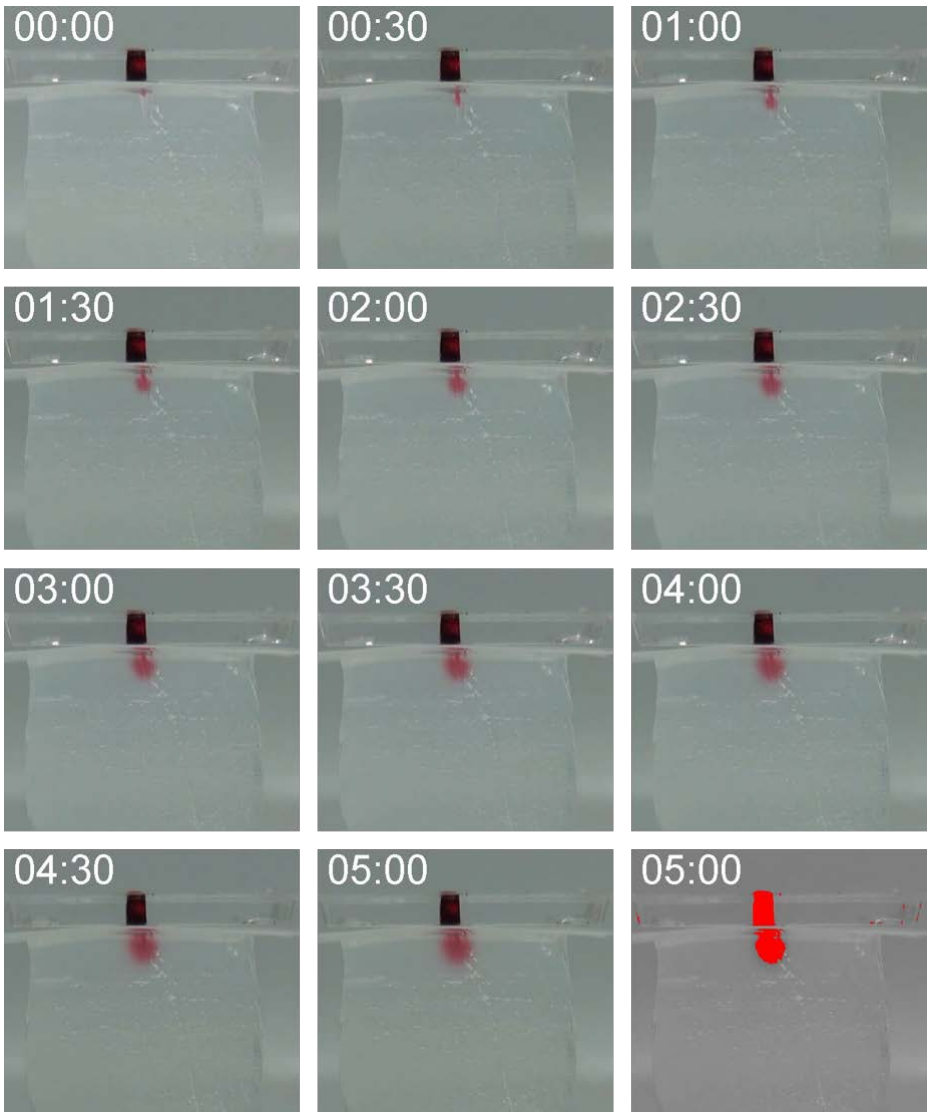

Figure 4.1.6 Time-lapse images in case of T2-① drug delivery at 1% agarose gel

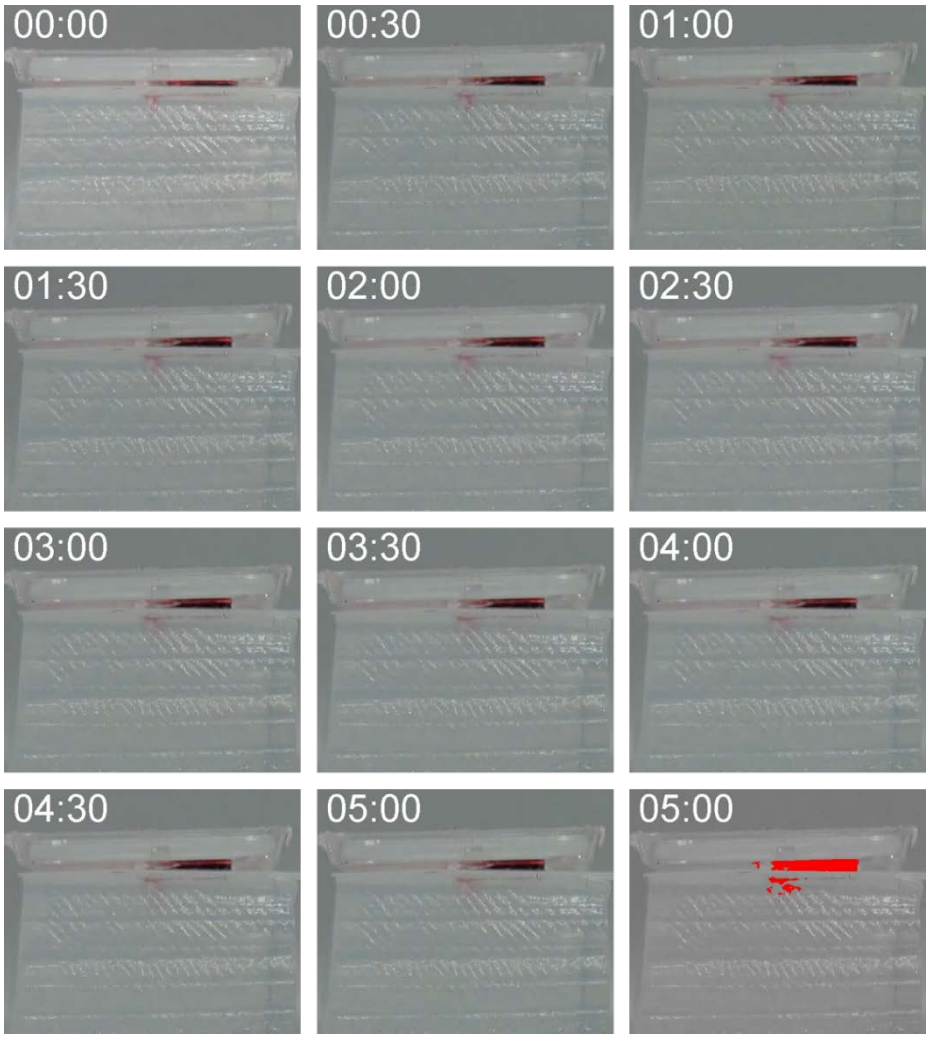

Figure 4.1.7 Time-lapse images of the insertion on the embrocated surface without additional drug influx at 1% agarose gel

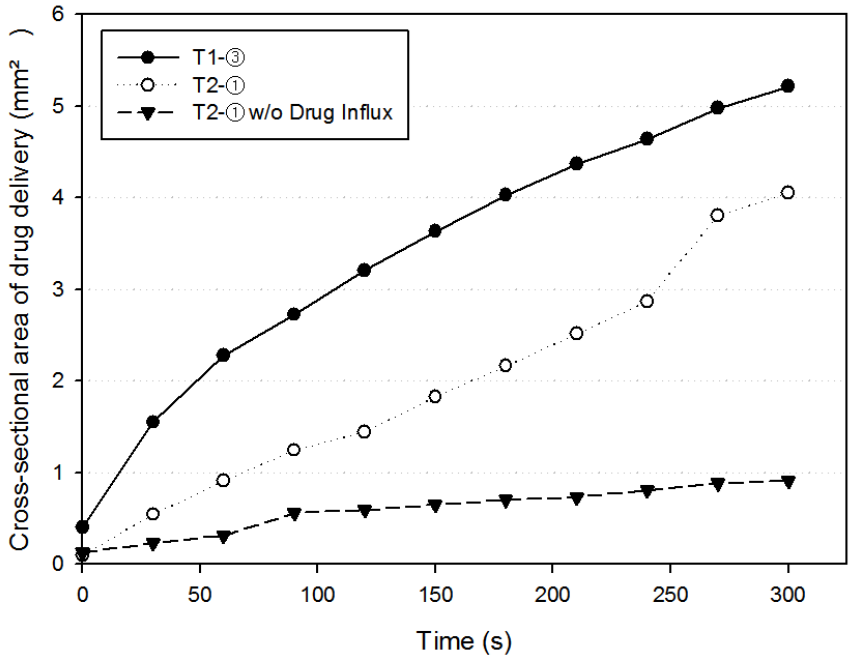

Figure 4.1.8 Plot of the cross-sectional area dimension of diffusion against times and type of microneedle (T1-③, T2-①, the T2-① insertion on the embrocated surface without additional drug influx)

Figure 4.1.6 and 4.1.7 shows the time-lapsed image of each case. Figure 4.1.8 demonstrates the plot of the cross-sectional area dimension of diffusion against times and method of drug influx. In case of T2-①, the efficiency of drug delivery is 45 ~ 61% compared to that of T1-③. This suggests that

having two outlets is more advantageous than an outlet having a large contact area to the groove. In the case of drug delivery by simple embrocation and insertion of microneedle, it is confirmed that only about 15 ~ 17% of the dose of drug is administered compared with T1-③. Immediately after the insertion of the microneedle, it is assumed that only the drugs around it flow into the body along the groove. That is, the drug is stagnant between the substrate of the microneedle and the skin, and is not delivered through the pore formed by the microneedle. On the other hand, the proposed microneedles can deliver the drug continuously by capillary force and wicking through a microfluidic channel formed between the groove and the inserted skin.

4.2 Evaluation of skin deformation and insertion depth

When the microneedles are inserted in to the skin, they are not completely inserted into the actual target tissue. Skin deformation occurs around the insertion site due to skin elasticity and damage. This means that there is a difference between the total microneedle length and the actual penetration length. In this study, optical coherence tomography (OCT) is performed to determine the depth of drug delivery and to measure skin deformation and insertion depth when microneedle is inserted into the skin. This technique scans near infrared rays while scanning, and receives reflected light from various tissues with various angles. Based on the acquired data, we can obtain reconstructed 3D images of the tissue.(Fig. 4.2.1) The microneedle is inserted into the Micropig® Franz cell membrane (Medi kinetics, Korea) and each experiment is repeated four times. The micro needle type used is T1-①, ②, ③, ④ (1500 ㎛, 1900 ㎛, 2400 ㎛, 2900 ㎛) and the results can be seen in figure 4.2.2. Skin deformation occurs around the microneedle insertion site are 713 ㎛, 806 ㎛, 954 ㎛, 1127 ㎛, respectively. As a results,

the depth of skin penetrated by microneedle is 686±103 ㎛, 1093±110 ㎛, 1445±100 ㎛, 1772±119 ㎛ in case of T1-①, ②, ③, ④. This represents the difference between the microneedle length and the actual insertion depth. It is valuable as an important reference for the design of microneedle to specify the desired insertion depth.

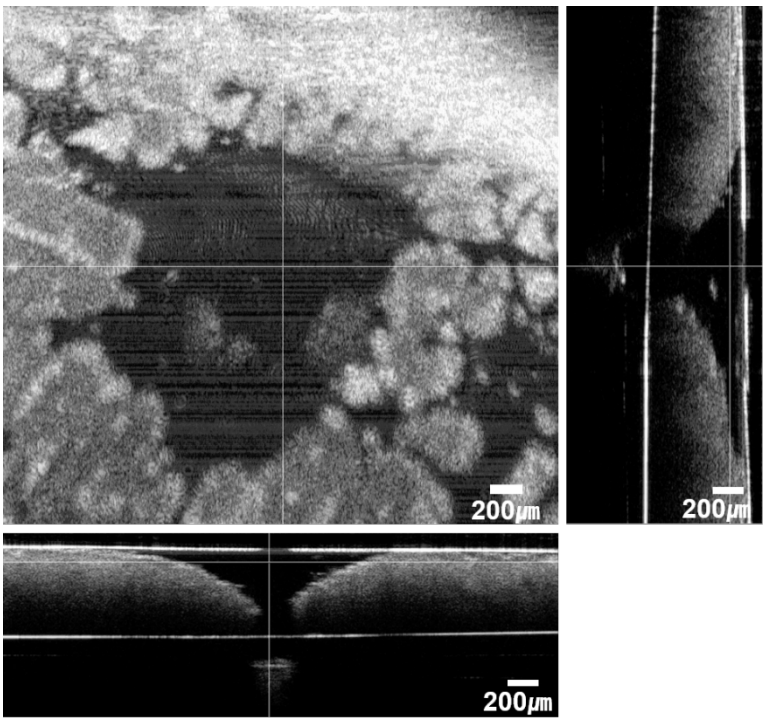

Figure 4.2.1 3D OCT Image of skin tissue inserted with microneedle**.**

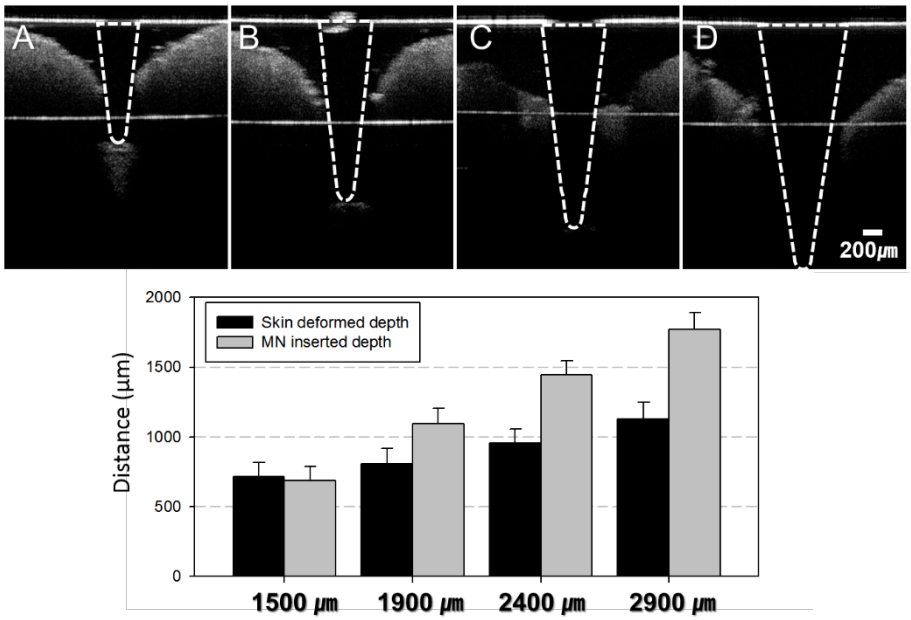

Figure 4.2.2 Cross-section image of skin inserted with microneedle

(A) T1-① (1500 ㎛) (B) T1-② (1900 ㎛), (C) T1-③ (2400 ㎛), (D) T1-④ (2900 ㎛). The graph presents the skin deformation occurs around the microneedle insertion site and the actual depth of skin penetrated by microneedle.

4.3 Drug delivery experiment *in vivo* using microneedle

To confirm the drug delivery using the micro needle in the actual body, the micro needle is inserted into the tail part of the mouse, and the drug delivery is performed. For the obvious visualization, we use blue oil-based ink. Compared with water-based inks, it is difficult to delivery oily inks into the body, and blue color ink is used to distinguish between the administered dye and the red blood in the body. In aspect of function, figure 4.3.1 demonstrate the oily inks successfully injected into the body using microneedles.

Experiments are conducted to determine whether there is a clear difference between the case of applied ink to the tail portion of adult mouse and the case of the drug delivery using microneedle.(Fig. 4.3.1 A &B) 5 minutes after the start of administration by each method, the treated site is sectioned to identify. Figure 4.3.1 (C) shows the cross-section of the area applied, and (D) is the cross-section of the site treated with the microneedle T2-①. As can be seen from the figure, the method through a microneedle can deliver the drugs successfully to the dermis and subcutaneous structure

whereas the applied drug permeates only the surface of the epidermis layer.

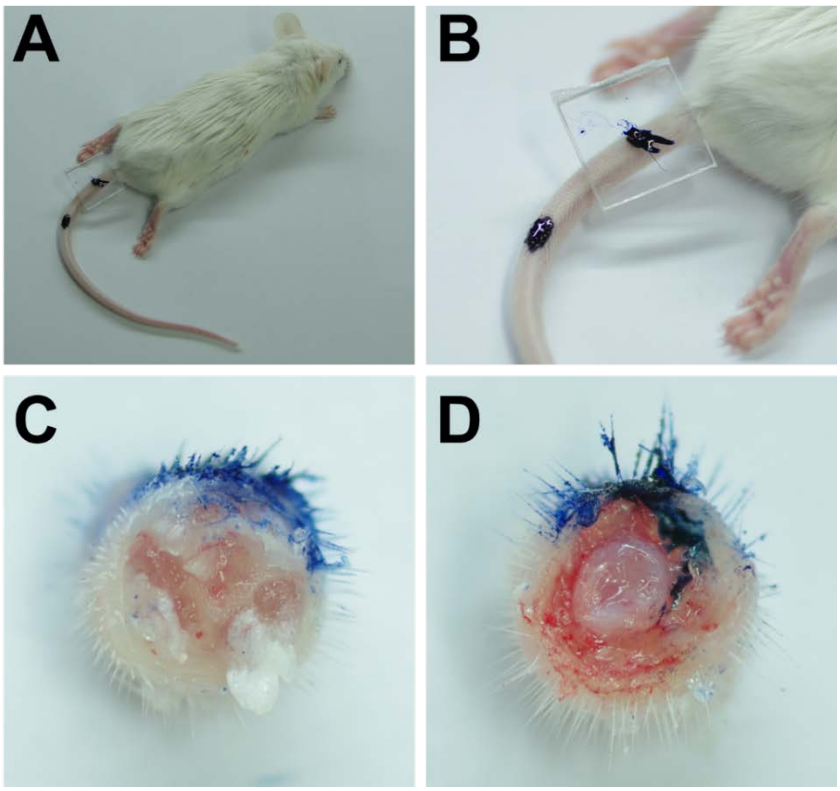

Figure 4.3.1 Drug delivery experiment *in vivo* using microneedle. (A,B) Drug embrocation and drug delivery using microneedles are performed on the tail portion of adult rats. (C) Section of the embrocation site (D) Section of drug delivered site by microneedle. Through the proposed method, it is confirm that the ink has been efficiently delivered to the *epidermis* and *subcutaneous*

tissue.

Chapter V

Conclusions

This thesis describes the design and utilization of microneedle for an efficient transdermal drug delivery and mass-produce it for commercialization. We discussed the formation of complex structures according to the mask design change using backside lithography process. Through this process, we demonstrated the trident-designed micro needle which mimic the tip of hypodermic needles. It has the advantage of fluid administration after infiltration into the skin. Particularly, this design combined with the drug delivery method using fiber sheet showed a more outstanding drug delivery effect.

One step further, we report mass production through the injection

molding process to commercialize the microneedle. We have realized the injection molding process of microneedle with fluid outlet for effective fluid influx while solving limitations such as machining of sharp point, gas trap and generation of burr, etc. The microneedles produced by the injection molding process demonstrated the functionality of drug delivery through *in vitro* and *in vivo* invasion experiments.

The microneedles of this study have various applications as a safe and advanced transdermal drug delivery method that anyone can use. In particular, it will serve as a starting point for solving problems that may arise from drug delivery through existing injections, but also will be a new step for human health and well-being with low production costs and easy accessibility.

Bibliography

1 Derler, S. & Gerhardt, L.-C. Tribology of skin: review and analysis of experimental results for the friction coefficient of human skin. *Tribology Letters* **45**, 1-27 (2012).

2 Prausnitz, M. R. & Langer, R. Transdermal drug delivery. *Nature biotechnology* **26**, 1261-1268 (2008).

3 Larrañeta, E., Lutton, R. E., Woolfson, A. D. & Donnelly, R. F. Microneedle arrays as transdermal and intradermal drug delivery systems: Materials science, manufacture and commercial development. *Materials Science and Engineering: R: Reports* **104**, 1-32 (2016).

4 Paudel, K. S. *et al.* Challenges and opportunities in dermal/transdermal delivery. *Therapeutic delivery* **1**, 109-131 (2010).

5 Tanner, T. & Marks, R. Delivering drugs by the transdermal route: review and comment. *Skin Research and Technology* **14**, 249-260 (2008).

6 McGrath, J. A., Eady, R. A. & Pope, F. M. *Rook's Textbook of Dermatology* Vol. 7th ed. 3.1–3.6 (Blackwell Publishing, 2004).

7 Breitkreutz, D., Mirancea, N. & Nischt, R. Basement membranes in skin: unique matrix structures with diverse functions? *Histochemistry and cell biology* **132**, 1-10 (2009).

8 Fenner, J. & Clark, R. A. Anatomy, Physiology, Histology, and Immunohistochemistry of Human Skin. *Skin Tissue Engineering and Regenerative Medicine*, 1-17 (2016).

9 Lee, Y. & Hwang, K. Skin thickness of Korean adults. *Surgical and radiologic anatomy* **24**, 183-189 (2002).

10 Coulman, S., Allender, C. & Birchall, J. Microneedles and other physical methods for overcoming the stratum corneum barrier for cutaneous gene therapy. *Critical Reviews™ in Therapeutic Drug Carrier Systems* **23** (2006).

11 Williams, A. *Transdermal and topical drug delivery from theory to clinical practice*. (Pharmaceutical Press, 2003).

12 Gerstel, M. S. & Place, V. A. (Google Patents, 1976).

13 Henry, S., McAllister, D. V., Allen, M. G. & Prausnitz, M. R. Microfabricated microneedles: a novel approach to transdermal drug delivery. *Journal of pharmaceutical sciences* **87**, 922-925 (1998).

14 Ma, B. *et al.* A PZT insulin pump integrated with a silicon microneedle array for transdermal drug delivery. *Microfluidics and Nanofluidics* **2**, 417-423 (2006).

15 Wilke, N. & Morrissey, A. Silicon microneedle formation using modified mask designs based on convex corner undercut. *Journal of micromechanics and microengineering* **17**, 238 (2006).

16 Izumi, H. & Aoyagi, S. Novel fabrication method for long silicon microneedles with three-dimensional sharp tips and complicated shank shapes by isotropic dry etching. *IEEJ Transactions on Electrical and Electronic Engineering* **2**, 328-334 (2007).

17 Omatsu, T. *et al.* Metal microneedle fabrication using twisted light with spin. *Optics express* **18**, 17967-17973 (2010).

18 Zhu, M. *et al.* Silica needle template fabrication of metal hollow microneedle arrays. *Journal of Micromechanics and Microengineering* **19**, 115010 (2009).

19 Sullivan, S. P. *et al.* Dissolving polymer microneedle patches for influenza vaccination. *Nature medicine* **16**, 915-920 (2010).

20 Wang, P.-C. *et al.* in *Engineering in Medicine and Biology Society, 2009. EMBC 2009. Annual International Conference of the IEEE.* 7026-7029 (IEEE).

21 Park, J.-H., Allen, M. G. & Prausnitz, M. R. Biodegradable polymer microneedles: fabrication, mechanics and transdermal drug delivery. *Journal of Controlled Release* **104**, 51-66 (2005).

22 Lee, I.-C., He, J.-S., Tsai, M.-T. & Lin, K.-C. Fabrication of a novel partially dissolving polymer microneedle patch for transdermal drug delivery. *Journal of Materials Chemistry B* **3**, 276-285 (2015).

23 Donnelly, R. F. *et al.* Hydrogel-forming microneedle arrays can be effectively inserted in skin by self-application: A pilot study centred on pharmacist intervention and a patient information leaflet. *Pharmaceutical research* **31**, 1989-1999 (2014).

24 Kim, Y.-C., Park, J.-H. & Prausnitz, M. R. Microneedles for drug and vaccine delivery. *Advanced drug delivery reviews* **64**, 1547-1568 (2012).

25 Wilke, N., Hibert, C., O'Brien, J. & Morrissey, A. Silicon microneedle electrode array with temperature monitoring for electroporation. *Sensors and Actuators A: Physical* **123**, 319-325 (2005).

26 Chen, B., Wei, J., Tay, F. E., Wong, Y. T. & Iliescu, C. Silicon microneedle array with biodegradable tips for transdermal drug delivery. *Microsystem Technologies* **14**, 1015-1019 (2008).

27 Grundfest, H., Sengstaken, R. W., Oettinger, W. H. & Gurry, R. Stainless Steel Micro-Needle Electrodes Made by Electrolytic Pointing. *Review of Scientific Instruments* **21**, 360-361 (1950).

28 Parker, E., Rao, M., Turner, K., Meinhart, C. & MacDonald, N. Bulk micromachined titanium microneedles. *Journal of microelectromechanical systems* **16**, 289-295 (2007).

29 Jin, C. Y., Han, M. H., Lee, S. S. & Choi, Y. H. Mass producible and biocompatible microneedle patch and functional verification of its usefulness for transdermal drug delivery. *Biomedical microdevices* **11**, 1195 (2009).

30 Watanabe, T., Hagino, K. & Sato, T. Evaluation of the effect of polymeric microneedle arrays of varying geometries in combination with a high-velocity applicator on skin permeability and irritation. *Biomedical microdevices* **16**, 591-597 (2014).

31 Gill, H. S. & Prausnitz, M. R. Coated microneedles for transdermal delivery. *Journal of controlled release* **117**, 227-237 (2007).

32 Stokes, R. J., Evans, D. F. & Errico, M. *Liquid Coating Processes*. (Wiley-VCH, 1997).

33 Chen, X. *et al.* Dry-coated microprojection array patches for targeted delivery of immunotherapeutics to the skin. *Journal of Controlled Release*

139, 212-220 (2009).

34 Gill, H. S. & Prausnitz, M. R. Coating formulations for microneedles. *Pharmaceutical research* **24**, 1369-1380 (2007).

35 Kim, M., Jung, B. & Park, J.-H. Hydrogel swelling as a trigger to release biodegradable polymer microneedles in skin. *Biomaterials* **33**, 668-678 (2012).

36 Kim, J. D., Kim, M., Yang, H., Lee, K. & Jung, H. Droplet-born air blowing: Novel dissolving microneedle fabrication. *Journal of controlled release* **170**, 430-436 (2013).

37 Gardeniers, H. J. *et al.* Silicon micromachined hollow microneedles for transdermal liquid transport. *Journal of Microelectromechanical systems* **12**, 855-862 (2003).

38 Moon, S. J. & Lee, S. S. A novel fabrication method of a microneedle array using inclined deep x-ray exposure. *Journal of Micromechanics and Microengineering* **15**, 903 (2005).

39 Davis, S., Prausnitz, M. & Allen, M. in *TRANSDUCERS, Solid-State Sensors, Actuators and Microsystems, 12th International Conference on, 2003.* 1435-1438 (IEEE).

40 Wang, P. M., Cornwell, M., Hill, J. & Prausnitz, M. R. Precise microinjection into skin using hollow microneedles. *Journal of investigative dermatology* **126**, 1080-1087 (2006).

41 Rodriguez, A. *et al.* Fabrication of silicon oxide microneedles from macroporous silicon. *Sensors and Actuators B: Chemical* **109**, 135-140 (2005).

42 Li, C. G., Lee, C. Y., Lee, K. & Jung, H. An optimized hollow microneedle for minimally invasive blood extraction. *Biomedical microdevices* **15**, 17-25 (2013).

43 Sullivan, S. P., Murthy, N. & Prausnitz, M. R. Minimally invasive protein delivery with rapidly dissolving polymer microneedles. *Advanced materials* **20**, 933-938 (2008).

44 Park, J.-H., Choi, S.-O., Seo, S., Choy, Y. B. & Prausnitz, M. R. A

microneedle roller for transdermal drug delivery. *European journal of pharmaceutics and biopharmaceutics* **76**, 282-289 (2010).

45 Zhang, P., Dalton, C. & Jullien, G. A. Design and fabrication of MEMS-based microneedle arrays for medical applications. *Microsystem technologies* **15**, 1073-1082 (2009).

46 Sammoura, F., Kang, J., Heo, Y.-M., Jung, T. & Lin, L. Polymeric microneedle fabrication using a microinjection molding technique. *Microsystem Technologies* **13**, 517-522 (2007).

47 Dick, L. A. Innovative drug delivery technology to meet evolving need of biologics & small molecules. *Transdermal Delivery & Microneedles* 4-6 (2015).

48 Lhernould, M. S. & Delchambre, A. Innovative design of hollow polymeric microneedles for transdermal drug delivery. *Microsystem technologies* **17**, 1675 (2011).

49 Wood, A. New Method of Treating Neuralgia by the Direct Application of Opiates to the Painful Points. *Survey of Anesthesiology* **28**, 350 (1984).

50 Simonsen, L., Kane, A., Lloyd, J., Zaffran, M. & Kane, M. In focus-unsafe injections in the developing world and transmission of bloodborne pathogens: a review. *Bulletin of the World Health Organization* **77**, 789-800 (1999).

51 Hamilton, J. G. Needle phobia: a neglected diagnosis. *Journal of Family Practice* **41**, 169-176 (1995).

52 Nir, Y., Paz, A., Sabo, E. & Potasman, I. Fear of injections in young adults: prevalence and associations. *The American journal of tropical medicine and hygiene* **68**, 341-344 (2003).

53 Lavoie, M. C., Verbeek, J. H. & Pahwa, M. Devices for preventing percutaneous exposure injuries caused by needles in healthcare personnel. *The Cochrane Library* (2014).

54 Whitesides, G. M., Ostuni, E., Takayama, S., Jiang, X. & Ingber, D. E. Soft lithography in biology and biochemistry. *Annual review of biomedical engineering* **3**, 335-373 (2001).

55 Xia, Y. & Whitesides, G. M. Soft lithography. *Annual review of materials*

science **28**, 153-184 (1998).

56 Mata, A., Fleischman, A. J. & Roy, S. Fabrication of multi-layer SU-8 microstructures. *Journal of micromechanics and microengineering* **16**, 276 (2006).

57 Chen, C., Hirdes, D. & Folch, A. Gray-scale photolithography using microfluidic photomasks. *Proceedings of the National Academy of Sciences* **100**, 1499-1504 (2003).

58 Kang, M., Byun, J. H., Na, S. & Jeon, N. L. Fabrication of functional 3D multi-level microstructures on transparent substrates by one step back-side UV photolithography. *RSC Advances* **7**, 13353-13361 (2017).

59 Lee, J.-H., Choi, W.-S., Lee, K.-H. & Yoon, J.-B. A simple and effective fabrication method for various 3D microstructures: backside 3D diffuser lithography. *Journal of micromechanics and microengineering* **18**, 125015 (2008).

60 Kochhar, J. S., Goh, W. J., Chan, S. Y. & Kang, L. A simple method of microneedle array fabrication for transdermal drug delivery. *Drug development and industrial pharmacy* **39**, 299-309 (2013).

61 Larrañeta, E. *et al.* A proposed model membrane and test method for microneedle insertion studies. *International journal of pharmaceutics* **472**, 65-73 (2014).

62 O'Mahony, C. Structural characterization and in-vivo reliability evaluation of silicon microneedles. *Biomedical microdevices* **16**, 333-343 (2014).

63 Lee, S. W. & Lee, S. S. Application of Huygens-Fresnel diffraction principle for high aspect ratio SU-8 micro-/nanotip array. *Optics letters* **33**, 40-42 (2008).

64 Beck, J. & Bardèche, J. in *Annales de biologie clinique.* 987-991.

65 Davies, P. Determination of diffusion coefficients of proteins in beaded agarose by gel filtration. *Journal of Chromatography A* **483**, 221-237 (1989).

66 Sjöberg, H., Persson, S. & Caram-Lelham, N. How interactions between drugs and agarose-carrageenan hydrogels influence the simultaneous transport of drugs. *Journal of controlled release* **59**, 391-400 (1999).

67 Fatin-Rouge, N., Starchev, K. & Buffle, J. Size effects on diffusion processes within agarose gels. *Biophysical Journal* **86**, 2710-2719 (2004).

68 Pluen, A., Netti, P. A., Jain, R. K. & Berk, D. A. Diffusion of macromolecules in agarose gels: comparison of linear and globular configurations. *Biophysical journal* **77**, 542-552 (1999).

69 Zhang, D., Das, D. B. & Rielly, C. D. Microneedle Assisted Micro-Particle Delivery from Gene Guns: Experiments Using Skin-Mimicking Agarose Gel. *Journal of pharmaceutical sciences* **103**, 613-627 (2014).

70 Lee, Y. *Mechanics of three dimensional cutting processes*. (DaeGa, 2005).

71 Tsuji, H. Poly (lactic acid). *Bio-Based Plastics: Materials and Applications*, 171-239 (2013).

72 Auras, R. Poly (lactic acid). *Encyclopedia Of Polymer Science and Technology* (2010).

73 Dwight, J. *Aluminium design and construction*. (CRC Press, 2002).

초 록

효과적인 약물 전달을 위한 마이크로니들 및 생산 공정 개발

현재 전 세계적으로 연간 12 조회의 약물주입이 주사기를 통해 일어나고 있으며 인류의 10% 가량은 주사공포증으로 고통받고 있다. 또한 전 세계 수많은 사람들이 당뇨 등의 크고 작은 만성질환을 앓으며 많게는 하루에 수 회 이상의 주사를 통한 약물공급을 필요로 한다. 주사를 이용한 경피 약물 전달 방법은 소화계 및 순환계의 대사과정을 거치지 않고 약물의 투입이 가능하고, 효과가 빠르며 적은 양의 약물로 약효를 낼 수 있는 장점이 있지만 많은 문제점을 수반하고 있다.

최근 일회용 주사기의 재사용으로 인한 C 형 간염 환자의 발생 등, WHO 가 2014 년에 추산한 바에 이르면 매년 200 만 건에 이르는 주사기 유발 의료사고가 일어나며 B, C 형 간염 및 HIV 등 25 종에 이르는 혈액매개 바이러스감염 사고가 보고되었다. 또한 개발도상국에서 행해지는 주사기 시술의 최소 50% 이상이 안전하지 못한 상태에서 행해진다. 해마다 백신접종비용이 증가하는 경제적인 이유 이

외에도, 주사를 통한 약물 전달은 기본적으로 전문 의료인에 의해 실시되어야만 하는 규제도 예방접종비율을 쉽게 늘리지 못하는 원인 중에 하나이다. 따라서 주사바늘로 인한 사고의 위험성이 없으며, 전문 의료진이 아닌 일반인도 사용할 수 있는 약물전달 기술로서 마이크로 니들의 개발이 요구된다.

이를 위해 본 연구에서는 피부를 통해 약물을 효과적으로 전달할 수 있는 마이크로니들의 디자인과 그 제조방법을 제시한다. 외피에 침습하여 미세한 구멍을 생성할 뿐 아니라 약물의 지속적인 투여가 가능한 채널을 형성하는 디자인으로 효율적인 약물전달을 구현한다. 단순히 피부에 상처를 내는 역할 외에 1) 마이크로 니들 배열의 사이에 섬유를 삽입하여 모세관 힘 및 위킹(wicking)을 이용, 투여된 약물을 지속적으로 공급할 수 있는 방법과 2) 마이크로 니들의 측면에 유체 흐름을 위한 홈과 여기에 연결되어 지속적인 약물 공급이 가능한 약물투입구를 설계하여 효율적인 약물 공급 방법을 개발하였다. 이러한 마이크로 니들을 낮은 제조 단가와 생산량을 구현할 수 있는 사출 공정을 이용하여 대량 생산의 가능성을 보인다. 사출 공정으로 형성한 마이크로니들을 이용한 지속적인 약물 투여 및 확산은 실험을 통해 실시간으로 확인할 수 있다. 또한 실제 성체

마우스의 체내에 삽입하여 성공적인 약물 전달이 가능함을 확인하였다.

본 연구의 마이크로니들은 누구나 사용할 수 있는 안전하고 진보된 경피 약물 전달 방법으로서 다양한 응용 가능성을 갖고 있다. 특히, 기존의 주사를 통한 약물전달에서 생길 수 있는 문제점들을 해결할 수 있는 단초로서 작용할 뿐 아니라 낮은 생산비용과 쉬운 접근성으로 인류의 건강과 복지를 위한 새로운 한걸음이 될 것이다.

주요어 : 마이크로니들; 경피 약물 전달; 배면노광; 사출공정; 3 차원 미세구조물 생성

학번 : 2011-22886